Mechanistic Studies on the Hydroxylation of Methane by Methane Monooxygenase

Mu-Hyun Baik,[†] Martin Newcomb,*[,‡] Richard A. Friesner,*[,†] and Stephen J. Lippard*[,§]

Departments of Chemistry, Columbia University, New York, New York 10027, University of Illinois at Chicago, Chicago, Illinois 60607, and Massachusetts Institute of Technology, Cambridge, Massachusetts 02139

Received December 16, 2002

Contents

1. Introduction

Methanotrophs are bacteria that live on methane as their only source of carbon.[1] The first step in their utilization of this simplest of all hydrocarbons is its selective conversion to methanol. Subsequent biochemical pathways transform methanol to formaldehyde, which in turn is processed into biomass. Further oxidation of formaldehyde to carbon dioxide provides energy that is stored for later use as NADH.[2] The conversion of methane to methanol is catalyzed at the active site of a metalloenzyme known as methane monooxygenase, or MMO.[3−9] As indicated in eq 1, one atom of the dioxygen molecule is assimilated into the alcohol and the other forms water. In methanotrophic organisms there are two

$$CH_4 + NADH + H^+ + O_2 \rightarrow CH_3OH + NAD^+ + H_2O \quad (1)$$

kinds of MMO systems, a soluble form (sMMO), comprising several protein components that have been isolated and structurally characterized, and a membrane-bound or particulate form (pMMO).[10,11] The hydroxylase responsible for dioxygen activation and hydrocarbon oxidation in pMMO, which is expressed in practically all methanotrophs, contains copper. Unfortunately, efforts to isolate and purify this hydroxylase have thus far not been sufficiently successful to afford an X-ray crystal structure determination.[12−14] Under copper-deficient conditions,[15,16] some methanotrophs express sMMO, the hydroxylase enzyme of which (MMOH) contains a carboxylate-bridged non-heme diiron center at its active site. MMOH has thus far attracted most of the attention because it is easier to purify and study than pMMO.

The ability of the MMO systems to activate inert C−H bonds under ambient conditions has captivated the imagination of many researchers over the past 20 years. If a biomimetic industrial catalyst could be devised that reproduced the reactivity of this enzyme, then large-scale conversion of methane gas (it is currently not economical[17] to transport and store methane gas from remote sites) into methanol might make available a new cost-effective energy source.[18,19] Although such a catalyst is not realistic for the near future,[20] there are valuable lessons to be learned for the design of compounds that can oxidize alkane and other substrates catalytically[21−27] by studying how nature utilizes a relatively small transition metal-based active site[28,29] to achieve a difficult chemical transformation.

Crystal structure data available for sMMO from a number of different investigations[30−38] have served as a valuable starting point for many mechanistic studies. The chemistry of sMMO is versatile, and oxidative activation of a wide variety of hydrocarbon substrates ranging from simple saturated and unsaturated alkanes to halogenated, aromatic, or heterocyclic compounds has been established.[39−50] Soluble MMOs, isolated from *Methylococcus capsulatus* (Bath), hereafter *Mc. capsulatus* (Bath), and *Methylosinus*

[†] Columbia University.
[‡] University of Illinois at Chicago.
[§] Massachusetts Institute of Technology.

10.1021/cr950244f CCC: $44.00 © 2003 American Chemical Society
Published on Web 05/17/2003

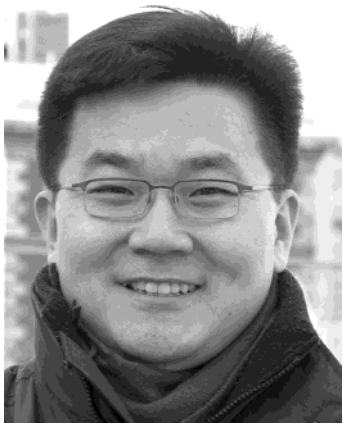

Mu-Hyun Baik was born in Seoul, South Korea, in 1970. In December 1980, he and his family moved to Dinslaken, a small town in Germany close to Düsseldorf. After obtaining a "Vordiplom" (B.S.) in chemistry from the Heinrich-Heine-Universität in Düsseldorf in 1994, he came to the United States as an exchange graduate student on a one-year fellowship from the German Academic Exchange Service (DAAD) at the Chemistry Department of the University of North Carolina Chapel Hill. He quickly fell in love with Chapel Hill and decided to stay, obtaining his Ph.D. from UNC in 2000 under the supervision of Cynthia K. Schauer. He then moved to Columbia University to work with Richard A. Friesner and in collaboration with Stephen J. Lippard on a number of different projects. In August 2003, he will be joining the Chemistry Department at Indiana University in Bloomington as an Assistant Professor. Baik's research interests lie in the areas of computational inorganic and bioinorganic chemistry.

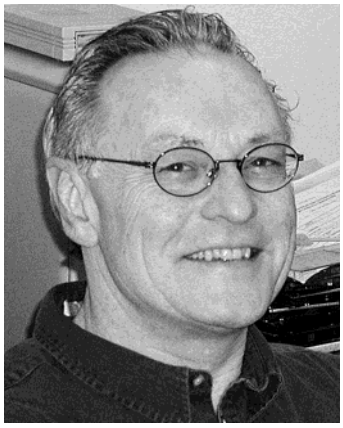

Martin Newcomb obtained his Ph.D. degree in 1973 with Warren Ford at the University of Illinois at Urbana and studied as a postdoctoral scholar with the late Donald J. Cram. Newcomb held faculty positions at Texas A&M University and Wayne State University, and he is currently an LAS Distinguished Professor of Chemistry at the University of Illinois at Chicago. Newcomb's research interests are in the areas of radical reactions in organic and biological chemistry.

Richard A. Friesner was born in New York, NY, in 1952. He received his B.S. degree in chemistry from the University of Chicago in 1973. He obtained his Ph.D. in 1979 at the University of California, Berkeley, working in the laboratory of Kenneth Sauer. He then spent three years as a postdoctoral fellow, working with Robert Silbey at the Massachusetts Institute of Technology. He joined the Chemistry Department at the University of Texas at Austin in 1982 as an Assistant Professor. In 1990, he became Professor of Chemistry at Columbia University. His interests include the application of quantum chemical methods to biological systems, development of molecular mechanics force fields and models for continuum solvation, computational methods for protein folding and structural refinement, prediction of protein–ligand binding affinities, and calculation of electron-transfer rates in complex molecules and materials.

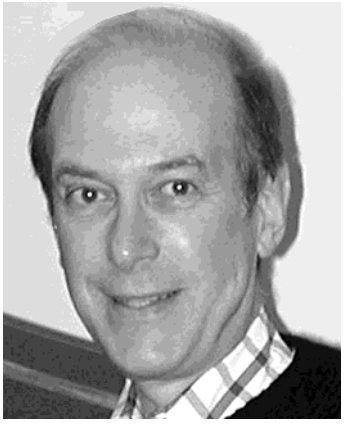

Stephen J. Lippard is the Arthur Amos Noyes Professor of Chemistry and Head of the Chemistry Department at the Massachusetts Institute of Technology. He was born in Pittsburgh, PA, and educated in Pittsburgh public schools. He studied at Haverford College (B.A.) and the Massachusetts Institute of Technology (Ph.D.). After a year as a NSF postdoctoral fellow at MIT, he served on the faculty of Columbia University before returning to MIT in 1983. His research activities span the fields of inorganic, biological chemistry, and neurochemistry. Included are mechanistic studies of platinum anticancer drugs, the synthesis of dimetallic complexes as models for non-heme iron enzymes, structural and mechanistic investigations of methane monooxygenase, and optical sensors for neurotransmitters.

trichosporium OB3b (*Ms. trichosporium* OB3b), have three component proteins.[51−54] In addition to MMOH, the system has a reductase, MMOR, which facilitates electron transfer from NADH to the diiron centers in the hydroxylase (eq 1),[55−58] and an auxiliary protein, MMOB, which couples the consumption of electrons with hydrocarbon oxidation in MMOH. Both MMOB and MMOR bind to MMOH during catalytic turnover,[54] and although there is some information about the structures of complexes that form between these components[59−63] and how they interact with each other,[64−68] X-ray structures are not yet available.[69]

Figure 1 illustrates the structure of MMOH from *Mc. capsulatus* (Bath). The hydroxylase is an $\alpha_2\beta_2\gamma_2$ heterodimer with two carboxylate-bridged diiron centers housed in four-helix bundle motifs of the α subunits of the two protomers. In the resting, oxidized state (H_{ox}), the positive charge of the two high-spin iron(III) atoms is precisely balanced by four glutamate and two bridging hydroxide ligands. Two additional histidine ligands complete the octahedral coordination spheres of the iron atoms (Figure 2). Upon reduction to the diiron(II) form (H_{red}), a necessary step in the catalytic cycle of the enzyme, MMOH loses the bridging hydroxide ions. In addition, one of the glutamate ligands undergoes a carboxylate shift,

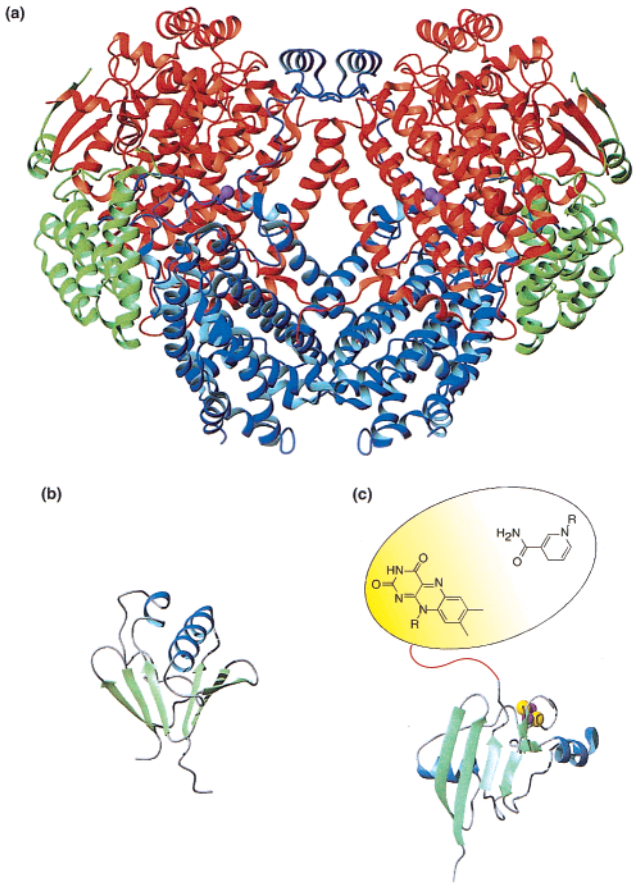

Figure 1. (a) X-ray crystal structure of MMOH from *Mc. capsulatus* (Bath).[31] The α subunit is colored red, the *β* subunit blue, and the *γ* subunit green. Iron atoms are shown as purple spheres. (b) Solution structure of MMOB. Flexible regions of N- and C-termini are not shown.[60] (c) Structure of MMOR. The solution structure of the [2Fe-2S] domain of MMOR[63] is shown with a cartoon representing the FAD and NAD(H) binding domains. The Fe and S atoms of the [2Fe-2S] cluster are shown as purple and yellow spheres, respectively. (Reprinted with permission from ref 7. Copyright 2002 Elsevier Science Ltd.)

bringing a previously dangling oxygen atom into the bridging position and shortening the Fe−Fe distance slightly (Figure 2). The system is thus poised to react with dioxygen, the second major step in the overall catalytic cycle (Scheme 1). Proceeding through several postulated or isolated intermediates, the system evolves to give the hydroxylating, diiron(IV) species **Q**. The catalytic cycle completes with the third part, in which the substrate methane is converted into methanol and H_{ox} is restored after losing the second oxygen atom as water released into the environment.

Scheme 1

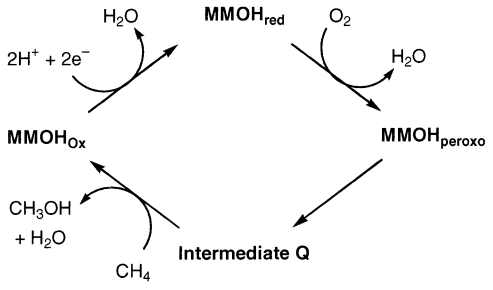

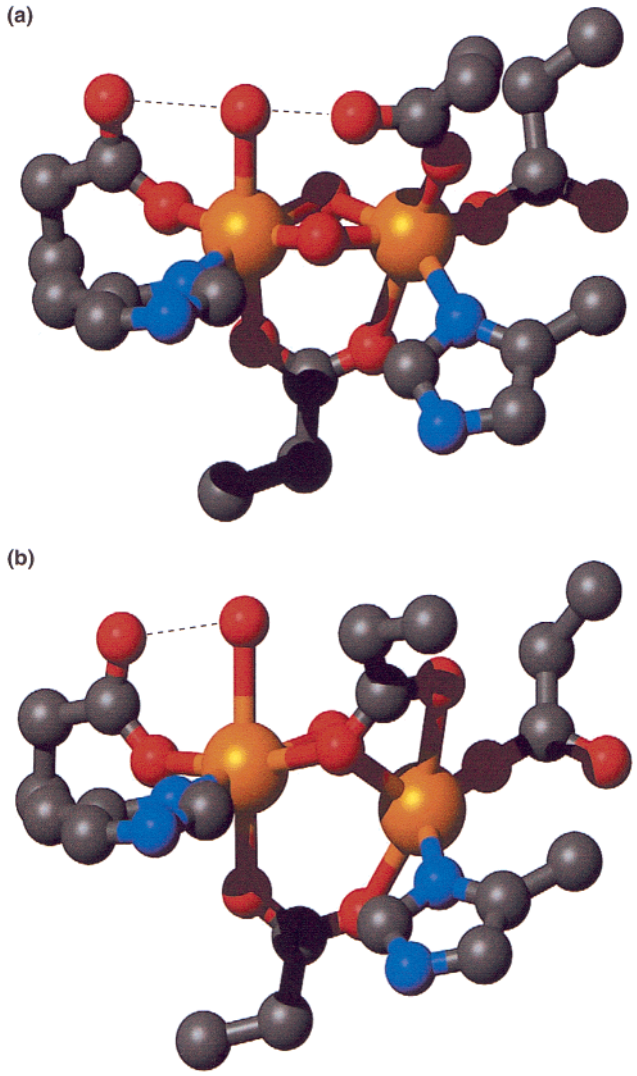

Figure 2. Active-site structures of (a) $MMOH_{ox}$ and (b) $MMOH_{red}$.[31] Colors: gray, carbon; red, oxygen; blue, nitrogen; orange, iron. (Reprinted with permission from ref 7. Copyright 2002 Elsevier Science Ltd.)

In this review we focus on this third leg of the catalytic cycle, limiting our discussion primarily to the final hydroxylation step. Extensive discussions of the earlier chemistry can be found elsewhere.[3−5]

The range of experimental methods utilized to examine the hydroxylation mechanism is remarkably broad. Spectroscopic studies using UV/vis,[51,70,99] EPR,[51,59,70−82,88] ENDOR/ESEEM,[74,80−89] EXAFS,[70,90−94] CD/MCD,[95−98] and Mössbauer[70,73,74,99,100] techniques at various stages of the catalytic cycle have been reported, and the results have been summarized.[3−5] In the past few years, substrate probes have been used with increasing frequency to address whether the reaction is concerted or involves the formation of a radical or a cationic intermediate. In general, such probes are substrates that are expected to report on the radical or cationic nature of intermediates by affording different products for different mechanistic pathways. The product distribution can be used as evidence to support or eliminate one or the other mechanistic scenario. In addition, the time scale required for a substrate intermediate to rearrange and generate products is, in principle, a powerful tool

for estimating the lifetimes of the short-lived species. Unfortunately, the interpretation of probe experiments has proved to be difficult, and a number of conflicting conclusions have been drawn. Recently, substantial progress has been made in delineating and better understanding substrate probe experiments, and these studies form the first main focus of this review. Another important line of experimental work that has also raised several issues is the measurement of kinetic isotope effects. Only recently has it been possible to delineate substrate binding and activation steps, each of which is subject to an isotope effect. The results of these experiments comprise the second major section of this review.

In the past few years, computational models of the active site of the MMOH have provided significant insight into the mechanism of catalysis. Theoretical studies provide a precise molecular-level picture of intermediate and transition-state structures, their energies, and electronic details of the mechanism. Although all prominent models are based upon density functional theory (DFT)[101,102] and common features can be identified, significant differences exist among proposals from different workers reflecting diverse model construction and validation philosophies. The level and nature of chemical interpretation schemes is similarly diverse. In this review we attempt to interpret, in addition to summarizing, the mechanistic proposals that exist in the recent literature. As is the case in experimental work, the choice of theoretical framework introduces some bias, and certain approximations tend to predetermine the final result. The electronically complicated magnetic behavior and characteristic structural features of the diiron core in MMOH have given rise to a number of theoretical models that propose very different mechanisms for steps in the catalytic cycle. Even when key features of two proposals resemble each other on first sight, significant differences are revealed upon more detailed inspection. To understand the origin of these nontrivial differences, which have significant consequences, the underlying theoretical framework has to be considered. We therefore present a brief overview of the theoretical challenges and methods commonly used to overcome them. Our goal is to help the nonexpert learn how to evaluate conflicting claims without introducing bias toward any single approach.

2. Probe Studies of the Alkane Hydroxylation by sMMO

2.1. General Remarks on Mechanistic Probes

Mechanistic probe studies of enzyme-catalyzed oxidation reactions have been applied with increasing frequency. In this method of investigation, one employs substrates that, if processed via a specific intermediate, will result in rearranged products. Probe studies can be used in a qualitative manner to implicate an intermediate, or, if the rate constant for the rearrangement reaction is known, they can be applied to "time" the reaction of the transient. A variety of transformations could be employed, but racemization and epimerization reactions and ring openings of cyclopropane-containing compounds have been most commonly used.

Racemization and epimerization reactions at sp^3-hybridized carbon centers will be very fast for both cationic and radical intermediates. These processes involve inversions at the radical or cation center or rotations that have essentially no activation energy for C−C single bonds between an sp^3-hybridized carbon and an sp^2-hybridized carbon. The barrier for rotation in the ethyl radical, for example, is quite small, on the order of 50 cal/mol,[103] and the rotation has a rate constant on the order of 5×10^{12} s^{-1} at ambient temperature. Radical and cationic centers are planar or nearly planar in most cases, and radical or cation intermediates will lose stereochemical information at the site that is functionalized if the lifetime is adequate.

Substituted cyclopropane probes (Scheme 2) provide no "timing" aspects for cationic intermediates

Scheme 2

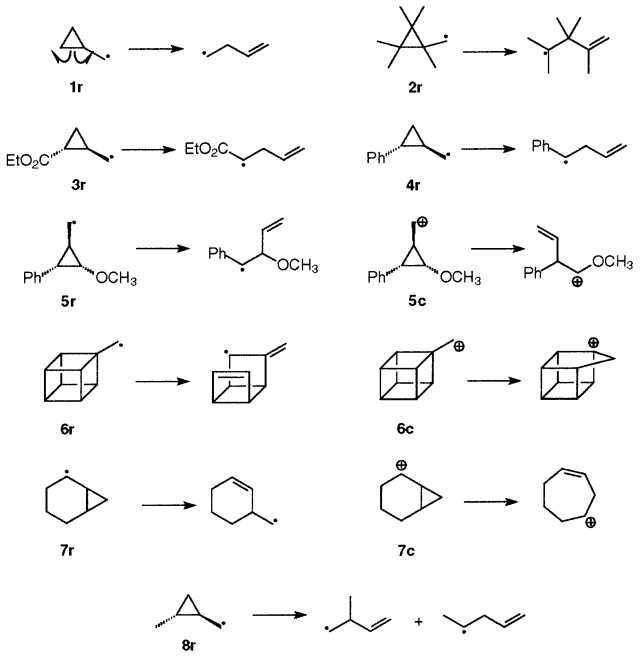

other than an assumption that processes have no barriers. Cyclopropane probes, however, give access to a wide window for timing of radical intermediates. Ring opening of the parent of the series, the cyclopropylcarbinyl radical (**1r**), occurs with a rate constant of 7×10^7 s^{-1} at ambient temperature.[104] Incorporating additional methyl groups on the ring increases strain, with a corresponding increase in the rate constant for ring opening. Ultimately, the permethylated system, the (1,2,2,3,3-pentamethylcyclopropyl)methyl radical (**2r**), has a rate constant for ring opening of 3×10^9 s^{-1} at ambient temperature.[105] The rates of ring openings of cyclopropylcarbinyl radicals are more strongly accelerated by incorporation of groups that stabilize the incipient radical product. The ester-substituted radical **3r** has a ring-opening rate constant of 7×10^{10} s^{-1}.[106] Aryl substitution at the incipient radical center strongly accelerates the ring-opening reaction; radical **4r** opens with a rate constant of 3×10^{11} s^{-1}.[107]

There is an important caution in the use of mechanistic probes. Often one is interested in identifying either a radical or cationic species, but many probe substrates will ultimately give the same rearrangement product if converted to a radical or cationic intermediate. Thus, racemizations of chiral substrates do not provide information about the character of an intermediate, nor do ring openings of most cyclopropane-based probes. A few probes will distinguish between radicals and cations, however. These include the cyclopropane probes that contain an aryl group on one position of the ring to bias a radical rearrangement and an alkoxy group on another position of the ring to bias a cationic rearrangement. An example is probe **5**, which opens to the benzylic radical from radical **5r** but to the oxonium ion from the incipient cationic species **5c**.[108,109] Methylcubane (**6**) provides differentiation between cations and radicals because the cubylmethyl radical (**6r**) ring-opens by bond cleavage,[110,111] whereas an incipient cubylmethyl cation (**6c**) ring-expands to the homocubyl system.[112] Unfortunately, radical-derived products from methylcubane ring openings are not expected to be stable.[110]

In principle, some simple cyclopropanes can be employed to differentiate between radicals and cations, but these are difficult to use in practice because the radical rearrangement reactions are relatively slow and the cationic reaction manifolds are highly biased toward cyclic products. Norcarane (**7**) can provide a differentiation between the two reactive intermediates in principle because radical **7r** ring-opens predominantly to the (2-cyclohexenyl)methyl radical,[113] whereas ring expansion of the 2-norcaranyl cation (**7c**) occurs.[114] One might also use the product distributions of unsymmetrical polymethylcyclopropanes to differentiate between the intermediates. For example, the (*trans*-2-methylcyclopropyl)-methyl radical (**8r**) ring-opens to the primary and secondary alkyl radical products with a partitioning ratio that is nearly 1:1,[105] and the observation of only one of the two possible alcohol products from oxidation of *trans*-1,2-dimethylcyclopropane would suggest that a radical intermediate *was not* formed in the reaction.

2.2. Evidence for Cationic Intermediates

The possibility that cationic intermediates of some type are produced in sMMO hydroxylations was suggested in an early mechanistic study of *Ms. trichosporium* OB3b.[115] 1,1-Dimethylcyclopropane was hydroxylated to give the unrearranged alcohol 1-methylcyclopropylmethanol, the cationic rearrangement product 1-methylcyclobutanol, and the radical rearrangement product 3-methyl-3-buten-1-ol (Scheme 3).

Scheme 3

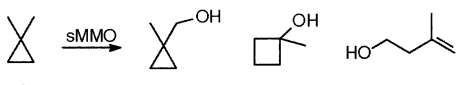

9

The products were formed smoothly in time-course studies over 10 min, and the average ratio of products was 81:13:6 (unrearranged:cationic:radical). The unrearranged alcohol isomerized to the cyclobutanol product when incubated under the enzymatic oxygenation conditions, but this reaction was "slower" than the oxidation reaction. Furthermore, labeling studies with $^{18}O_2$ and with $H_2{}^{18}O$ resulted in partial label incorporation into the cyclobutanol, suggesting that a cationic species was formed as an intermediate in the enzyme-catalyzed reaction, which subsequently reacted with the labeled water.[115]

Further evidence for production of cationic species in sMMO hydroxylations was not provided for nearly a decade, until two probes that could differentiate between cations and radicals, methylcubane (**6**) and the "phenyl-methoxy"cyclopropane probe **5**, were studied. An early study of methylcubane oxidation by the sMMO from *Mc. capsulatus* (Bath) did not find rearranged products.[116] A report of methylcubane oxidation by the sMMO from *Ms. trichosporium* OB3b concluded, however, that a radical-derived rearrangement product was obtained on the basis of analysis of the mass spectrum of a product.[117] A reinvestigation of methylcubane oxidation by sMMO enzymes from both *Mc. capsulatus* (Bath) and *Ms. trichosporium* OB3b found the same rearrangement product as in the preceding study, as determined by mass spectral fragmentation patterns, but the rearrangement product was identified as homocubanol by comparison to an authentic sample (Scheme 4).[118]

Scheme 4

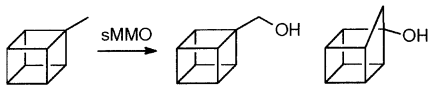

6

Homocubanol is the ring-expanded alcohol that would be produced by trapping the homocubyl cation with water, and there is no evidence that a ring enlargement reaction occurs to any measurable extent in the reaction of the cubylmethyl radical (**6r**).[110] Thus, the methylcubane results implicate a cationic pathway but provide no evidence for a radical intermediate.

In recent experiments, cationic rearrangement products were found in small amounts from hydroxylation of probe **5** by the sMMO from *Mc. capsulatus* (Bath),[118] and from oxidation of norcarane (**7**) by the sMMO enzymes from both *Ms. trichosporium* OB3b[119] and *Mc. capsulatus* (Bath).[132] Thus, cation-derived products have been found in every mechanistic probe study where some rearrangement occurred and the substrate permitted differentiation between cationic and radical rearrangements. The amounts are small in all cases, however, which leads to concerns about minor reaction pathways or secondary reactions. Whereas there is now little dispute that cationic products are obtained in sMMO hydroxylations, there is not a consensus as to the mechanistic interpretation of these results.

2.3. Evidence for Radical Intermediates

In determining whether a radical intermediate is formed in a sMMO hydroxylation reaction, we set a minimum lifetime of the radical of several picoseconds. If the lifetime were shorter, then translation

of the species from the reactive iron−oxygen complex would not be possible, and any rearrangement would have to occur while the "radical" moiety is in intimate contact with these atoms. Such a situation would exist if a shallow energy minimum separated two transition states in the hydroxylation reaction. Because the reaction is committed to completion from the shallow energy well, the definition of a species in such a situation as an intermediate becomes a semantic point, but it clearly is not a "solvent-separated" pair nor equivalent to a diffusionally free intermediate. Some computational works have referred to such a species as a "bound radical".

Mechanistic probe studies searching for evidence of radical intermediates in sMMO oxidation reactions have been conducted for years, but, until recently, an implicit assumption of the studies was that any rearranged product should be ascribed to a radical intermediate. That is, there has been little effort to determine whether rearranged products actually came from radicals. Unfortunately, that view has been propagated into recent literature, where discussions of previous work that could not possibly provide information about the type of intermediates that gave rearranged products were presented in the context that they did provide such evidence. The situation now exists whereby conflicting conclusions about the demonstrations of radical intermediates are presented, even when the same studies are being discussed!

Many studies seeking evidence of radical intermediates in sMMO hydroxylations used probes that could not provide information about the type of intermediates. Because there is strong evidence that cationic species are formed in the hydroxylation reactions, *those results are vitiated* with regard to their ability to demonstrate that a radical intermediate was formed. The results are useful only for providing an *upper limit* on the lifetime of a possible radical intermediate. The general result with radical probes is that there is no conclusive evidence for a radical intermediate with a lifetime of ≥1 ps from studies of the sMMO systems from *Mc. capsulatus* (Bath) and *Ms. trichosporium* OB3b. A single exception to these results exists with studies of norcarane with both enzymes, which now represents the *only* evidence for radical intermediates in sMMO-catalyzed hydroxylation reactions. We discuss this substrate in greater detail below.

In a study patterned after one conducted with cytochrome P450 enzymes,[48] tetradeuterated cyclohexene **10** was hydroxylated by the sMMO from *Ms. trichosporium* OB3b with 20% allylic rearrangement to give product **12** (Scheme 5). The "allylic shift" product **12** was obtained in higher yield (33%) when the hydroxylation was catalyzed by cytochrome P450.[120] It was also reported[48] that hydroxylation of tetradeuterated norbornane **13** gave predominantly the endo alcohol **14** and exo alcohol **15** with retention of stereochemistry (Scheme 5). A small amount of epimerization occurred in the norbornane hydroxylations; ca. 2% of the "H" functionalized product was *exo*-nobornanol-d_4, and ca. 5% of the "D" functionalized product was *endo*-norbornanol-d_3. Again, larger

Scheme 5

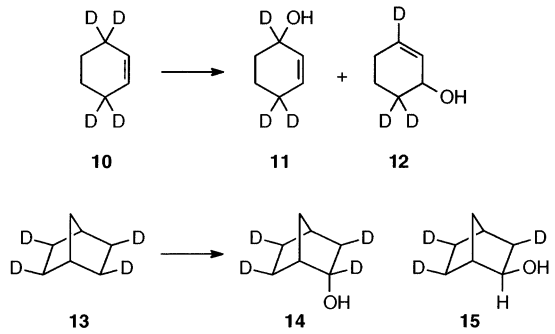

amounts of epimerization had been found when the same substrate was oxidized by cytochrome P450.[121]

Studies with the sMMO from *Mc. capsulatus* (Bath) found hydroxylation of *cis*- and *trans*-2-butene with no isomerization.[45] The rate constants for rotation of allyl and substituted allyl radicals are in the range from 100 to 1×10^5 s^{-1} at ambient temperature,[122] and these results exclude intermediates with lifetimes in the microsecond to millisecond range. Several isomerized products were found in the work, however (Scheme 6).[45] Stereochemical scrambling

Scheme 6

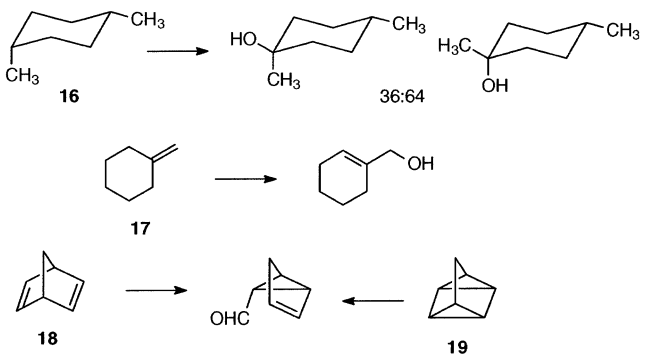

was observed with *cis*-1,4-dimethylcyclohexane (**16**), allylic shifts occurred as shown in the hydroxylation of methylenecyclohexane (**17**), and norbornadiene (**18**) and quadracyclane (**19**) were oxidized to a common carbonyl-containing product assumed to be the aldehyde shown in the figure by analogy to the product isolated in a related cytochrome P450 study.[123]

The detection of rearrangement products in the above studies was taken as evidence that the reaction proceeded by hydrogen abstraction to give a radical intermediate,[48,124] which was the consensus mechanism for hydroxylation by cytochrome P450 enzymes at the time of the study. In fact, the rearrangements do not implicate species with lifetimes adequate for intermediates. If an allylic radical or cationic intermediate were formed from cyclohexene, then nearly complete randomization would occur, biased only by a secondary kinetic isotope effect (KIE) in the trapping of the intermediate. No electrons "shift" in an allylic radical, and the high degree of retention requires that the "intermediate" had a subpicosecond lifetime. In a similar manner, if norbornane were converted to the norbornyl radical, then the position of functionalization should have been randomized. The norbornyl radical should be planar or nearly so,

and the same mixture of *exo*- and *endo*-2-norbornanols would be found from trapping this radical if it had been formed as an intermediate from abstraction at either the endo or exo face. The low level of epimerization found requires that the norbornyl moiety did not have adequate time to rotate in the course of the reaction, which again places the lifetime in the subpicosecond range. Such a lifetime is too short for an intermediate and would be consistent with a small minimum well on the reaction surface.

A number of simple cyclopropane probes and aryl-substituted cyclopropane probes were oxidized in mechanistic studies of *Mc. capsulatus* (Bath) without the detection of rearranged alcohol products. In one such study,[125] only cyclopropylmethanol was detected from oxidation of methylcyclopropane. Scheme 7 shows probes that gave no rearrangement products and the deduced limits of the lifetimes of a transient radical if it were formed in the oxidation reaction.[126,127] The limits on the radical lifetime decrease as the rate constants for the radical fragmentation reactions increase, reflecting conservative assumptions that the detection limits for rearranged products were 1% (or even 10%) of the total of oxidized products. A small amount of radical-derived rearrangement product appeared in the product mixture from oxidation of probe **5**, although the compound was not a good substrate.[118] From the ratio of radical-derived oxidation product to other products, a radical lifetime of 0.1−0.2 ps was deduced.

Scheme 7. Radical Lifetime Limits from Mechanistic Studies of the sMMO of *Mc. capsulatus* (Bath)

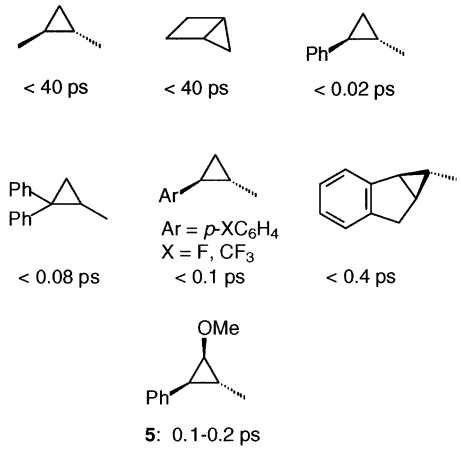

Mechanistic studies of hydroxylations of cyclopropane probes catalyzed by the sMMO from *Ms. trichosporium* OB3b have afforded small amounts of rearranged products that might derive from radicals or cationic species. The formation of ring-opened rearrangement product in the oxidation of 1,1-dimethylcyclopropane by this enzyme was noted previously.[115] The assumption made[115] was that the ring-opened product derives from a radical intermediate, but there is no evidence that such was the case. Note that the cyclobutane product from a cationic rearrangement was also detected in this work. If a radical were involved, its lifetime would be on the order of 1 ns.

Oxidation of *trans*-2-phenylmethylcyclopropane (**4**)[126] at 30 °C affords 3−5% rearranged product alcohol relative to unrearranged alcohol; this result indicates a lifetime ($\tau = 1/k$) in the range of 0.11−0.16 ps if a radical were involved in the reaction. In this study, reductase and component B enzymes from *Mc. capsulatus* (Bath) were mixed with the *Ms. trichosporium* OB3b hydroxylase enzyme. Subsequently, the oxidation of **4** was repeated with all protein components from *Ms. trichosporium* OB3b.[128] No detectable amount of rearranged product from **4** was observed, and an upper limit on the radical lifetime was set as $\tau < 0.03$ ps.

Simple cyclopropane probes were also examined in this latter study with the sMMO from *Ms. trichosporium* OB3b.[128] Oxidation of both *cis*- and *trans*-1,2-dimethylcyclopropane resulted in no detectable rearranged product, and the authors set limits of the radical lifetime of $\tau < 8$ ps and < 34 ps, respectively, for the two probes. Oxidation of 1,1,2,2-tetramethylcyclopropane (**20**) (Scheme 8) was reported to give unrearranged alcohol **21** and a small amount of ring-opened product **22**; at 45 °C, the ratio of **21**:**22** was 22:1. From these results it was concluded that the formation of product **22** demonstrated that a radical intermediate was formed with a lifetime of $\tau = 30$ ps,[128] but there is no obvious reason to exclude a cationic intermediate as the source of this product. Probe **20** does provide an opportunity to implicate a radical intermediate because the radical derived from **20** partitions to give both the primary and tertiary ring-opened product radicals in a 1:10 ratio.[105] Thus, the detection of product **23** at about 10% of the amount of product **22** would have provided an indication that a radical intermediate had formed, whereas the absence of **23** would be an indication that **22** did not arise from a radical reaction. Unfortunately, the oxidation products were not completely characterized; the authors stated that they did not have an authentic sample of **23** for comparison to the products they detected by GC.[128]

Scheme 8

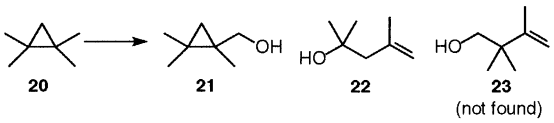

The oxidation of methylcubane (**6**) by the sMMO from *Ms. trichosporium* OB3b was reported[117] to give a rearrangement product that was thought to arise from a radical intermediate. The product was later demonstrated[118] to be homocubanol by comparison to an authentic sample. Ring expansion of the cubylmethyl radical to the homocubyl radical does not occur.[110] As a consequence, the formation of homocubanol provides evidence that a cationic species was formed but no support for formation of a radical intermediate. After the misidentification of homocubanol was corrected in the literature, the results were again presented as evidence for a radical intermediate with the statement that "radical species may be generated prior to the cation".[128] The argument[128] apparently is that it is possible that the cubylmethyl

radical was formed and then very rapidly (because radical rearrangement to cube-ruptured products has a rate constant of 3×10^{10} s^{-1})[111] was oxidized to the cubylmethyl cation, which in turn rearranged to the homocubyl cation.

2.4. Norcarane—A Unique Result

Mechanistic studies with norcarane (**7**) have provided unique results that deserve special attention. As noted earlier, norcarane has the potential to provide information concerning whether a radical or cationic species was involved in a rearrangement. It was first used as a probe in an enzyme-catalyzed hydroxylation reaction[129] by cytochrome P450, in which no rearranged products were detected. Later, it was applied in a study of the alkane hydroxylase enzyme from *Pseudomonas oleovorans*,[130] where substantial amounts of radical-derived ring-opening products were obtained. The alkane hydroxylase enzyme is a diiron species that might be similar to sMMO, but the products observed following hydroxylations of probe substrates by the two enzymes are quite different. A high yield of radical-derived rearrangement product from norcarane was found with this enzyme,[130] whereas only a small amount of rearranged products formed in sMMO-catalyzed hydroxylations (vide infra). In addition, when *trans*-2-phenylmethylcyclopropane was oxidized with this enzyme, ring-opened products were exclusively formed,[131] but little or no rearrangement products occur when this probe is hydroxylated with sMMO enzymes.[126,128]

Norcarane was recently investigated in mechanistic studies of the sMMO enzymes from *Ms. trichosporium* OB3b[119] and *Mc. capsulatus* (Bath)[132] with similar results. The major products by far were the isomers of 2-norcaranol. In addition, small amounts of 3-norcaranols, 2- and 3-norcaranones, the radical-derived rearrangement product (2-cyclohexenyl)-methanol, and the cation-derived rearrangement product 3-cycloheptenol were obtained. The yields of radical-derived rearrangement product relative to the total amounts of product from oxidation of the C(2) position of norcarane were 1−3%.[119,132] The 2-norcaranyl radical ring-opens with a rate constant $k \approx 2 \times 10^8$ s^{-1},[130] which gives a rate constant for the trapping reaction of $(0.6-2) \times 10^{10}$ s^{-1}. That is, the radical lifetime would be $\tau = 50-150$ ps. Although this is a short lifetime, it is much greater than that indicated by other mechanistic probe studies and would require a short-lived radical intermediate in the oxidation reaction.

The interpretation of the norcarane results differs for the two groups that performed the studies. Brazeau et al.[119] concluded that the results demonstrated that a radical intermediate was involved in the hydroxylation reaction. Newcomb et al.[132] concluded that a radical was indicated but that the results were so unique that one should not generalize them for the hydroxylation mechanism. One concern is that very small amounts of radical-derived product were obtained not only with the sMMO enzymes but also for oxidation of norcarane with several cytochrome P450 enzymes.[132,133] For reactions where absolute yields are reported, the relative percentages of the radical-derived product varied; nevertheless, the absolute yields were consistently in the range of 1 nmol of product when ca. 0.5 nmol of cytochrome P450 or 10 nmol of sMMO enzymes was used.[132]

2.5. Reactions with a Chiral Alkane Substrate

One issue to be considered is that the diagnostic probes used in the above-described studies might not be representative of the natural substrate methane and therefore give rise to mechanistic information that is not applicable to the hydroxylation of simple alkanes. An elegant method for improving this situation is the use of isotopomers of the natural substrates. Here, a chiral carbon center is prepared by using both deuterium and tritium substitution at the terminal carbon atom of ethane or longer chain alkane.[134,135] The product distribution of the resulting chiral alkane substrates, such as (*S*)- or (*R*)-[1-^{2}H,1-^{3}H]-ethane, reports on the course of the reaction by evolving alcohols that reflect the nature of intermediates that might form upon oxidation by the MMOs. The amounts of retention in the product alcohols are determined by ^{3}H NMR spectroscopy of diastereomeric derivatives. Figure 3 illustrates the use of

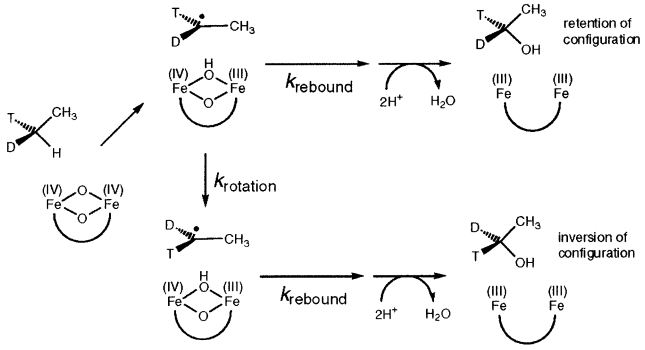

Figure 3. Oxidation of (*S*)-[1-^{2}H,1-^{3}H]-ethane, assuming formation of a substrate radical intermediate. Depending on the lifetime of the intermediate, retention or inversion of configuration at the chiral carbon center is expected. (Adapted from ref 134.)

chiral ethane as a reporter for probing a putative H-atom abstraction mechanism for reaction of an alkane with intermediate **Q** of MMOH. After the formal abstraction of a hydrogen atom from the chiral substrate, an alkyl radical might be formed that can recoil and then rebound to form the alcohol product. If the lifetime of the radical intermediate with a planar sp^2-carbon center is appreciably longer than the time needed for rotation around the C−C axis in the ethyl radical, complete loss of stereochemistry is expected and the product alcohols will be a racemic mixture. Alternatively, the reaction might proceed in a concerted manner (not shown), without any radical character. Between these two extremes are reaction pathways that allow for both concerted and radical-like character, the nature of which is best interpreted with the aid of computational chemistry. Studies using sMMO from *Mc. capsulatus* (Bath)[134] and *Ms. trichosporium* OB3b[135] fall into this latter category. Both systems gave essentially the same result when used to convert chiral ethane and butane into their

corresponding alcohols. A 70:30 retention:inversion ratio was observed, a peculiar result that could not simply be explained with either a simple radical recoil−rebound or concerted mechanism alone. From the known lifetime of the ethyl radical,[103] however, one could exclude the participation of a radical intermediate, as defined above. These results are discussed further in the section on computational model studies. By comparison, the hydroxylation of chiral ethane by pMMO using the same technique[136] gave 100% retention of configuration, establishing a concerted reaction pathway for that enzyme.

3. Kinetic Isotope Effects

Studies of isotope effects in MMO oxidations have resulted in some of the more confusing experimental results, which have been compounded by erroneous mechanistic interpretations in some cases. A kinetic isotope effect (KIE) for a reaction is a measure of the ratio of rates of reactions of isotopomers. Usually, hydrogen and deuterium reactions are compared because the difference in the zero-point vibrational levels for a C−H and C−D bond is large and deuterated isotopomers are relatively easy to prepare. Primary KIEs are determined for reactions at the site of isotopic substitution, and secondary KIEs are determined for reactions at other positions.

The origin of the KIE is the change in bonding between the ground state of the molecule and the transition state. In the classical model, the maximum primary H/D KIE would be obtained when the transition state is symmetrical, such that a C−H bond-stretching mode is lost in the transition state. Because the zero-point energy of a C−H bond is greater than that of a C−D bond, the loss of the vibrational mode in the transition state will result in a difference in activation energies for the H/D pair, with a higher barrier for the deuterated substrate. At ambient temperature the maximum difference in rates would give $k_H/k_D \approx 7$. It is important to emphasize that the maximum effect would be found when the bond is partially broken in the transition state. In some reports of KIEs in MMO hydroxylations, the authors have stated that the maximum effect would result when a C−H bond is fully broken, which is not correct.

Bond bending modes are lower in energy than stretches, and loss of a bending mode in the transition state would give a smaller KIE in the classical model.[137] Secondary KIEs are much smaller than primary KIEs because they reflect changes in the character of a bond that is not in the act of breaking. For example, a secondary KIE would result from the change in the bond strength as an sp^3-hybridized C−H bond changes to an sp^2-hybridized bond in the transition state. Whereas primary H/D KIEs are greater than 1, secondary H/D KIEs can be normal ($k_H/k_D > 1$) or inverse ($k_H/k_D < 1$).

The classical model for KIEs seemingly served organic chemists well, but high-level computational work shows that the model is much too simplified. Stretching and bending modes are not isolated from one another, nor are they mixed to the same extent in ground and transition states. One result of mode mixing is that the value of the KIE does not indicate the angle defined by the breaking X−H and forming H−Y bonds as assumed in the classical model. Moreover, in the case of H/D KIEs, tunneling effects add another complication. Tunneling rates are temperature independent but reflect the mass of the tunneling species. In practical terms, if the reaction is conducted at a temperature where H-atom tunneling is an important contributor to the overall rate, then D-atom tunneling might not occur to an appreciable extent, and the observed k_H/k_D could be very large.

An example illustrates the serious problem one encounters with the simple classical model. A linear abstraction of a hydrogen atom in the rate-limiting step of methane oxidation might be expected to have a large KIE from the classical model, whereas a four-center transition state for reaction of Fe−O with C−H should have a KIE no larger than 2.[137] Yoshizawa[138] addressed isotope effects expected for various reaction pathways for MMO and cytochrome P450 enzymes. For an sMMO model reacting with methane at ambient temperature, H/D KIEs for four-center transition states were computed to be 8.6 (singlet reaction surface) and 9.2 (triplet reaction surface). The computed KIE for a linear hydrogen atom abstraction reaction in the singlet state was 10.6. If tunneling corrections derived using the Wigner function are included, these values change to 13.1, 14.3, and 13.0, respectively. In light of these computational results demonstrating that essentially the same KIE can be obtained for both the four-center and the linear transition states, the observation of a KIE of $k_H/k_D \approx 2$ for oxidation of methane and methane-d_4, which is the KIE value found in k_{cat}, is rather meaningless with regard to the details of the mechanism of the oxidation reaction.

The inadequacy of the classical description for KIEs has important ramifications. The KIE for a specific reaction pathway cannot be predicted from assumptions. As a corollary, a mechanistic description cannot be formulated from an observed KIE without the aid of robust computational results. These features have not been well appreciated in the past, and this failure has led to unjustified conclusions regarding mechanisms. It has commonly been assumed that a large H/D KIE requires that the C−H−O angle in the transition state of a hydroxylation reaction is 180°. Similarly, the assumption has been made that, if the H/D KIE for an enzyme-catalyzed hydroxylation is similar in magnitude to that involving, for example, H-atom abstraction by an alkoxyl radical, a hydrogen atom was abstracted in the enzyme reaction. Perhaps more disturbing for studies of enzyme-catalyzed hydroxylation reactions has been the assumption, often implicit, that the observation of any H/D KIE requires that a hydrogen atom abstraction reaction occurred to give a radical intermediate. Although it is correct that an abstraction reaction should demonstrate an H/D KIE, it would be difficult to conceive of any type of C−H functionalization mechanism that should not have a KIE.

Kinetic studies of enzyme-catalyzed reactions are complicated because multiple reactions are involved in the processes, and this feature adds an additional

layer of complexity to KIE studies. Enzyme kinetics are described in terms of the rate constant for the catalytic reaction (k_{cat}) and the rate constants for other processes, which can include substrate binding, conformational changes, and product release that are often not separated but treated as a composite observable, the Michaelis constant K_M. The kinetics of the enzyme-catalyzed reaction are described by the formalism of a prior equilibration followed by a rate-limiting reaction according to eq 2, where V_{max} is the

$$V_{obs} = (V_{max}[Sub])/([Sub] + K_M) \quad (2)$$

maximum velocity of the reaction under saturation conditions and [Sub] is the concentration of substrate. Note that $V_{max} = [E]_0 k_{cat}$, where $[E]_0$ is the initial enzyme concentration. The Michaelis constant K_M is a kinetic parameter, and KIEs in enzyme-catalyzed reactions can occur in the K_M term, the k_{cat} term, or both. When a single concentration of substrate is studied, one cannot separate the possible KIEs, and the most reliable results are obtained when Michaelis−Menten studies are performed. Such studies involve determining the velocity of the reaction for a range of substrate concentrations.

Either intermolecular or intramolecular KIEs can be determined, and the two will not necessarily give the same value. An intermolecular KIE study involves the use of, for example, a nondeuterated substrate RCH_3 and a deuterated substrate RCD_3 in independent experiments. The most secure KIE values are found when one determines both K_M and V_{max} for each substrate. The data are most readily interpreted when the KIE in K_M is unity. Note that the KIE found in k_{cat} in this example of an intermolecular study would actually be a primary KIE multiplied by two secondary KIEs because funtionalization of a C−D position in RCD_3 leaves two deuterium atoms at the functionalized position.

An intramolecular KIE study is performed with a partially deuterated substrate; for example, hydroxylation of $RCHD_2$ to give RCHDOH and RCD_2OH might be studied. Because the competition is at one site in the substrate, the K_M value is not important as long as the methyl group freely rotates to provide access to both the D and H positions. Furthermore, the measured KIE is an intrinsic KIE because it cannot be masked (vide infra). In this example of an intramolecular KIE study, the observed KIE after statistical correction for the number of reactive atoms is actually a primary KIE divided by a secondary KIE, because functionalization of an "H" position leaves one more "D" atom in the product than does functionalization of a "D" position.

Intermolecular KIEs observed in enzyme-catalyzed reactions can be further complicated by masking effects.[139] This phenomenon occurs when substrate binding is irreversible, and no alternative reaction pathways exist after binding. For example, in the MMO hydroxylation reaction by intermediate **Q**, an observed H/D KIE of unity could be found due to masking, even if the rates of oxidation of RCH_3 and RCD_3 by **Q** were different. The necessary conditions for complete masking are that (1) substrate binding is fast, not sensitive to isotopic substitution, and irreversible, (2) no alternative reaction for intermediate **Q** exists, and (3) product release is not isotope sensitive. The masking effect can be partially or completely unmasked if there is an alternative reaction channel for **Q** that competes with the substrate hydroxylation reaction.

3.1. KIE in Methane Oxidations

In early isotope effect studies of oxidations of methane, large KIEs were found, typically in single-concentration experiments. Rates of reactions of methane and methane-d_4 were determined by competition or by comparing the rates of reactions of single-substrate experiments. Oxidations by cells of *Methylomonus rubrum* indicated that the rate of CH_4 oxidation was 12.5 times faster than the rate of oxidation of CD_4.[140] A similarly large KIE (k_H/k_D = 11.8) was reported for oxidation of CH_4 and CD_4 by purified sMMO from *Mc. capsulatus* (Bath).[45] These studies provided no method for determining if the KIE was in the K_M term, the V_{max} term, or both.

Subsequently,[48] oxidations of CH_4 and CD_4 were investigated in Michaelis−Menten studies. A large intermolecular KIE was determined for oxidation by sMMO from *Ms. trichosporium* OB3b, but the origin of the measured KIE was a combination of a small KIE in V_{max} and a large KIE in K_M (Table 1). Thus, the KIE in the k_{cat} terms (equal to the KIE in the V_{max} terms) was $k_H/k_D = 1.7$.[48] Similarly, a small KIE in k_{cat} and large KIE in K_M were found when the same enzyme was studied at 4 °C.[141] In the case of sMMO from *Mc. capsulatus* (Bath) studied by a different group,[142] the KIE in K_M for methane and methane-d_4 oxidation was nearly unity, and the KIE in k_{cat} was small and similar in value to that found with the *Ms. trichosporium* OB3b enzyme. On the basis of this study, one would expect that the single-concentration study of the sMMO from *Mc. capsulatus* (Bath) reported earlier[45] should have found a KIE for methane oxidation of about 2. The small KIEs in the k_{cat} terms for methane deserve special note because, owing to the intermolecular design of the studies, the measured KIEs in these terms result from a primary KIE times three secondary KIEs, and the implication is that the primary KIE in k_{cat} for functionalization of methane is quite small.

Intramolecular KIEs in oxidations of partially deuterated methane give intrinsic KIEs in k_{cat} that are independent of a KIE in K_M because a single substrate is studied. Experimental values are listed in Table 1. As previously noted, intramolecular KIE values should not be the same as those found in an intermolecular KIE study. This difference can be used to separate primary and secondary KIEs, as discussed below.

Nesheim and Lipscomb[141] reported both intermolecular and intramolecular KIEs for oxidations by the sMMO from *Ms. trichosporium* OB3b conducted at 4 °C. However, the results for the intramolecular KIEs appear to be internally inconsistent. Specifically, the statistically corrected intramolecular KIEs for CH_3D, CH_2D_2, and CHD_3 should be the same, in each case equal to a primary KIE divided by a secondary KIE, but they are reported to be 12, 9.3, and 4, respec-

Table 1. Kinetic Isotope Effects in sMMO Oxidations of Deuterated Substrates

Intermoleculear

substrate	enzyme[a]	temp (°C)	K^H_M/K^D_M	V^H_{max}/V^D_{max}	$(V/K)_H/(V/K)_D$	ref
CH_4/CD_4	OB3b	30	0.20	1.7	8.4	48
	OB3b	4	0.065 ± 0.011	1.7 ± 0.2	26 ± 5	141
	OB3b	4			19 ± 4	141[b]
	Bath	45	0.88 ± 0.12	1.75 ± 0.10	2.0 ± 0.3	142

Intramoleculear

substrate	enzyme[a]	temp (°C)	k_H/k_D	BDE[c]	ref
CH_3D	OB3b	4	12 ± 1	105	141[d]
CH_2D_2	OB3b	4	9.3 ± 0.5		141[d]
CHD_3	OB3b	4	3.9 ± 1		141[d]
CH_2D_2	Bath	45	1.29 ± 0.07	105	142
CH_3CHDT	OB3b	30	4.2 ± 0.2	101	135
CH_3CHDT	Bath	45	3.4 ± 0.4	101	134
$CH_3(CH_2)_2CHDT$	Bath	45	2.2 ± 0.4	101	134
CH_3CHDT	pMMO	45	5.2 ± 0.4	101	136
CD_3CHDT	pMMO	45	5.5 ± 0.7	101	136
Ph-*c*-$C_3H_4CH_2D$	Bath	45	5.1	98	126[e]

[a] OB3b, sMMO from *Ms. trichosporium* OB3b; Bath, *Mc. capsulatus* (Bath); pMMO, MMO in particulate form. [b] Results from competition between equal amounts of methane and methane-d_4. [c] Bond dissociation energies are enthalpies for the C−H homolysis reaction at 298 K (ΔH_{298}), from refs 245 and 246. [d] Values are those given in the original report;[141] in principle, the values should be identical, and they should be smaller than the intermolecular KIE of 1.7 if the secondary KIE is normal (see text). [e] The value listed is the average value from oxidation of the mono- and dideuterated substrates.

tively.[141] Moreover, the intramolecular KIEs (equal to a primary KIE multiplied by one or more secondary KIEs) should be *smaller* than the intermolecular KIE in V_{max} (equal to a primary KIE multiplied by one or more secondary KIEs), which was found to be 1.7. We list the published values in Table 1, but we would caution that the internal inconsistency of the values invites a reevaluation of the original data, which were not reported in the publication.[141]

The stereochemical studies with chiral alkanes discussed in section 2.5 also provided intramolecular KIEs. In these experiments, chiral ethane and chiral butane, each chiral by virtue of isotopic substitution on one methyl group with deuterium and tritium, were oxidized by MMOs, and the amounts of retention in the product alcohols were determined by ^{3}H NMR spectroscopy of diastereomeric derivatives. In the ^{3}H NMR spectrum, one can differentiate between RCH_2CDTOR^* and RCH_2CHTOR^*, which permits a calculation of the intramolecular KIE. It is noteworthy that, in principle, one also can determine the secondary KIE at the chiral atom by comparing the amount of oxidation at each terminal carbon (vide infra). Intramolecular KIEs for oxidation of chiral ethane by sMMO from *Ms. trichosporium* OB3b[135] and both the sMMO[134] and pMMO[136] from *Mc. capsulatus* (Bath) have been reported. The oxidation of chiral butane by sMMO from *Mc. capsulatus* (Bath)[134] also was studied. In addition, intramolecular KIEs for hydroxylation of *trans*-2-phenylmethylcyclopropane by the sMMO from *Mc. capsulatus* (Bath) have been reported.[126]

The KIE values permit some general conclusions about the nature of the functionalization reaction. The k_H/k_D values for sMMO (Bath)-catalyzed hydroxylations show an increase that correlates inversely with the bond energy of the C−H bond undergoing functionalization. The increasing KIE suggests an increasing amount of bond-breaking in the transition states as the C−H BDE of the substrate decreases. This result indicates that the isotopically sensitive step is exergonic, as one might expect for the actual oxidation reaction. The same conclusion would be reached regarding the sMMO extracted from *Ms. trichosporium* OB3b if the intermolecular KIE in V_{max} for methane were compared to the intramolecular KIE from ethane; our reservations concerning the intramolecular KIEs reported for methane oxidation by sMMO extracted from *Ms. trichosporium* OB3b were noted above.

KIEs determined in internal competition experiments are listed in Table 2. This type of study is performed with a substrate that can be oxidized at more than one position, such as toluene, which can be functionalized by sMMO to give benzyl alcohol or *p*-cresol. Oxidations are performed on unlabeled substrate and substrate with one position isotopically labeled. If the multiple positions of the substrate have free access to the active site and if there is no secondary KIE on the functionalization of the reference position, then the ratio of products from the unlabeled substrate divided by the ratio of products from the labeled substrate gives the KIE at the labeled position. The phenomenon of increased oxidation at a second position when the first position is isotopically labeled with deuterium is called "meta-

Table 2. Results of Internal Competition Kinetic Isotope Effect Studies

substrate	enzyme[a]	temp (°C)	k_H/k_D	ref
toluene[b]	Bath	45	11.6 ± 2.4	142
toluene[c]	Bath	45	8.4 ± 1.9	142
norbornane[d]	OB3b	30	≥5.5	48
substrate **4**[e]	Bath	45	1[f]	126

[a] OB3b, sMMO from *Ms. trichosporium* OB3b; Bath, *Mc. capsulatus* (Bath). [b] Toluene-d_0 and methyl-d_3. [c] Toluene-d_0 and -d_8. [d] Norbornane-*exo*-d_0 and *exo*-d_4. [e] *trans*-2-Phenylmethylcyclopropane-d_0 and methyl-d_3. [f] No metabolic switching; the partially deuterated substrate displays a KIE of 5.1; see Table 1.

bolic switching" [143] or "isotopically sensitive branching". The internal competition experiments provide intermolecular KIEs, but they can have the advantage of intramolecular KIE studies in that the KIE is only in k_{cat}.

The disadvantage of internal competition experiments is that the substrate might not tumble freely on the time scale of the oxidation reaction. In such a situation, when the multiple oxidizable positions do not have free access to the active site, a KIE of unity can be found. This property was apparent in a study of a sMMO oxidation of a cyclopropane probe, *trans*-2-phenylmethylcyclopropane; a KIE of unity was found for methyl group oxidations of Ph-*c*-$C_3H_4CH_3$ and Ph-*c*-$C_3H_4CD_3$, but oxidations of Ph-*c*-$C_3H_4CH_2D$ and Ph-*c*-$C_3H_4CHD_2$ gave, after statistical correction, intramolecular KIEs of 5.1.[126]

3.2 Primary and Secondary KIEs

In principle, observed intermolecular and intramolecular KIEs in k_{cat} can be used to give primary and secondary KIEs. The intermolecular KIE in k_{cat} for CH_4 and CD_4 is equal to a primary KIE (π) times three secondary KIEs (σ). If the values for σ for each D atom are equal, then one has $KIE_{inter} = \pi\sigma^3$. The intramolecular KIE, after correction for statistical effects, is $KIE_{intra} = \pi/\sigma$, again if secondary KIEs have equal values when more than one D is present. The intermolecular and intramolecular KIEs thus give two equations and two unknowns and can be solved to give π and σ.

Wilkins et al.[142] solved for π and σ for oxidation of methane by the sMMO of *Mc. capsulatus* (Bath) using the intermolecular KIEs in V_{max} determined in a Michaelis−Menten study and the intramolecular KIE from oxidation of CH_2D_2. They obtained $\sigma = 1.37 \pm 0.08$ and $\pi = 1.08 \pm 0.03$. In principle, a similar analysis of data for sMMO from *Ms. trichosporium* OB3b can be performed, but as noted above, the reported intramolecular KIEs are internally inconsistent.[141]

Secondary KIEs also can be deduced from the oxidations of chiral ethane and chiral butane by the sMMO from *Mc. capsulatus* (Bath) described above.[134] In the ^3H NMR spectrum of the diastereomeric derivatives, one can differentiate between RCH_2-CDTOR* and RCH_2CHTOR*, which permits a calculation of the intramolecular KIEs. In addition, the ratios of oxidation at the terminal methyl group compared to the labeled methyl group were available. For CH_3CHDT, the average ratio of oxidation at C2 to C1 was 3.35, and the average ratio of C4 to C1 oxidation of chiral butane was 3.55. The collected results indicate that a CH_3 group is oxidized 3.45 times as fast as a CHDT group. Correcting for the statistical advantage of three C−H bonds in the CH_3 group and for the fact that a portion of the C−D bonds in the CHDT group react, we compute that a C−H position on the CH_3 group is about 1.5 times as reactive as the C−H position on the labeled methyl group. Thus, the cumulative effect of the D and T atoms on the labeled group is to give a secondary KIE that is inverse, with $k_{HH}/k_{DT} = 0.7$.

The finding of a normal secondary KIE for methane oxidation and an inverse secondary KIE for ethane and butane oxidation might indicate a mechanistic difference for the reactions. We would caution, however, that the data are quite limited, and such a conclusion would require further investigation to confirm.

3.3. Other KIEs

Limited studies of heavy atom KIEs in MMO oxidations have been reported. Huang et al.[144] found $^{12}C/^{13}C$ KIEs of unity for oxidation of propane at C2 by both the sMMO and the pMMO from *Mc. capsulatus* (Bath). The conclusion from these results was that there was little structural change in the transition states for the propane hydroxylation reactions, consistent with a concerted mechanism for hydroxylation by both enzymes.[144]

Using sMMO from *Mc. capsulatus* (Bath), Stahl et al.[145] reported $^{16}O/^{18}O$ KIEs in reactions with acetonitrile. For this substrate, the hydroxylation reaction competes with an oxidase reaction (formation of water from dioxygen) that results from further reduction of the intermediate oxidant **Q**. Oxygen atom KIEs were 1.0167(10) and 1.0152(7) for the oxidase and hydroxylation of acetonitrile reactions, respectively. The identity in the KIEs indicates that the isotoptically sensitive step precedes the reaction with substrate. Furthermore, the magnitude of the KIE was not consistent with irreversible formation of a Michaelis complex between substrate and enzyme, nor was it consistent with rapid reversible binding of dioxygen. Alternatively, irreversible formation of a superoxide adduct is one mechanistic description that is consistent with the $^{16}O/^{18}O$ KIE values. The conclusions from this study have implications for other KIE studies; specifically, the reversible formation of the Michaelis complex indicates that a KIE in substrate binding is possible, and this will appear as a KIE in the K_M terms.

Solvent isotope effects in the reaction of the sMMO from *Ms. trichosporium* OB3b have been reported.[146] The solvent kinetic isotope effect in formation of intermediate **P** (or H_{peroxo}) at 5 °C was $k_H/k_D = 1.3 \pm 0.1$, and the solvent KIE in formation of intermediate **Q** was $k_H/k_D = 1.4 \pm 0.1$. In addition, proton inventory plots (plots of the change in rate with percentage of deuterium in the solvent) were linear, indicating that a single proton was delivered in the isotopically sensitive step. The results are consistent with concurrent formation of water and intermediate **Q**.

3.4. KIEs in Reactions with Intermediate Q

As illustrated in Scheme 1, the reactive intermediate **Q** accumulates in the reactions of sMMO enzymes from both *Ms. trichosporium* OB3b and *Mc. capsulatus* (Bath), permitting kinetic studies of its reactions with various substrates. In principle, such studies should provide straightforward results because one is following only a single reaction. In practice, the results of kinetic isotope effect studies of the reactions of **Q** have proved to be complicated.

KIE studies have been reported for reactions of **Q**, which can be prepared in the absence of substrate, from both sMMO enzymes (Table 3).[141,147−150] The

Table 3. Second-Order Rate Constants and KIEs for the Reaction of Intermediate Q with Derivatized Methane Substrates

substrate	enzyme[a]	$k_{obs} \times 10^{-2}$, M^{-1} s^{-1} [b]	k_2, s^{-1} [c]	KIE, k_H/k_D
CH_4	OB3b[148]	140 ± 6		42
CD_4	OB3b[148]	3.3 ± 0.2		
C_2H_6	OB3b[148]	140 ± 10		1
C_2D_6	OB3b[148]	150 ± 10		
C_3H_8	OB3b[148]	9.5 ± 0.2		1
C_3D_8	OB3b[148]	9.0 ± 0.3		
CH_4	Bath[150]	287 ± 9		23.1 ± 1.1
CD_4	Bath[150]	12.4 ± 0.5		
C_2H_6	Bath[150]	265 ± 11		1.00 ± 0.04
C_2D_6	Bath[150]	266 ± 3		
CH_3CN	Bath[150]		282 ± 10	46.4 ± 2.3
CD_3CN	Bath[150]		6.06 ± 0.14	
CH_3NO_2	Bath[150]		5.34 ± 0.02	8.1 ± 0.2
CD_3NO_2	Bath[150]		0.66 ± 0.02	
CH_3OH	Bath[150]	7.27 ± 0.06		1.01 ± 0.01
CD_3OH	Bath[150]	7.19 ± 0.04		

[a] OB3b, sMMO from *Ms. trichosporium* OB3b; Bath, *Mc. capsulatus* (Bath). [b] The k_{obs} values might be the products of an equilibrium constant times a rate constant; see the discussion of eq 5 in the text. [c] The k_2 values are first-order rate constants for reaction of the **Q**−substrate complex; see eq 3 and the discussion in the text.

unusual feature of the reactions of **Q** with methane and methane-d_4 is that the velocity of the reaction of **Q** with methane is much greater than that with CD_4. In one report,[141] the KIE in overall reaction rates of **Q** from *Ms. trichosporium* OB3b at 4 °C was stated to be in the range of 50−100. More recently, the same laboratory[148] reported a refined value for the KIE for CH_4/CD_4 reaction with **Q** at 4 °C of 42 (Table 3). Two reports by another group[149,150] gave similarly large KIEs of 23−28 (Table 3) for the methane reaction with **Q** from *Mc. capsulatus* (Bath).

The large overall KIEs for reaction of **Q** with methane have been interpreted as possibly arising from hydrogen atom tunneling in the C−H functionalization reaction, as confirmed partially by the computational study reported by Yoshizawa,[138] which predicted an increase of the KIEs by ∼5 when tunneling corrections are added. It is possible, however, that the KIEs in the methane oxidation step are smaller than the observed KIEs, and possibly similar in magnitude to the KIEs in k_{cat} for oxidations of methane and methane-d_4. Reactions of **Q** with nitromethane and acetonitrile clearly demonstrate saturation kinetic behavior, as shown in Figure 4.[150]

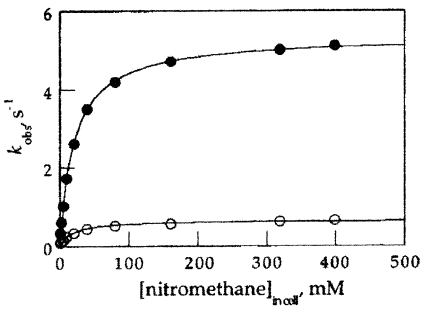

Figure 4. Plot of k_{obs} versus nitromethane concentration for the decay of **Q** at pH = 7 and 20 °C. Solid circles represent CH_3NO_2, and open circles represent CD_3NO_2. (Reprinted with permission from ref 150. Copyright 2002 American Chemical Society.)

Such kinetic results require that a fast equilibrium is established between substrate and enzyme prior to the reaction of **Q** (eq 3). The kinetic description for the observed rate constant (k_{obs}) for reaction of **Q** under these conditions is given by eq 4. When the concentration of substrate S is small and/or the equilibrium binding constant is small, the observed rate constant simplifies to eq 5, and a plot of k_{obs} versus substrate concentration will appear to be linear.

$$Q + S \overset{K_{bind}}{\rightleftharpoons} QS \xrightarrow{k_2} \text{product} \quad (3)$$

$$k_{obs} = K_{bind}k_2[S]/(1 + K_{bind}[S]) \quad (4)$$

$$k_{obs} = K_{bind}k_2[S] \quad (5)$$

Only low concentrations of methane in water (<1 mM) can be achieved. It is possible, therefore, that the observed rate constants for reactions of methane with **Q** are actually the products of the binding equilibrium constant and the rate constant for the reaction. If that is the case, then the KIEs for reaction of **Q** with methane and methane-d_4 will be given by eqs 6 and 7.

$$KIE = (K_{bind}k_2)_H/(K_{bind}k_2)_D \quad (6)$$

$$KIE = (k_{2H}/k_{2D})(K_{bind-H}/K_{bind-D}) \quad (7)$$

In the case of the sMMO from *Ms. trichosporium* OB3b at 4 °C, the KIE in k_{cat} at 4 °C determined under steady-state turnover conditions is k_H/k_D = 1.7.[141] This value is the same as that found at 30 °C. The observation of a large KIE in K_M for methane oxidation by this enzyme in Michaelis−Menten kinetic studies (KIE = 15)[141] suggests that substrate binding is reversible. That is, the large KIE in K_M is likely to reflect differential solvation and binding of CH_4 versus CD_4. If the ratio of the equilibrium binding constants in eq 7 is equal to the inverse of the ratio of the experimental Michaelis constants (K_M), then the observed KIE for CH_4 and CD_4 of 42[148] would give $k_H/k_D \approx 2.8$, which is similar to the KIE in k_{cat} determined under steady-state conditions.

Subsequent studies of KIEs in reactions of **Q** from from *Ms. trichosporium* OB3b employing mutant coupling protein MMOB indicated that substrate binding rates (and presumably equilibria) were important.[148] When coupling protein MMOB containing a mutation was used in place of the wild-type MMOB, the velocity of the methane reaction with **Q** was reduced by a factor of 7, whereas the velocity of the reaction of methane-d_4 with **Q** was unaffected. The observed KIE in velocities of the methane reaction with **Q** was reduced from 42 with wild-type MMOB to 6 with the mutant MMOB.[148] This behavior suggests that the rate or equilibrium of methane binding was limited with the mutant MMOB, but the rate of CD_4 binding was not.

For the sMMO from *Mc. capsulatus* (Bath), the KIE in k_{cat} at 20 °C can be anticipated to be similar to that found at 45 °C (ca. 1.7).[142] In this case, however, the KIE in the Michaelis constant K_M for methane and methane-d_4 was nearly unity.[142] Thus, the overall

KIE under steady-state turnover conditions (KIE = 2)[142] is much smaller than the KIE of 23 found in reaction of **Q** with methane at 20 °C.[150] Nonetheless, there is close similarity in the KIEs for k_{cat} for both sMMO enzymes as well as in the overall KIEs for reaction of **Q** from both enzymes with methane, and it seems likely that the two enzymes react similarly. The inconsistency of the results for the two sMMO enzymes might invite a reinvestigation of the KIE in K_M for *Mc. capsulatus* (Bath).

The difficulty in determining substrate concentration effects on the reaction of **Q** with methane suggests that it is premature to use the large KIE values for mechanistic interpretations in general and as evidence for hydrogen atom tunneling in particular. Especially noteworthy in regard to the latter point is the absence of evidence for tunneling in the intramolecular KIE found in the oxidation of CH_2D_2 by the sMMO from *Mc. capsulatus* (Bath), which is only $k_H/k_D = 1.3$.[142] Because K_M cannot be affected in an intramolecular KIE determination, the observed KIE must be the intrinsic value for k_{cat}, which is most likely to be the rate constant for the reaction of **Q** with substrate. Thus, the intramolecular KIE values suggest no hydrogen atom tunneling in the methane oxidation reaction.

In reactions of partially deuterated methanes with **Q**, Nesheim and Lipscomb[141] found a linear reduction in overall rates according to the number of deuterium atoms in the substrate. The interpretation was that the C−D bonds were nearly inert, but that interpretation is based on the implicit assumption that irreversible binding occurred. If the binding equilibrium is fast, then the observed rate constants are described by eq 7. It would seem logical that the binding equilibrium constants for partially deuterated methane would be approximately equal to the statistically corrected averages of the binding constants for methane and methane-d_4. In addition, support for hydrogen atom tunneling is not apparent in the intramolecular KIE studies, which were internally inconsistent.[141]

KIEs for reactions of ethane and propane with **Q** from both enzymes also have been reported (Table 3).[147,148,150] The velocities of reaction of **Q** with ethane and ethane-d_6 were equal in studies of **Q** from both enzymes, as were the velocities of reactions of propane and propane-d_8 with **Q** from *Ms. trichosporium* OB3b. Substituting the mutant MMOB for wild-type MMOB had an effect on the velocity of ethane reaction with **Q**. The mutant MMOB results, when coupled with the methane results with mutant MMOB, indicate that there is probably a change in the rate-determining step between oxidation of methane, ethane, and propane. It was concluded[148] that, with wild-type MMOB, C−H functionalization was limiting in the oxidation of methane, and that substrate binding was limiting in the oxidations of ethane and propane. For ethane reactions with **Q** from *Mc. capsulatus* (Bath),[150] it was concluded that substrate access to **Q** was rate-limiting. We note that, if this interpretation is correct, then the observed KIEs in the oxidation of methane and methane-d_4 discussed above are likely to be the products of the binding equilibrium constants and the catalytic rate constants as shown in eq 7.

The KIEs found in reactions of larger, more polar substrates with **Q** from *Mc. capsulatus* (Bath) are intriguing (Table 3). Reaction of **Q** with methanol and methanol-d_3 had a KIE of unity.[150] A rather large KIE was observed for reaction of **Q** with nitromethane at 20 °C (KIE = 8.1), and a very large KIE was found for reaction of **Q** with acetonitrile (KIE = 46). In the case of the nitromethane oxidations, saturation kinetics were apparent for reactions of both the protio and deuterio substrates, and the KIE is for the rate constant of the catalytic reaction. In the case of acetonitrile, the protio substrate clearly demonstrated saturation kinetics, but it was difficult to determine if the deuterated substrate (CD_3CN) did. It appears possible that the limiting step for reaction of CD_3CN with **Q** was substrate access, in which case the KIE for the oxidation step cannot be determined. If CD_3CN equilibrated freely, however, then the large KIE suggests a unique reaction pathway for acetonitrile.

These latest studies[148,150] are interesting in the sense that they propose an elegant solution that might unify the diverse KIE trends observed with different substrates and seemingly with sMMO from different organisms that exist in the literature. In addition to the intrinsic reaction barrier for the C−H bond activation, which is rate-limiting in the case of CH_4, the hypothesis is that the diffusion/binding of the substrate might become rate-limiting for different substrates, giving rise to completely different KIEs. The latter will depend not only on the size, dipole moment, and solubility of the substrate both in water and in the hydrophobic protein pocket, but also on specific interactions of the substrate with the protein environment immediately around the active site, such as hydrogen-bonding and electrostatic interactions. This hypothesis is difficult to examine experimentally and poses a new challenge to large-scale computational studies that are best suited to deliver quantitative, atomic-level details about each of the interactions that are suspected to control the rate-limiting process.

In summary, the large KIEs found for reactions of **Q** are clearly dramatic, but the origins of the effects remain to be determined. Conclusions that hydrogen atom tunneling reactions are involved in methane oxidations should be considered provisional until the inconsistencies between the intramolecular KIE values for partially deuterated methane and the intermolecular results with **Q** are sorted out.

4. Computational Model Studies

4.1. Overview of Computational Methodology

The advent in the past decade of new DFT[101] methods has made it possible to carry out quantitative investigations of large, transition metal-containing systems by using high-level quantum chemical techniques. The most efficient DFT approaches currently allow treatment of ~150 atoms without the imposition of symmetry at a reasonable level of theory with relatively modest computational effort. Calculations of this type can provide a detailed

atomic-level picture of the structural and energetic features of chemical reactions in MMO and other metalloenzymes.

Although all of the recent studies of MMO utilize DFT methods, there are nevertheless significant differences in the details of the calculations that have been carried out, which have important effects on the conclusions that have been drawn. In this section, we begin by briefly considering the key issues involved in designing these calculations and the likely effects on accuracy. These issues can be enumerated as follows.

(1) Physical model: The largest variation in results arises from differing assumptions concerning the physical model for the various proposed intermediates and transition states. In principle, one should include the entire protein and surrounding solvent environment in the calculations. New computational methods that utilized a combined quantum mechanics/molecular mechanics (QM/MM) approach[151−160] allow such inclusion, albeit with a potentially less accurate representation of the surroundings. Only one preliminary QM/MM study,[161] which was concerned with refining the structure of **Q** in a larger ligand environment, exists in the literature. A more detailed study that addresses structural and energetic issues connected to the hydroxylation mechanism in a QM/MM framework has not yet been reported. Hence, we focus on purely quantum mechanical calculations on model complexes that have been employed to date. Even if an accurate representation of the entire protein were to be used, it still would be necessary to investigate different local structures in the reactive core.[162] Identification of such structures with experimentally observed intermediates is a nontrivial task, requiring the integration of experimental and theoretical results in a complex fashion. We discuss specific issues along these lines for MMO below.

(2) DFT functional: A number of DFT functionals have been used in both the chemistry and physics communities. The studies we discuss below all employ a hybrid functional, B3LYP,[163,164] which contains an admixture of exact exchange along with correlation and gradient terms. Such functionals are in general significantly more accurate, e.g., in computed heats of atomization of small organic molecules,[165,166] than density functionals containing "pure" exchange functionals only, such as BLYP[164,167] or PW91xc.[168,169] Data with regard to accuracy for transition metal-containing species are more anecdotal, but the preponderance of evidence at present suggests that hybrid functionals are significantly more accurate for these applications as well.[170,171]

(3) Basis sets: In general, larger and more flexible basis sets will lead to more accurate results in DFT calculations;[172] however, it is also desirable to limit basis set size in the interest of computational efficiency. A number of strategies can be used to do so without substantially degrading accuracy: (a) smaller basis sets, such as the standard double-ζ set of Gaussian-type basis 6-31G**, can be used for geometry optimization, followed by a larger basis set for single-point energy evaluations. In most of the recently reported studies, triple-ζ quality basis sets are employed for computing more reliable energies. Geometries are in general less sensitive to basis set than total energies. (b) If a large structural model is used, a smaller basis set can be utilized on the periphery of the model than near the reactive core. (c) The core electrons of iron typically are not treated explicitly in modern quantum chemical calculations. Instead, either effective core potentials[173−177] or the frozen core approximation is utilized. These techniques can now be considered mature quantum chemical methods and are widely accepted. Within the framework of these general considerations, however, different calculations reported below represent different compromises between speed and accuracy.

(4) Treatment of spin: The MMO models that we consider below mostly contain a large number of unpaired electrons on the Fe atoms. The only approach available to treat spin multiplets in a DFT calculation is the use of unrestricted DFT (UDFT). Results for ferromagnetic (high-spin) coupling with such methods are unproblematic. However, the wave functions obtained from such calculations do not rigorously describe states in which some of the spins are antiparallel, i.e., couple antiferromagnetically to each other. Approximate methods based on the use of a broken-symmetry wave function can be usefully applied; we discuss this approach further below.

We consider below results from four different efforts to model MMO: Yoshizawa, Morokuma−Basch, Siegbahn, and Friesner−Lippard. The Yoshizawa model is fundamentally different from the other three models with regard to its proposal for where the reactive methane chemistry takes place, coordination numbers of the iron atoms in **Q**, total charge, etc. Furthermore, the modeling is carried out using a very small number of atoms, making it impossible to compare total energies with those of alternative formulations. Hence, the only way to evaluate this model is on the basis of internal consistency, comparison with experimental data, and plausibility of the underlying physical assumptions; we do so in sections 4.5−4.8.

The remaining three models have a number of similarities but also significant differences. The Friesner−Lippard model is nearly twice the size of the later Siegbahn and Morokuma models and roughly 3 times the size of their original models. There are also nontrivial differences in the specific structures investigated by each group. Geometry optimizations in the Siegbahn and Morokuma protocols are carried out at the double-ζ (DZ) level, whereas the Friesner−Lippard geometry optimizations are performed at the DZP level. Both the Friesner−Lippard and Siegbahn protocols mandate a final energy evaluation using an extended basis set, whereas the Morokuma protocol contains no such step. Finally, the Friesner−Lippard model incorporates antiferromagnetic coupling when appropriate, e.g., in modeling **Q** and its reaction with methane, as do later models produced by Siegbahn. In contrast, the Morokuma models use ferromagnetic coupling to represent every structure. Some of these differences stem from the different electronic structure codes employed by each group (some types of calculations are much harder to carry out with one

program rather than another), while others reflect different philosophies with regard to what is necessary and sufficient to obtain an accurate model.

The question of what effects each of the various approximations discussed above has on the results is a complex, system-dependent issue, which is examined in detail in the sections that follow. The traditional view has been that small models, and small basis sets, are sufficient to obtain reasonable results for enzyme active-site modeling, on the grounds that the chemistry taking place is highly localized, that small variations in geometry are unimportant, and that DFT does not require large basis sets to achieve a reasonable level of convergence. This general protocol is not sufficiently accurate if one is trying to understand the role of the protein environment in enzymatic catalysis—for example, the carboxylate shifts[178] that are central to the functioning of MMO in the catalytic cycle (Figure 2) require significant rearrangement of the protein at the active site, which cannot be accounted for in a small model system. However, the methane reaction itself conforms more to this picture. It is the case that three of the four models considered identify the rate-determining step in hydroxylation as proton-coupled electron transfer from the substrate by one of the bridging oxygens in the diiron core. The quantitative bond lengths, bond angles, wave functions, and energies that constitute an atomic level of detail can, however, exhibit substantial variation as the model assumptions are altered.

When such differences occur, it is reasonable to suppose that calculations carried out with a larger structural model that retains better fidelity to the existing experimental X-ray structures, uses larger basis sets, and employs a treatment of spin that is closer to that mandated by experimental observations—even if such a treatment is imperfect—will yield more accurate and robust results from a quantitative point of view. One set of quantities that are particularly important and difficult to calculate are total free energy differences of the various intermediates and transition states in the catalytic cycle. In many cases, small structural models evaluated with small basis sets are unable to obtain results for these differences that are even in qualitative agreement with experiment. On the other hand, one would hope that methods which in essence converge the model with regard to the various components, e.g., systematically increasing the basis set size until the results are more or less invariant, would provide agreement with experiment in the range of what is expected from the intrinsic accuracy of the DFT functional—on the order of 2−5 kcal/mol.

4.2. Electronic Structure of Q

Although it has been established[179,180] that both iron atoms in the reactive intermediate **Q** are in an oxidation state of IV,[180] neither the structural arrangement of the first shell ligands around the Fe_2O_2 core nor the electronic configuration is known exactly. In principle, the four metal-based electrons of the d^4-Fe(IV) configuration at each metal center can adopt three different spin states, labeled as "low-spin" (LS), "intermediate-spin" (IS), and "high-spin" (HS) in Figure 5. In addition, the orientation of the

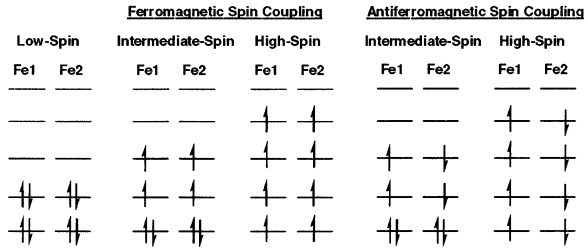

Figure 5. Illustration of the possible spin states of a $[Fe(IV)]_2$ center.

unpaired electrons at the iron centers to each other gives rise to a second degree of freedom resulting in either a ferromagnetic (F) or antiferromagnetic (AF) spin-coupling of the diiron centers for the IS and HS cases. Experimentally, antiferromagnetic behavior is observed in Mössbauer studies of the intermediate **Q** with a coupling constant of $J < -30\ cm^{-1}$.[180] These measurements strongly suggest high-valent iron centers with unpaired electron that couple with one another, ruling out the LS case. The LS state for Fe(IV) is also intuitively unlikely given that, to date, not one example of a complex displaying a low-spin d^4-Fe(IV) configuration is known. The Mössbauer data are, however, consistent with both the IS and HS cases. As discussed below, all three spin states have been explored in theoretical models.

Modeling ferromagnetic (F) spin-coupling in a computational study is not problematic, whereas the antiferromagnetic (AF) coupling is substantially more challenging because computationally efficient methods, such as DFT or Møller−Plesset perturbation theory (MPx), are single reference methods that can only describe pure spin states. Populating the molecular orbitals in a pattern as to mimic AF spin-coupling gives rise to inaccurate solutions in the single reference framework indicated by substantially spin-contaminated wave functions, rendering the computed solution unreliable by default. In principle, a proper quantum mechanical description of the AF-coupled wave function requires a multireference method, such as CASSCF,[181,182] expressing the final wave function as a linear combination of different spin states. While theoretically more justified, these calculations are computationally expensive and currently beyond reach for transition metal-containing systems of reasonable size. There are two approaches to resolve this issue, both of which have been pursued in the literature. A number of studies have simply ignored the AF coupling and used F coupling instead. Typically, the coupling constants in the species involved in the catalytic cycle of MMO are small, and, consequently, the energy difference between the AF-coupled state and the F-coupled analogue is similarly small. Thus, the error introduced by evaluating the energies on F-coupled models of the AF-coupled complex is probably tolerable. This argument has been subject to some criticism based upon the notion that the electronic structure of a F-coupled Fe(IV) dimer is substantially different from that of a AF-coupled dimer, potentially leading to very different

chemical behavior, especially in redox reactions. An alternative approach that allows AF coupling in DFT was suggested first by Noodleman[183] and extended later by Yamaguchi et al.[184] using broken-symmetry (BS) orbitals to populate spin-polarized, i.e., unrestricted, orbitals centered around each of the metal centers more independently from one another.

4.3. Broken Symmetry Calculations

The BS approach makes use of localized orbitals and ignores the usual procedure of combining atomic orbitals that belong to the same symmetry to form in-phase and out-of-phase linear combinations of atomic orbitals. One misconception that has caused much confusion is concerned with the meaning of BS wave functions. Typically, the S vs S^2 analysis reveals significant spin contamination of the BS wave function, and it has been argued repeatedly that the energies based upon BS wave functions are therefore flawed.[185,186] This view ignores the fact that the BS wave function is formally an average of different spin-state wave functions and thus is required to display a mismatch of the S and S^2 values, which is the very indication of the spin-state average nature.[187] If a BS wave function does not display spin contamination, one has reached the totally delocalized limit, and the BS wave function is exactly the same as the symmetric wave function. Thus, it is important to recognize that Noodleman's BS approach does not result in a rigorously valid wave function for the intrinsically multiconfigurational problem but rather gives access to a working approximation in a single-determinant framework subject to the limiting condition that the spin−spin coupling is relatively weak. The energy of the properly AF-coupled system can be estimated by using Heisenberg's spin Hamiltonian combined with Noodleman's spin projection techniques, allowing for evaluating the true energy of the AF-coupled state. The most important features of the broken-symmetry approach can be summarized as follows.[183,188] The Heisenberg spin Hamiltonian simply relates the two spin vectors at the two metal centers with the Heisenberg exchange coupling constant J (eq 8). Consequently, the coupling constant

$$H_{\text{spin}} = (-2J)\vec{S}_1\cdot\vec{S}_2 \tag{8}$$

J gives the relative energies, $E(S)$, of all possible spin states, characterized by the total spin quantum number S (e.g., $S = {}^8/_2$ for the F-coupled Fe(IV) dimer). The relative energies can be computed by using eq 9. The difference between the energy of the

$$E(S) = -JS(S+1) \tag{9}$$

F-coupled state where all metal-based electrons are parallel to each other, E(F), and that of the broken-symmetry case, E(BS), where the spin directions of the unpaired electrons on each of the iron centers are antiparallel to each other, can be calculated by using eq 10. Thus, the coupling constant J can be computedby using eq 11, from the energies of the F-coupled and the broken-symmetry states, with both S_1 and S_2 being ${}^4/_2$ in the case of the Fe(IV) dimer. The true energy of the pure singlet state can be obtained from the computed energy of the broken-symmetry state by subtracting $\Delta E = -4J$. Typically, these corrections are less than a few kilocalories per mole.[187,189,190]

$$E(\text{F}) - E(\text{BS}) = (-4J)(S_1S_2) \tag{10}$$

$$J = -[E(\text{F}) - E(\text{BS})]/(4S_1S_2) \tag{11}$$

An important question, for which theoretically rigorous answers do not exist to date, is concerned with the validity of interpreting BS orbitals in a classical orbital analysis scheme. For example, it is unclear whether examining the BS frontier orbitals as the main promoters of electrophilic or nucleophilic reactivity is a valid procedure. Detailed analyses of the BS wave functions in a classical orbital analysis scheme suggest that BS wave functions are physically meaningful representations. The physical meaning and usefulness of the BS orbital analysis are open questions for future work and resemble the ongoing discussion about the meaning of the Kohn−Sham orbitals[191−197] from DFT calculations in comparison to classical orbitals from Schrödinger theory.

4.4. Model Validation and Analysis

The electronic flexibility and the presence of many spin states that are energetically close to each other requires a careful inspection of the electronic structure calculation results. In addition to traditional benchmarks, such as the ability of the computer model to reproduce experimentally observed structural features, the convergence to the correct or at least a reasonable electronic structure must be confirmed before any conclusion can be drawn. Electron spin densities, computed on the basis of Mulliken population analysis,[198,199] proved to be a valuable tool for monitoring the electronic spin state of the iron centers. Mulliken population analysis uses the trace of the product matrix of the electron density and the orbital overlap to divide and assign the total electron density in partial electron density contributions from each of the atomic basis orbitals. By simply adding contributions of all orbitals that are centered around each of the atomic centers in the molecule, partial charges, spin densities, and other electronic features can be extracted from the computed wave function. It is important to recognize that this simple procedure relies on a balanced representation of all atoms, and the results are highly dependent on the size and nature of the basis set used. Thus, population analyses are not uniquely determined and have to be done within one consistent computational framework using similar technical parameters. The absolute spin densities that characterize, e.g., a typical Fe(IV) center are therefore expected to be somewhat different when different theoretical methods are applied. In addition, covalent bonds and other electronic interactions between the metal center and the ligand moieties give rise to spin density flux from the metal center to the ligands and often result in reduction of formally computed spin densities from integer numbers that might have been expected from simplistic considerations. For example, typical spin densities of a d^4-Fe(IV) center range from 3.2 to 3.7, depending on the nature of the first-shell ligands.

More significant deviations from these expected values usually indicate different electronic states, requiring a careful inspection of the results to confirm that the electronic structure of the model is reasonable.

The lack of unambiguous structural data on **Q**, for which a crystal structure is not available, has posed a significant challenge to computational studies. Instead of starting from a consensus structure for **Q**, a proposal must be made on the basis of computations which proved to give rise to a number of different suggestions, depending on the approaches taken. Currently, there are four model systems available that fall into two distinctively different classes resulting from divergent strategies in evaluating and emphasizing experimental observations. The first class, proposed by Yoshizawa and Hoffmann,[200] implicates the metal as an actor in the C−H bond activation. The majority of the computational models, however, propose that the actual oxidation reaction takes place at the bridging oxo moiety. A number of models that differ by size and the underlying electronic states have been examined. In the following section, the characteristics and differences of these models will be examined.

One of the most influential experimental studies has been the combined Mössbauer and extended X-ray absorption fine structure (EXAFS) experiment by Shu et al.[201] that indicated a "diamond core" for the (μ-oxo)diiron quadrilateral with two short (1.74 Å) and two long (1.82 Å) Fe−O bonds and a metal-to-metal distance of 2.46 Å. The computed pre-edge area of 28 units for **Q** in the EXAFS experiment was interpreted as an indicator for a coordination number around each iron center not greater than 5.

4.5. Yoshizawa Model

An interesting proposal is to treat the catalytically active diiron center as an analogue to the bare $Fe{=}O^+$ ion. This cation has been shown to hydroxylate methane in gas phase under ion cyclotron resonance conditions.[202−204] The consensus mechanism for the C−H activation in the gas phase is shown in Figure 6.[205−207] Starting from the initial

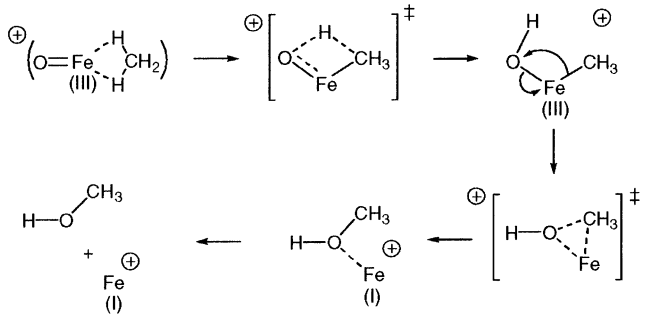

Figure 6. Mechanism of methane hydroxylation by FeO^+.[205]

methane complex, the C−H bond is activated in the first transition state that is proposed to involve a four-center interaction (Figure 6), resulting in a hydroxo intermediate, which can reductively eliminate methanol to give a free iron cation. This last step is usually labeled "methyl migration" to indicate that the Fe−C bond cleavage and C−O bond formation is the dominating event of the second transition state. Although this simple gas-phase reaction involves an Fe(III) center and is not catalytic in nature, Yoshizawa et al. argued that this reaction may be a good model for the methane hydroxylation reaction in the enzyme and its models.[138,185,200,207−214] From a purely inorganic perspective, such a proposal is unusual in the sense that Fe(III) complexes typically display a very different chemistry than Fe(IV) systems. However, the structural and functional resemblance, that is, an iron-oxo species carrying out the same transformation as the metalloenzyme, makes this approach an interesting possibility. To test this idea, Yoshizawa and co-workers constructed a simplest possible model of **Q** by replacing all first-shell ligands with H_2O[200] and in later studies with OH^- and maintaining Glu144, modeled as a formate, at the bridging position.[213] The main emphasis was placed on deriving an intuitive understanding rather than quantitative accuracy, which led to a number of dramatic approximations.

In accord with the EXAFS results, the iron centers are four- and five-coordinate in approximately tetrahedral and square-pyramidal geometries, respectively (Figure 7). The experimentally observed antiferromagnetic coupling of the unpaired spins at the iron centers to each other was ignored. Although the procedure of using ferromagnetic coupling is widespread for the reasons described above, a very different and unusual approximation was introduced by Yoshizawa and co-workers that potentially has a decisive consequence for the model chemistry. All spins are assumed to be paired by enforcing an overall singlet state in a closed-shell (restricted spin) theoretical framework. As a result, the model complex of **Q** contains two low-spin Fe(IV) centers formally with two doubly occupied iron-based MOs on each metal centers and three unoccupied, metal-dominated MOs, which play a key role in promoting the catalysis. These unoccupied MOs are proposed to function as electron-accepting orbitals. This proposal is problematic mainly for two reasons. First, there is no example of a low-spin Fe(IV) complex in the vast inorganic and organometallic literature to date. To enforce such an unusual configuration, an exceptionally strong ligand field would be required. It is difficult to imagine how the first-shell ligands present at the active site, carboxylate and imidazole fragments derived from glutamate and histidine residues, can accomplish this task. Second, Mössbauer spectroscopy[180,201] indicated that the Fe(IV) centers are either in intermediate-spin ($S = 1$) or high-spin ($S = 2$) states. Thus, the electronics of the proposed model chemistry is not well supported by experimental evidence.

Mechanistically, methane hydroxylation is proposed to be a two-step reaction progressing as shown in Figure 7.[213] As seen in the case of $Fe{=}O^+$, methane is proposed to bind directly to the iron center, forming a reactant complex with a relative energy of −6.1 kcal/mol. There is no direct experimental evidence to support the formation of an Fe−C bond in the catalytic cycle,[215] but it is also difficult to rule out

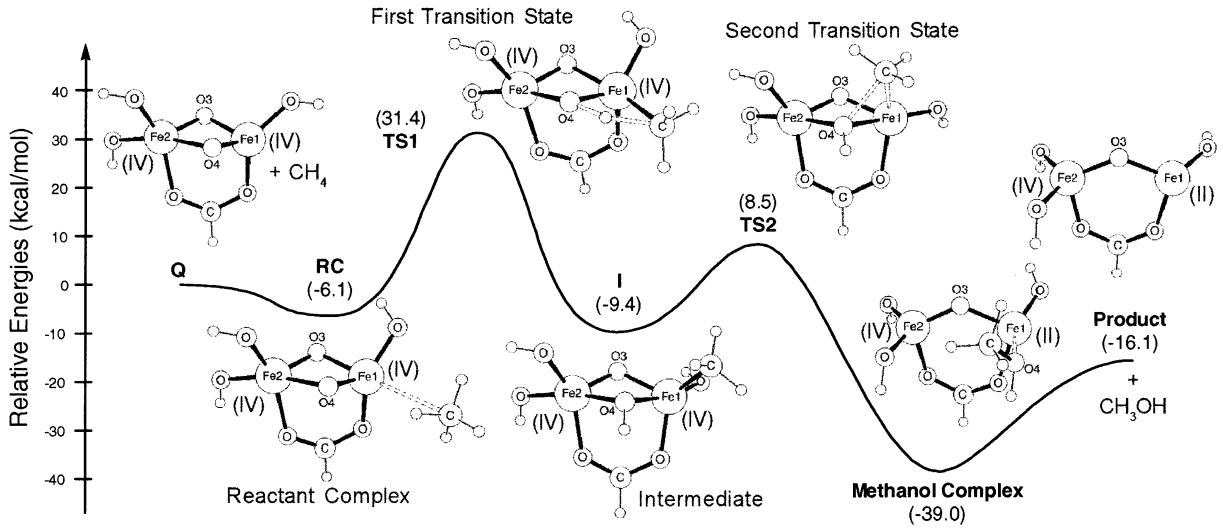

Figure 7. Methane hydroxylation mechanism proposed by Yoshizawa et al.[213]

such a mechanism. The rate-limiting step is hydrogen migration to the bridging oxo group involving a four-center transition state, labeled **TS1** in Figure 7, that is 37.5 kcal/mol uphill with respect to the reactant complex. The initial product of this first redox reaction is the reaction intermediate **I** containing a bridging hydroxide. The next step, C−O bond formation, is accomplished by methyl migration and is 17.9 kcal/mol uphill with respect to the hydroxy intermediate. The C−O distance of 1.93 Å at **TS2** indicates that the transition state is "early" and the C−O bond is not formed to an appreciable extent at the transition state. After this transition state is traversed, the Fe2−O4 bond breaks and methanol formation completes to give the product complex, which releases methanol to form the final complex.

This proposal is attractive in the sense that it incorporates a number of familiar features from catalysis performed by simple transition metal complexes.[24,25] The metal center interacts directly with the substrate, assigning an intuitive role for the iron center and explaining the unsaturated coordination geometry of Fe1. The conversion of methane to methanol is decomposed into a rate-limiting C−H activation step and a reductive elimination step where the C−O bond is formed. As is to be expected for a drastically simplified model, quantitative agreement with the experimental activation energy $\Delta G^{\ddagger}$, which has been estimated to be ∼14−17 kcal/mol,[149] is poor. It is interesting to note that the most difficult step, the C−H bond cleavage, does not involve a change of oxidation state at the iron center in this model. The two-electron redox reaction is associated with the reductive elimination step **I → Methanol Complex**. Analogous to the template reaction of the $Fe{=}O^{+}$ ion, this reaction would require the **Methanol Complex** to be an Fe(IV)−Fe(II) mixed-valence complex, where both iron centers are again in a low-spin state. Figure 8a shows the schematic MO diagram[212] of **Q** and the first transition state **TS1**. This MO diagram illustrates clearly the low-spin nature of both iron centers in the diiron complex. Four lowest energy MOs are doubly occupied, while six empty MOs complete the expected set of 10 in-phase and out-of-phase combinations of the metal d-orbitals, shown as delocalized combinations of d-orbitals from both metal centers. Figure 8b is the corresponding "localized" cartoon commonly drawn by inorganic chemists for simplicity. The electron count for the metal centers does not change with methane addition; that is, the first step is not a redox reaction. This scenario translates into a MO interaction diagram that shows two occupied CH_4-based orbitals interacting with one empty metal-based orbital to give two occupied low-lying MOs and a high-energy, metal-dominated MO (Figure 8b). The unusual proposal of an Fe(IV)−Fe(II) mixed-valence state is the only possible result in a closed-shell/restricted-spin framework of theory—the alternative, an Fe(III)−Fe(III) complex, would require unrestricted-spin wave functions to allow an uneven number of electrons at each iron center. Similarly, the restricted-spin formalism is unable to describe a radical reaction pathway, thus predetermining the reaction to be nonradicaloid in character. Consequently, the complicated spin-exchange problem for the stepwise two-electron redox process that poses a major challenge to overcome in other model studies (vide infra) is not present here. The two electrons of the metal−carbon σ-bond formed in the first step of the reaction are simply injected into the metal as a pair, and the C−O bond is formed as indicated for the $Fe{=}O^{+}$ template reaction in Figure 6. Although these approximations are dramatic, they allowed the construction of simple molecular orbital-based arguments, and, until recently, this was the only model that provided an intuitively understandable molecular orbital analysis of a proposed mechanism.

In an attempt to quantify the effect of the closed-shell formalism and to consider alternative electronic states that have been examined by other researchers (vide infra), Yoshizawa and co-workers have also conducted broken-symmetry calculations[185] on the same model system modeling the AF-coupled singlet state. Surprisingly, the energy of this alternative transition state was computed to be 32.4 kcal/mol lower than that of the original transition state **TS1**, placing it at an energy of −1.0 kcal/mol on the

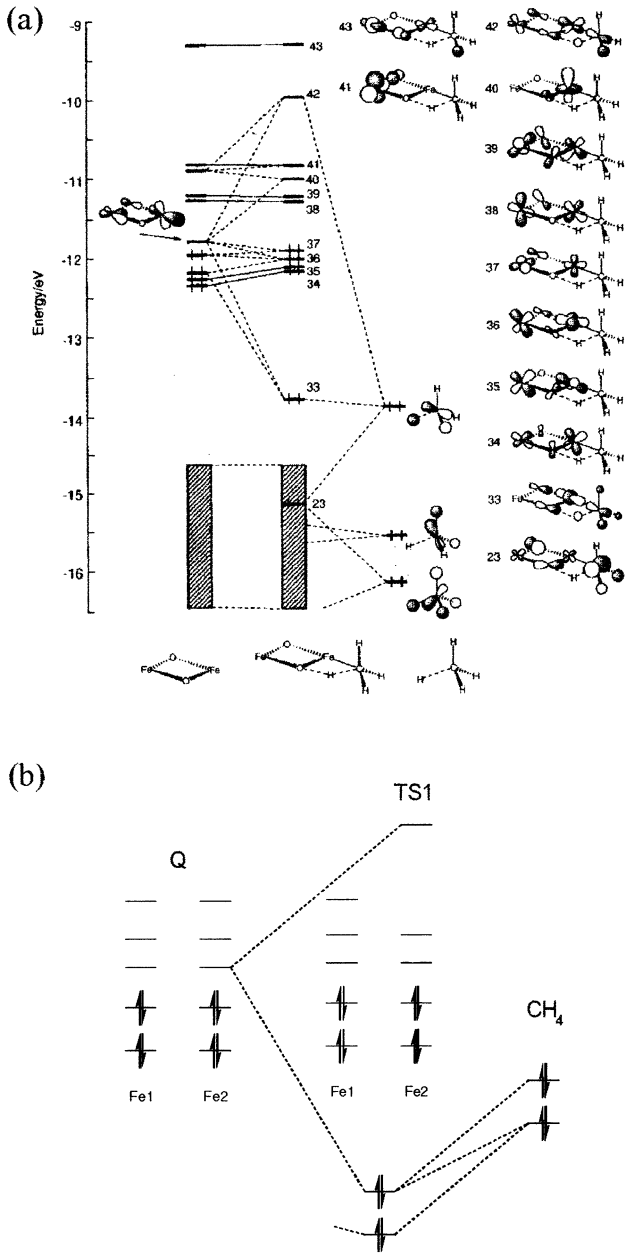

Figure 8. (a) MO interaction diagram **Q** → **TS1**. (b) Schematic cartoon of the MO diagram illustrating the electronic configuration. (Reprinted with permission from ref 212. Copyright 1998 The Chemical Society of Japan.)

relative energy scale used in Figure 7. Consequently, the activation barrier from the reactant complex to the AF-coupled analogue of **TS1** is only +5 kcal/mol, making the first step unlikely to be rate-limiting. This AF-coupled analogue was dismissed on the basis of the incorrect notion (vide supra) that the spin contamination found in the BS calculation would invalidate the model. To project from the BS wave function to the true pure singlet spin state energy, the ferromagnetically coupled analogue is required, which has not been considered by these authors—note that the original transition state **TS1** is the closed-shell solution without any unpaired spins. The energy mismatch of the AF-coupled analogue of **TS1** is most likely a simple reflection of the fact that it is not appropriate to compare its energy to those of reaction intermediates computed on the closed-shell singlet surface. More appropriately, the AF-coupled analogues of all species shown in Figure 7 must be computed and the activation energy determined by comparing the energy of the AF-coupled **TS1** to an AF-coupled reactant complex. Intuitively, one would expect all AF-coupled analogues of the intermediates shown in Figure 7 to display significantly lower energies simply because they are the high-spin analogues of the nonintuitive low-spin iron complexes. Thus, the entire reaction energy profile will probably shift to lower energies and give more reasonable and consistent reaction energy barriers. These high-spin analogues have not been explored to date, and it is not possible to compare the two electronic scenarios systematically.

The small size of the model allowed for carrying out full harmonic vibrational frequency analyses, which not only are important for confirming that the computed intermediates and transition states are true local minima and maxima on the potential energy surface but also give access to a theoretical evaluation of the kinetic isotope effect. The KIE, that is, the ratio (k_H/k_D), was evaluated on the basis of the transition-state theory formula (eq 12).[216] In

$$\frac{k_{CH_4}}{k_{CD_4}} = \left(\frac{m^R_{CD_4} m^\#_{CH_4}}{m^R_{CH_4} m^\#_{CD_4}}\right)^{3/2} \left(\frac{I^R_{xCD_4} I^R_{yCD_4} I^R_{zCD_4}}{I^R_{xCH_4} I^R_{yCH_4} I^R_{zCH_4}}\right)^{1/2} \left(\frac{I^\#_{xCH_4} I^\#_{yCH_4} I^\#_{zCH_4}}{I^\#_{xCD_4} I^\#_{yCD_4} I^\#_{zCD_4}}\right)^{1/2} \frac{q^R_{\nu CD_4} q^\#_{\nu CH_4}}{q^R_{\nu CH_4} q^\#_{\nu CD_4}} \exp\left(-\frac{E^\#_{CH_4} - E^\#_{CD_4}}{RT}\right) \quad (12)$$

addition to the closed-shell singlet transition state **TS1** shown in Figure 7, a triplet analogue of **TS1** was conceived by comparison to the two-state model suggested by Shaik et al.[217−219] for the hydroxylation of alkane by cytochrome P450, where energetically nearly degenerate doublet and quartet states were considered. The triplet analogue of **TS1** is ∼20 kcal/mol lower than the closed-shell singlet transition states, which is a confusing result because of the unusual magnitude of the energy difference. If taken as physically meaningful, this scenario would suggest a significant thermodynamic driving force for intersystem crossing to the triplet surface, putting much of the proposed mechanism in question. A more detailed electronic structure analysis of the triplet state and its relevance to the proposed mechanism was not explored. Thus, the nature of the triplet state, in particular regarding the location of the two radicaloid electrons in the molecule and the exact formal electronic states of the iron centers, is unclear. The authors noted that the relative energies of these alternative transition states are not enlightening and dismissed them for further mechanistic discussions. However, KIEs were computed for both the singlet and triplet species of the transition state. Despite the energetic and electronic differences, the computed KIEs for the singlet and triplet states, 8.6 and 9.2 at 300 K, respectively, are remarkably similar, as discussed in section 3. As can be expected from inspection of the transition-state structure (Figure 7) and the considerations given in section 3, the

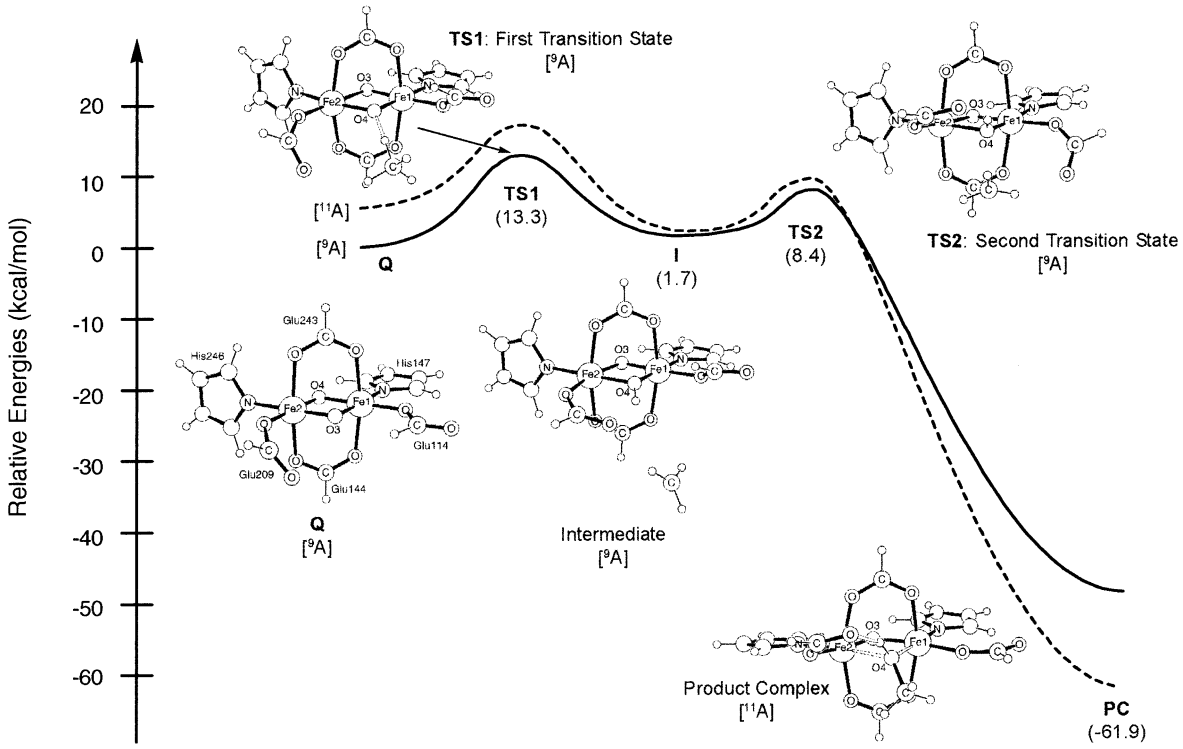

Figure 9. Methane hydroxylation mechanism proposed by Morokama, Basch, et al.[226]

addition of the tunneling effects derived by using the Wigner function increases the KIE significantly to give 13.1 and 14.3 at 300 K for the singlet and triplet states, respectively. Unfortunately, the Yoshizawa model is, to date, the only theoretical model for which KIEs have been derived explicitly, making it difficult to evaluate the results in the context of other theoretical work. Clearly, further studies in this direction will be pursued in the future, which might resolve some of the conflicting results outlined above.

4.6. Morokuma–Basch Model

Morokuma, Basch, and co-workers proposed a high-spin model for **Q** enforcing the presence of four unpaired spins at each Fe(IV) center of **Q** in unrestricted-spin DFT calculations.[161,186,220−226] One of the design features introduced at an early stage of study is a neutral net charge of the model. Recognizing that the active site of the metalloenzyme is buried in a hydrophobic pocket, and that the carboxylate ligands from glutamates and the two bridging oxo groups generate the neutral intermediate **Q**, it was argued that zero net charge is the most natural choice for the computational model. In comparison, the early Yoshizawa models[200,207,212] carried an artificial positive charge of +3. Most of the model studies by Morokuma, Basch, and co-workers are performed on a small model system that uses NH_2^- and H_2O ligands to represent histidine and glutamate residues, respectively. The bridging glutamate found in the crystal structures of the precursor H_{red} were modeled by a formate group.[220,224] Recently,[226] the model size was enlarged significantly to give a "medium-sized" model, shown in Figure 9. The histidine residues are represented by imidazole rings, and all glutamate ligands, both bridging and terminal, are modeled as formate. Ferromagnetic coupling was used in all cases to avoid computational complications. It is noteworthy that this enlargement of the model size is not only a technical improvement but also has an important chemical implication. In the enzymatic environment, the N-donor ligands are imidazole rings from histidine residues, which are neutral moieties. The O-donor ligands, on the other hand, are carboxylate groups from glutamate fragments. Thus, while the N-donor ligands are neutral and the O-donor ligands are negatively charged in the enzymatic environment, the small model used by Morokuma and co-workers reversed the ligand charges by using NH_2^- and H_2O ligands. The electronic effects of this improper ligand charge distribution are difficult to estimate, since significant error cancellation is expected for energy evaluations. A comparison with the recently employed medium-sized model indicates that the differences between these two models are significant (vide infra), although the overall trends and fundamental conclusions derived from the small model studies remain fully valid.[226] One intuitive effect of the ligand charge reversal might be an artificially increased polarizability on the N side of the dimer simply through means of Coulombic forces introduced by the NH_2^- ligands, while the originally more electron-rich O side of the dimer becomes less polarizable. The terms "N side" and "O side" refer to the fact that the cis orientation of the N- and O-donor ligands creates distinguishable "sides" of the iron dimer (Figure 9). Consequently, one might expect an enhanced reactivity on the N side compared to a model that is more faithful to the nature of the ligands in the enzymatic environment. Morokuma and co-workers initially proposed the hydroxylation reaction to occur on the N side of the dimer,[220] which

is preferable by 3.7 kcal/mol with a rate-limiting activation barrier of 19.5 kcal/mol compared to 23.2 kcal/mol[224] when the O side was chosen as the reactive center. Inspection of the metalloprotein structure and consideration of the steric demands of a more realistic portion of the amino acid ligands directly bound to the iron sites reveals, however, that the N side is not accessible for methane or any other substrate. Thus, we limit the following discussion to the O-side attack.[224,226]

The structures and energies computed by Morokuma and co-workers are shown in Figure 9. The proposed structure of **Q** is significantly different from the Yoshizawa model and contains two six-coordinate iron centers with two bridging carboxylate ligands in addition to the two bridging oxo groups. The latter and the iron centers form the "diamond" core structure, where each bridging oxygen atom forms a short and a long bond to the iron centers, respectively. The remaining coordination sites are occupied by a nitrogen- and an oxygen-donor ligand, respectively, to complete the approximately octahedral coordination geometry around each iron atom. This model is not in complete agreement with the EXAFS result,[201] which estimated the coordination number to be not larger than 5. However, given the usual uncertainty in determining coordination numbers from EXAFS experiments, which can be assumed to be around ±1, and the fact that the precursor complex H_{red} clearly shows two histidine and four carboxylate groups at the active center that could serve as ligands, this structural proposal is at least reasonable. The overall spin state of **Q** is nonet, ^{9}A, reflecting on the four unpaired electrons each on the Fe(IV) centers that display ferromagnetic coupling. In all studies, the authors considered a second spin state with a total of 10 unpaired electrons, thus giving an ^{11}A state, at any given point of the reaction energy profile. While this protocol gives a theoretically complete picture, it created much confusion because it is difficult to understand the chemical meaning of a reactive intermediate **Q** in a ^{11}A state. Similarly nonintuitive is the explicit consideration of the ^{9}A state for the final methanol complex, which is expected to consist of two d^5-Fe(III) centers, thus naturally suggesting the ^{11}A state when the unpaired metal d-electrons are coupled ferromagnetically. That both potential energy surfaces must be considered for a proper exploration of the mechanism, as demonstrated by these authors, is a logical consequence of the single-determinant nature of DFT. Because it does not offer an intrinsic and consistent way of describing the intersystem crossing between the ^{9}A state of the reactant **Q** + **CH$_4$** and the ^{11}A state of the final methanol complex, the reaction energy profile cannot be constructed as a smoothly connected single surface. Consequently, both electronic states must be sampled for the whole reaction, regardless of the physical relevance, giving rise to two reaction energy profiles, as shown in Figure 9. One of the most important points of such a composite reaction energy profile is the crossing point, where both states become energetically degenerate, which is the most appropriate point where intersystem crossing is expected to occur. Evaluating the actual transition probability or the coupling between the two states is demanding and usually beyond the capabilities of the DFT or any other single-determinant method. The exact position of the intersystem crossing appears to be dependent on the model size. Whereas the mid-sized model predicted the second transition state, **TS2**, to be a ^{9}A state and intersystem crossing to occur after **TS2** is traversed, the small model predicted **TS2** to be a ^{11}A state.[224]

Although the above-described protocol for constructing the reaction energy profile is theoretically appropriate, it proved to be misleading, especially to nontheorists. It is important to realize that the existence of the two spin states, ^{9}A and ^{11}A, is mainly a computational artifact. It is the result of the ferromagnetic coupling scheme adopted to obtain a physically meaningful wave function in a standard quantum mechanical procedure. In reality, Mössbauer and EPR spectroscopy[70,73,74] clearly established an overall singlet configuration for **Q** and the final methanol product. Thus, both the reactant and the product are most likely on the same singlet energy surface, and there is no need for switching to the F-coupled surface. If the computer model explicitly incorporates an AF-coupled singlet state, then the reaction path from **Q** + **CH$_4$** to the methanol product can be connected smoothly without proposing an intersystem crossing or any physically meaningless electronic states.

Enforcing the ^{11}A state for the reactant **Q** + **CH$_4$** leads to a peculiar electronic structure for **Q**. Mulliken spin population analysis reveals a spin distribution in **Q** (^{11}A) that is consistent with an Fe1(IV)−Fe2(III) mixed-valence state with five unpaired electrons on Fe2 (vide infra). Furthermore, full radical character is developed on the bridging O3, with an unpaired spin density of 1.03 (Table 4), confirming that the ^{11}A state for the reactant is physically meaningless. Unlike in the Yoshizawa model, C−H activation takes place at the bridging oxo group, labeled O4 in Figure 9. The first electron transfer occurs at the transition state, **TS1**, which shows a linear arrangement of the O···H···C moiety, indicative of a typical proton-coupled electron-transfer (PCET) transition state.[227] This oxidative C−H acti-

Table 4. Mulliken Spin Densities of the Structures Involved in the Methane Hydroxylation Mechanism Proposed by Morokuma et al.[224]

	spin density[a]				
atom	L_nFe1	L_nFe2	O3	O4	CH_3
Q (^{9}A)	3.55	3.44	0.44	0.30	
Q (^{11}A)	3.47	4.62	1.03	0.43	
TS-1 (^{9}A)	3.54	4.59	0.40	−0.37	−0.55
TS-1 (^{11}A)	3.52	4.63	0.43	0.55	0.59
I (^{9}A)	3.51	4.64	0.43	0.08	−0.99
I (^{11}A)	3.58	4.67	0.43	0.10	0.98
TS-2 (^{9}A)	3.23	4.58	0.38	0.20	−0.73
TS-2 (^{11}A)	3.97	4.57	0.50	0.01	0.81
methanol complex (^{9}A)	2.95	4.49	0.38	0.00	0.00
methanol complex (^{11}A)	4.59	4.48	0.66	0.00	0.00

[a] Negative sign denotes excess of β-electron density. L_nFe: $(H_2O)(NH_2)$Fe fragment.

vation step is rate-limiting with an activation enthalpy barrier of 13.3 kcal/mol. Once this electron-transfer step accompanied by formation of the O−H bond at the bridging oxygen moiety is complete, the methyl radical recoils to give the hydroxyl intermediate **I**, which was labeled as a "bound-radical" species by the authors. The reaction proceeds by a second attack of the methyl radical at the newly formed bridging hydroxide group to give the final methanol complex after traversing the second transition state, **TS2**. This transition state is 6.7 kcal/mol uphill from the radical intermediate. As described above, the intersystem crossing is computed to occur after the second transition state is traversed to give the energetically more favorable and chemically more intuitive ^{11}A state with two Fe(III) d^5 centers coupling ferromagnetically. Mulliken spin densities of the radical intermediate **I** and the second transition state **TS2** indicate that there is an electron-transfer component in the step **I** → **TS2**. The amount of unpaired electron spin at the methyl moiety decreases by 0.26 and 0.17 electron on the ^{9}A and ^{11}A surfaces, respectively. Note that the relative orientation of the unpaired electron on the methyl group is not the same. Whereas the spin is parallel to that of the ferromagnetically coupled iron centers in the case of the ^{11}A state, it is antiparallel for the ^{9}A state. Consequently, an α-electron is transferred from the CH_3 moiety to Fe1 in the ^{11}A case, whereas there is a β-electron transfer on the ^{9}A surface. The spin density at the electron acceptor, Fe1, increases by 0.39, from 3.58 to 3.97, for the ^{11}A case whereas it decreases by 0.28, from 3.51 to 3.23, for the ^{9}A state. The former spin flux is consistent with a simple electron-transfer mechanism, but the latter describes a chemically meaningless situation. As indicated by the spin density of 3.51, the electron-accepting Fe1(IV) center is in a high-spin state, with all four electrons having α-spin. Therefore, the electronic driving force for accepting an electron originates from the stability of the high-spin Fe(III) configuration with a half-filled d-shell. Transferring a β-electron without the involvement of a spin-exchange mechanism leads to an unreasonable electronic state where, from the five d-electrons of the Fe(III) configuration, two would be paired while three remain unpaired. This situation is impossible for an approximately octahedral Fe(III) center. This peculiar electronic structure progresses further upon completion of the methanol formation, and a spin density of 2.95 is indicated for Fe1 in the final methanol complex on the ^{9}A surface. This scenario can be resolved by considering that intersystem crossing is proposed to occur before **TS-2** is reached in the small model calculations. However, the mid-sized model that should be a better model for the enzymatic environment, as pointed out above, suggests the intersystem crossing to occur after traversing **TS2**. Unfortunately, these details have not been explored to date, and the spin densities of the mid-sized models have not been reported. These considerations further support the notion that the ^{11}A state should be ignored at the early part of the reaction, while the ^{9}A state should be disregarded at the end of the hydroxylation reaction.

In a recent study, the hydroxylation of derivatized methane substrates RCH_3 (R = H, CH_3, F) were examined explicitly using the Morokuma−Basch model.[226] Since the rate-limiting transition state (**TS1**) is characterized by partial cleavage of the C−H bond in all computational models proposed to date, the intrinsic reaction barrier of the C−H activation is expected to decrease as the C−H bonds become weaker[228] in the series of H−CH_3 (104.8 kcal/mol), H−CH_2F (101.3 kcal/mol), and H−CH_2CH_3 (100.5 kcal/mol), assuming that essentially the same mechanism remains valid. In good agreement with these expectations, Musaev et al.[226] reported activation energies of 21.8, 18.8, and 18.5 kcal/mol for H−CH_3, H−CH_2F, and H−CH_2CH_3, respectively. The energy difference of ∼3 kcal/mol between methane and ethane would translate into 2 orders of magnitude faster reaction kinetics for ethane compared to methane at room temperature. Experimentally,[148,150] no appreciable rate differences have been determined for methane and ethane hydroxylation reactions (Table 3). These computational results therefore support the hypothesis derived from experimental KIE studies that a different process, such as substrate binding, becomes rate-limiting in the case of ethane.

Although the quantitative confirmation of the transition-state energy trends as a function of C−H bond strength is reassuring, the details of the hydroxylation mechanism for the ethane and fluoromethane suggested by Musaev et al.[226] are dramatically different from the original mechanism for the methane hydroxylation reaction. Figure 10 shows the proposed structures for the "bound-radical" intermediate species and the final product complexes.

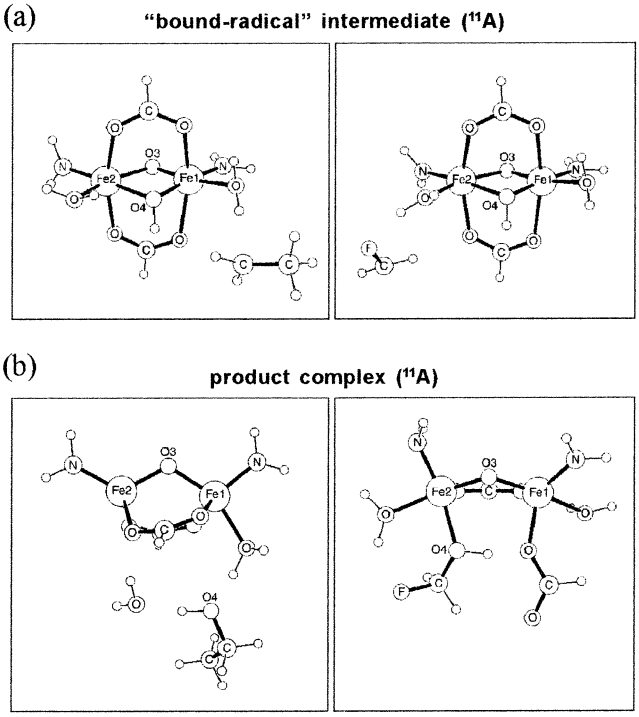

Figure 10. Structures for (a) bound-radical intermediate and (b) final product complex for the derivatized methane substrates RCH_3 (R = CH_3, F) proposed by Morokuma et al.[226] Note that (a) and (b) use different perspectives for clarity. The figures in (b) show a view that is approximately orthogonal to what constituted the Fe_2O_2 plane in (a).

Whereas the intersystem crossing from the ^{9}A state to the ^{11}A state was found to occur after traversing the second transition state **TS2** when methane is the substrate, for both C_2H_6 and CH_3F the intersystem crossing is computed to take place between the first transition state and the "bound-radical" intermediate state. The ^{11}A state intermediate is preferred by 2.6 and 3.2 kcal/mol for C_2H_6 and CH_3F, respectively, while energetic degeneracy or a slight preference was computed for the ^{9}A state intermediate when methane was used as substrate. Interestingly, the "bound" character of the radical in the intermediate structure is also lost for these two substrates. The distance between the hydrogen of the newly formed bridging hydroxyl group and the radicaloid carbon is 3.43 and 6.11 Å, respectively. Last, substantial and different structural changes are proposed for the two substrates once the C−O bond is formed to give the alcohol. Unlike in the case of methane, where all ligands except the bridging oxo (labeled O4 in all figures) remain bound and largely maintain their ligand position, affording an approximately octahedral coordination geometry around each of the iron center, formation of ethanol is proposed to lead to cleavage of an additional Fe−O bond, giving rise to a four-coordinate iron center (Fe2 in Figure 10b) in a distorted tetrahedral geometry. The essentially "free" water ligand shown in Figure 10b is a model ligand for a glutamate moiety. Similar dramatic structural changes are proposed for the product complex containing CH_2FOH. In this case, the Fe−O bond of one of the two bridging carboxylate groups is broken. Interestingly, the now terminal carboxylate changes its ligand position from axial to equatorial while the second oxo ligand, labeled O3 in Figure 10, rotates up to become "axial". The newly formed alcohol (CH_2FOH) acts as a tightly bound ligand of Fe2, with an Fe−O4 distance of 2.08 Å. Both iron centers display a distorted square-pyramidal coordination geometry. A more detailed analysis that might explain and describe the different electronic structures, which are expected to be substantial given the range of different coordination geometries (distorted octahedral, tetrahedral, and square-pyramidal) adopted by the iron centers, was not reported.

4.7. Siegbahn Model

Siegbahn reported one of the first rigorous attempts[229] in the literature to compute the electronic structure of the key intermediate **Q**. In these early studies, a highly simplified model of the diiron core was constructed using formate as the bridging ligand. Water and hydroxide were used to model all terminal ligands of the first coordination sphere, affording a model with an overall neutral net charge. Although a number of structural features established for the diiron core of **Q** could be predicted with good qualitative success, the key structural feature of an unusually short Fe−Fe distance of 2.46 Å, suggested on the basis of EXAFS data,[201] could not be reproduced. The simple model gave a distance of 2.79 Å. In a systematic search for alternative structural motifs that would give rise to a better agreement between theory and experiment, a model for **Q** with two bridging carboxylate ligands was proposed, displaying an Fe−Fe distance of 2.54 Å.[230] In recent years, the Siegbahn model has undergone significant refinements,[231−235] and the latest system contains as many as 60 atoms and uses imidazole and formate ligands to represent the histidine and glutamate residues, respectively. Inspired by a study by Friesner et al.[189] (vide infra), the structural motif of two bridging carboxylate ligands was reinvestigated, and the latest model[236] contains only one bridging carboxylate group; the second bridging ligand has undergone a carboxylate shift to become terminally bound to one of the iron centers, as was suggested by Friesner et al. This new structure was found to be 10 kcal/mol lower in energy than the former model of **Q** that contained two bridging carboxylate ligands. The treatment of the magnetic coupling between the two iron centers has also been revised. While the first two model generations ignored the experimental data and used ferromagnetic coupling for all intermediates along the reaction path, the latest model incorporates antiferromagnetic coupling via broken-symmetry orbitals for the reactant **Q** and product (methanol complex).

Despite the structural resemblance and the fact that antiferromagnetic spin-coupling was included, which are both features that had been pointed out by Friesner, Lippard, and co-workers to be crucial in recent years, the latest mechanism proposed by Siegbahn displays a number of features that are significantly different from the mechanism put forth by Friesner, Lippard, and co-workers. Siegbahn's proposal for the methane hydroxylation reaction mechanism is shown in Figure 11. Unlike in the works of any other researchers, a new key intermediate is proposed to exist, labeled as **Q′** in Figure 11, which is the actual reactive species carrying out the oxidative activation of the C−H bond. When compared to the AF-coupled **Q**, **Q′** is characterized by a structural distortion leading to an asymmetric Fe_2O_2 core and ferromagnetic coupling of the two iron centers. The transformation of **Q** to **Q′** requires formally an intramolecular electron transfer to give a mixed-valence Fe(III)−Fe(IV) species and an intersystem crossing from the AF-coupled configuration space to that of a F-coupled potential energy surface. This transformation is crucial for the proposal, because it offers answers to a number of key questions in the C−H activation process, such as the problem of transferring two electrons of opposite spin to a ferromagnetically coupled diiron core of **Q′** that serves as a two-electron acceptor. Figure 12 shows schematically and in intuitively understandable steps the different electronic reconfigurations required to obtain **Q′** starting from **Q**. Note that this is a simple illustration of the required transformations and does not suggest a precise mechanistic chain of reactions. The original studies by Siegbahn have not addressed the kinetics and the exact mechanistic pathways that might give access to **Q′**, as indicated by the dotted line connecting the two intermediates **Q** and **Q′** in Figure 11. The first required event is an intramolecular β-electron transfer from one of the lone-pair orbitals of the bridging oxo groups to the Fe2 center to generate a α-radicaloid oxygen at the bridging oxo

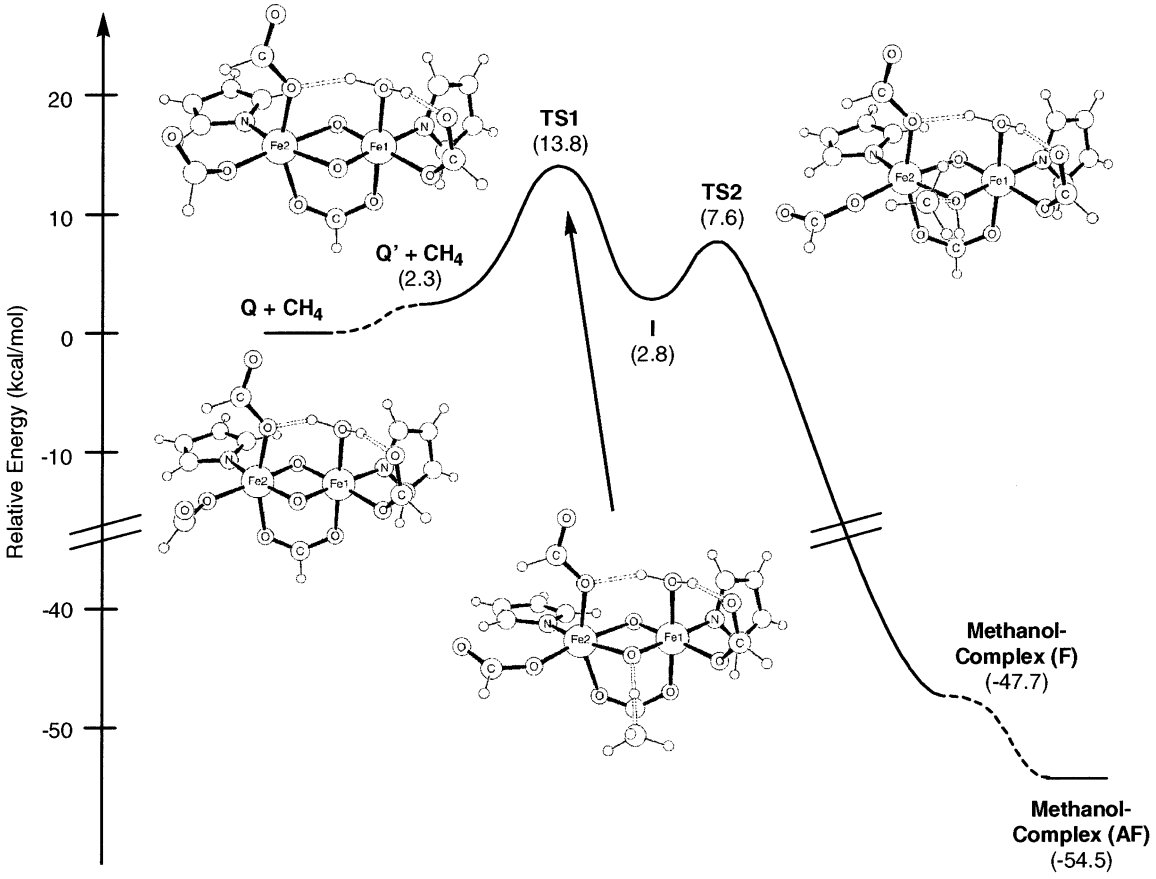

Figure 11. Methane hydroxylation reaction energy profile proposed by Siegbahn.[236]

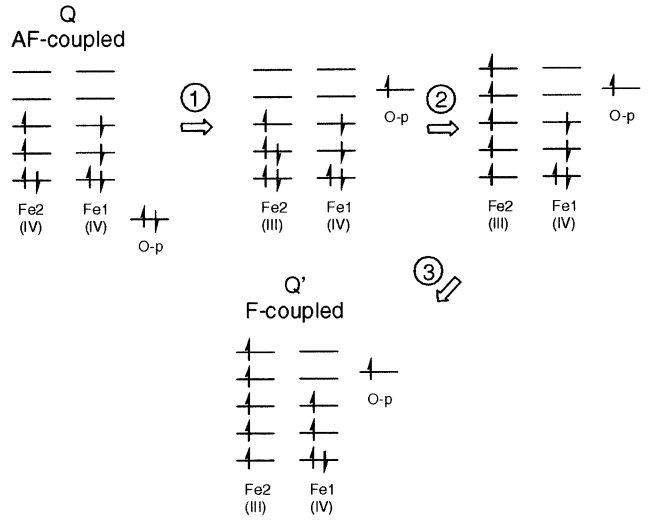

Figure 12. Schematic illustration of the electronic reconfigurations necessary to transform **Q** to **Q′** in the Siegbahn model.

moiety. Since the Fe2 center is the site with an excess of α-electrons in the antiferromagnetically coupled model of **Q**, the injection of a β-electron gives formally a low-spin Fe2(III) center. The next logical step toward **Q′** is an intersystem crossing involving the promotion of two β-electrons to the α-orbital space, resulting in an Fe(III) high-spin configuration of Fe2. It is important to recognize that this serves the same purpose as the intersystem crossing proposed by Morokuma an co-workers. Unlike in the Morokuma model, this crucial step, necessary to allow the accommodation of the two redox-active electrons with opposite spin, is proposed as a part of the preparation process of the active species **Q′**. In the Morokuma model this step was computed to occur late in the chain of reactions. The last logical step is another intersystem crossing that flips all unpaired spins at Fe1 to give an intermediate-spin Fe(IV) center, which is now coupled ferromagnetically to the second, high-spin Fe(III) center. The electronic structure of **Q′** is remarkable in view of the fact that it not only is an Fe(IV)−Fe(III) mixed-valence complex but also constitutes a diiron system with one iron center displaying high-spin and the other intermediate-spin iron centers. Surprisingly, the overall energy difference between **Q** and **Q′** is negligibly small, 2.3 kcal/mol. The kinetics of the required electronic reconfigurations, which is likely to be a challenging task to model in the DFT framework, were not explored. The result of this complex transformation is a redox-active iron dimer capable of promoting the two-electron oxidation of methane without further complications. The first electron transfer involves the β-electron from the C−H σ-bond in a classical proton-coupled electron-transfer reaction with an activation energy of 13.8 kcal/mol. The spin density analysis reveals that this first step is a highly localized process between the C−H bond and the radicaloid oxo bridge to give a radical intermediate, labeled **I** in Figure 11. The second electron transfer is coupled to a migration of the CH_3 radical to attack the bridging hydroxyl group, which completes the C−O bond formation to give the final product. The last step is another

intersystem crossing between the ferromagnetically coupled Fe(III)−Fe(III) ^{9}A state to an Fe(III)−Fe(III) ^{11}A state, where both iron centers become high-spin metal sites with five unpaired metal d-electrons, respectively.

In evaluating this proposal, it is important to recognize that a significant portion of the mechanistic details might simply be the result of technical limitations of the computational procedure. The bias toward the ferromagnetically coupled intermediates is a reflection of this computational procedure. In principle, the antiferromagnetic analogues of the transition states and intermediates, which would eliminate the highly complicated intersystem crossings and reconfigurations, would also have to be considered and the relative energies between the optimized structures compared to find the lowest energy procedure. Due to technical problems, the antiferromagnetically coupled analogues have not been considered properly for all species examined along the reaction energy profile. The unusual mixed-valence systems, where high-spin and intermediate-spin metal centers are proposed to coexist along the reaction profile, require some justification. Intuitively, it is unclear how such dramatically different ligand field strengths can be generated by the nearly identical set of ligands that surround each of the metal centers.

A related but simpler question is concerned with the actual electronic configuration of **Q**. As mentioned above, the experimental data do not allow for distinguishing between the intermediate- and high-spin situations with two or four unpaired electrons on each of the iron centers, respectively. Recently, Noodleman[190] investigated the equilibrium structures and relative energies of these two possibilities in both F-coupled and AF-coupled frameworks based upon the doubly bridged structural motif proposed earlier by Siegbahn. Table 5 summarizes the most important results. The AF-coupled high-spin model is found to be the lowest energy species, and the AF-coupled intermediate-spin analogue used in the latest Siegbahn model is computed to be 7.5 kcal/mol higher in energy. Interestingly, the F-coupled species is 3.5 kcal/mol lower in energy than the AF-coupled model when the intermediate spin state is considered, whereas AF coupling is preferred by 11.8 kcal/mol over the F-coupled alternative when both iron centers are assumed to be in a weak ligand field, thus giving the high-spin case. The agreement between the optimized core structure and that suggested by EXAFS experiment[201] improves notably when intermediate spin is assumed. The best match of the Fe−Fe distance with the experimental estimate of 2.46 Å is obtained using the AF-coupled intermediate-spin case, where the Fe−Fe distance is optimized to be 2.42 Å. All other cases considered show a larger Fe−Fe separation with the lowest energy structure, the AF-coupled high-spin dimer, displaying a separation of 2.63 Å. Given the relative energies of the four species considered, the structural mismatch of the AF-coupled high-spin system appears tolerable, however.

Table 5. Structural and Energetic Comparison of Intermediate-Spin (IS) and High-Spin (HS) Models of Q Coupled Both Ferromagnetically (F) and Antiferromagnetically to Each Other, Computed by Noodleman et al.[190]

	spin states/ magnetic coupling			
	IS/AF	IS/F	HS/AF	HS/F
Fe−Fe distance (Å)	2.42	2.58	2.63	2.73
Mulliken spin population Fe1[a]	−1.27	1.50	2.54	2.99
Mulliken spin population Fe2[a]	1.27	1.54	−2.72	3.07
ΔE (kcal/mol)	7.53	3.99	0.00	11.82
J (cm^{-1})	−118		−376	

[a] Spin densities of 1.3−1.5 and 2.5−3.0 indicate intermediate-spin and high-spin cases with formally two and four unpaired electrons, respectively. While these Mulliken spin densities are somewhat low compared to those found in other studies, where 3.2−3.8 have been routinely observed for high-spin Fe(IV), they are still in a fully consistent and expected range and reflect the usual variation of the absolute number with the basis set and other technical parameters.

A last interesting feature of the Siegbahn model mentioned here concerns the *trans*-2-phenylmethylcyclopropane (**4** in Scheme 2) probe experiments. Siegbahn offered a unique explanation for the unusually short lifetime of the radical intermediate that was deduced from these studies. Using methylcyclopropane as a representative model substrate, Siegbahn argued that the energy of the second transition state would be substantially lowered compared to the reaction profile obtained for the methane substrate, giving rise to a mechanism that is quite different from the methane reaction, possibly avoiding the radical intermediate state altogether and proceeding via direct insertion of the oxygen moiety into the C−H bond. Unfortunately, an extensive analysis of this hypothesis has not appeared to date and remains an area of future work. Recognizing that the ionization potential of the cyclopropylcarbinyl radical, which was computed to be 151 kcal/mol for methylcyclopropane, is significantly lower than that of the methyl radical (229 kcal/mol), it was further determined that the second electron transfer is significantly enhanced in the case of the probe compared to the methane substrate. Although not rigorously examined, some theoretical evidence led to the suggestion that ionization of the cyclopropylcarbinyl radical takes place readily to give a cationic species. This process would explain the *trans*-2-phenylmethylcyclopropane probe results and consequently discredit the suitability of such probes as a mimic of the methane reaction, because they change the reaction mechanism in a decisive manner.

4.8. Friesner−Lippard Model

A distinctively different approach to computer model design has been adopted by Friesner, Lippard, and co-workers.[162,189,237−241] These authors made use of the crystal structure of $MMOH_{red}$,[31] one of two components of the catalytic cycle for which X-ray crystal structures are available, and attempted to reproduce the structural features of $MMOH_{red}$ by systematically increasing the size of the computer model. The core structure could not be reproduced successfully with small models, as found before by others. For example, the small model used in the

Morokuma−Basch studies, with NH_2^- ligands representing histidine and H_2O groups representing glutamate residues, mentioned above, was also used previously as a model for $MMOH_{red}$.[223] The Fe−Fe distance, which is considered one of the main characteristic structural features, is experimentally observed to be 3.3 Å in X-ray crystal structure studies.[31] The small model system gave an Fe−Fe distance of 4.56 Å, indicating that a very different species is obtained in these studies. Friesner, Lippard, and coworkers observed that the diiron core structure found in the crystal structure (Figure 2) is enforced by a network of hydrogen bonds and structural strain from the protein environment that could be reproduced accurately in a simulation only by using a large-scale model containing approximately 100 atoms.[189] Recently, the structures and the exchange-coupling behavior of the diiron core in the oxidized and reduced forms of the enzyme ($MMOH_{ox}$ and $MMOH_{red}$ in Scheme 1) have been reexamined in detail by Noodleman and co-workers using the BS formalism and taking the protein field energies into account by embedding the fully quantum mechanically optimized structures into the protein, the charges of which are allowed to interact with the quantum mechanical Fe_2O_2 entity.[242−244] These authors confirm that the protein environment has an appreciable impact on the energetics of the active site, supporting the view that modeling the enzymatic catalysis with a minimum-sized computational model with dramatic simplifications of the electronic structure at the active center is not appropriate. The first part of the catalytic cycle of MMO, involving the activation of dioxygen to prepare the reactive intermediate **Q**, is not discussed in this review, but Figure 13 shows an illustration of the structural models of

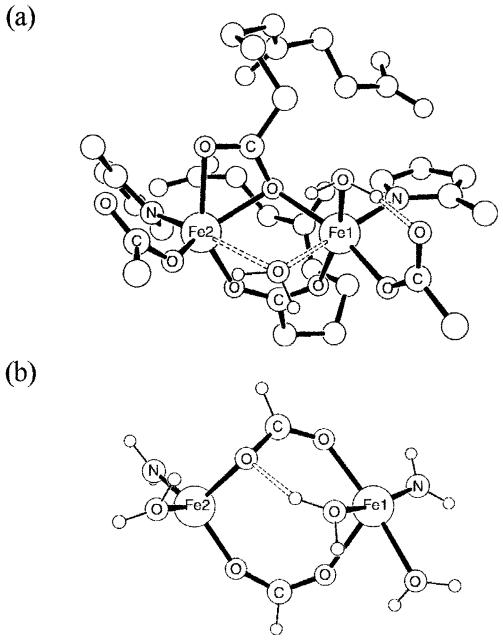

Figure 13. (a) 100-atom model of $MMOH_{red}$ (Friesner−Lippard).[189] Some hydrogen atoms are not shown, for clarity. (b) Small model of $MMOH_{red}$ (Morokuma−Basch).[223]

$MMOH_{red}$ obtained using the large-scale model in the Friesner−Lippard studies and that obtained using a minimum size model in the Morokuma−Basch studies. Comparing the large-scale model to the X-ray crystal structure, illustrated in Figure 2, two important structural features were reproduced: (i) the computed Fe−Fe distance is 3.5 Å, which is in good agreement with the X-ray crystal structure value, and (ii) the distinctive bridging coordination mode of Glu243 is obtained properly. Upon reduction of the computer model size to ∼60 atoms, loss of the bridging mode and substantial increase of the iron−iron distance were observed. Consequently, the large-scale model was used in all subsequent studies.

A second emphasis was concerned with the spin-coupling between the metal centers, and antiferromagnetic coupling in **Q** was included in the model explicitly using the broken-symmetry orbital approach. The proposal for the structure of **Q** is shown in Figure 14. The conclusion from the EXAFS experiment that the coordination number around each iron centers is not greater than 5 could not be supported in this model. The authors argued that the accuracy of the EXAFS experiment cannot rule out unambiguously a six-coordinate iron center. A five-coordinate iron center was calculated to be impossible if one includes two histidines and four glutamates, of which at least one remains as a bridging ligand, bound to the iron centers. In addition, two bridging oxo groups, resulting from reductive dioxygen activation, have to be included as ligands. To obtain a five-coordinate structure for **Q**, at least one of the ligands has to dissociate and move out of the active site. Both the Fe−O and Fe−N bonds formed between the metal and the glutamate and histidine ligands, respectively, are strong and were not calculated to be available for possible dissociation. In addition, removal of the carboxylate ligands would give rise to a charge imbalance and create a cationic diiron unit, which is highly unfavorable in the hydrophobic environment. In conclusion, the pseudo-octahedral environment was found to be the most realistic coordination geometry for each iron centers. Unlike in the small model studies, the carboxylate group of Glu243 is proposed to undergo a carboxylate shift. The open coordination site on Fe1 is occupied by a tightly bound water, creating nonidentical ligand environments for the two iron centers. The water ligand is stabilized by a hydrogen bond network between Glu243 and Glu114, which in turn enforces the orientation of the carboxylate ligands in the course of the reaction.

The hydroxylation mechanism proposed on the basis of this large-scale model of **Q** is shown in Figure 14. The reaction starts with nucleophilic attack of the methane substrate at the bridging oxo moiety. The rate-determining step involves a proton-coupled transfer of the first electron with an activation enthalpy of 17.9 kcal/mol. A detailed molecular orbital analysis has revealed that this PCET is strongly coupled to structural distortion of the (μ-oxo)diiron core, which facilitates an intramolecular electron transfer from the bridging oxo group to Fe2. After traversing the first transition state, two channels were discovered to exist. The first pathway is, in principle, a recoil/rebound mechanism. After completion of the PCET,

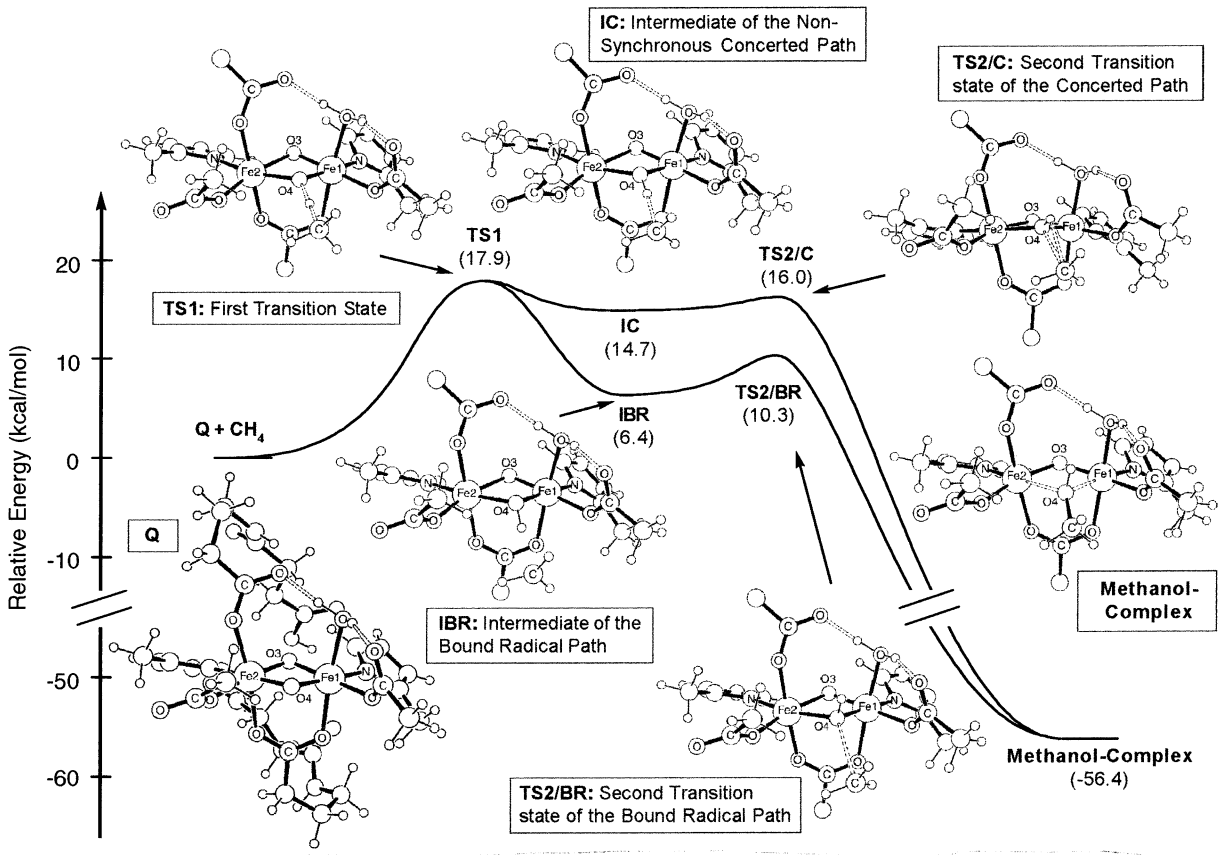

Figure 14. Methane hydroxylation mechanism proposed by Friesner, Lippard, et al.[237] The full model (~100 atoms) is shown for **Q**. In all other structures, only the most important core structure is displayed, for simplicity.

an intermediate is formed with the methyl radical recoiled to a position with an O—H···C distance of 1.97 Å. This distance is unusually short and does not allow free motion of the methyl radical; thus, the pathway has been characterized as a "bound-radical" pathway. The consideration of such a bound radical was suggested by experiments using the chiral ethane substrate, CH_3CHDT,[134,135] which revealed a 2:1 ratio of retention to inversion in the chiral ethanol products (vide infra). Since ethane racemizes typically in less than 100 ps in gas phase, one possible explanation for the experimental observations was a reduced degree of rotational freedom by a weak interaction of the radical substrate fragment with the diiron core. The pathway in the Morokuma—Basch model has also been labeled as a "bound-radical" mechanism. It is important, however, to recognize a significant difference between these two proposals. In the Friesner—Lippard model, the methyl radical recoil motion is substantially hindered in the bound-radical intermediate (**IBR**), while the Morokuma—Basch model predicted an O—H···C distance of 3.47 Å using the mid-sized model,[226] which is significantly longer than the distance of 1.97 Å predicted in the Friesner—Lippard model. In the case of the ethane and fluoromethane substrates, the distances are predicted to be 3.43 and 6.11 Å, respectively, in the Morokuma—Basch model.[226] A mechanism involving a radical substrate intermediate at distances of 3.47 Å from the active site that is well separated from the final product by an energetic barrier of 6.3 kcal/mol (Figure 9), as is the case for the methane substrate, can be interpreted only as a free radical recoil mechanism. For such a mechanism, full racemization of the chiral ethane probe should take place, although the authors have labeled this a "bound-radical" mechanism to reflect the experimentally observed retention of configuration described in section 2.5.

The next step of the bound-radical pathway in the Friesner—Lippard model is the formation of a C—O bond accompanied by a second electron-transfer reaction. The second transition state, labeled **TS2/BR**, is 3.9 kcal/mol uphill from the intermediate species and leads to a highly exothermic completion of the hydroxylation step to give the final methanol complex. A distinctive feature of the Friesner—Lippard model is the existence of a second reaction channel, labeled the "nonsynchronous concerted" pathway (Figure 14), where the recoil motion of the radicaloid methyl group is further suppressed compared to the bound-radical pathway. The intermediate of this second channel, **IC**, is 8.3 kcal/mol higher in energy than the bound-radical intermediate. Both pathways proceed in a very similar fashion to complete the overall two-electron redox process. In the bound-radical pathway, the bridging O—H group formed in the first step rotates upward and exposes the oxygen moiety toward the methyl radical fragment, which forms the C—O bond in a radical recombination-type mechanism to complete the hydroxylation process. The same motion is also present in the second, concerted pathway, with the methyl fragment being tightly connected to the hydroxo group at all times. The barrier for this reaction is

negligibly small, 1.3 kcal/mol. Both channels are available for the second redox reaction, and the preference for using one or the other will depend on the actual substrate. In most cases, however, both channels will be utilized because they are very close in energy. Rather than being two different mechanisms, the two computed pathways are proposed to be upper and lower limits both mechanistically and energetically, with the true reaction being an admixture of the two extreme cases. The nonsynchronous concerted channel, which is the higher energy pathway, will give rise to extremely short lifetimes of the radicaloid substrate fragments. The bound-radical pathway displays a slightly higher barrier for the C−O bond formation of 3.9 kcal/mol. These two features are key elements of the proposal and provide an explanation for the experimentally observed product distribution when chiral ethane is used as substrate. The Friesner−Lippard model is in good agreement with these experiments, which suggest a shallow potential well for the radical intermediate. The "bound-radical" mechanism proposed in the Morokuma−Basch model suggested a notably higher barrier of 6.9 and 9.5 kcal/mol for the second step using the medium and small model systems, respectively. The proposal of a radical intermediate that is not a discrete entity, but rather a "bound radical" with a significantly reduced lifetime, is a qualitatively intuitive possibility that follows from the radical clock experiments.

To quantify explicitly the correlation between the theoretical proposal and the chiral ethane experiments, the Friesner−Lippard model has been subjected to semiclassical molecular dynamics (MD) simulation[240] using the quantum mechanically computed potential energy surfaces. The reaction energy profiles and intermediate structures computed using methane and ethane as substrates, respectively, are very similar. The energy of the intermediate **I** is ∼4 kcal/mol lower when ethane is used as the substrate, owing to the inductive effect of the additional methyl group that stabilizes the radical intermediate. Including zero-point energy corrections, which amounts to approximately 2 kcal/mol, the transition state **TS1** was predicted to be also lower in energy by 3.5 kcal/mol for ethane.

The two-channel mechanism provides a unique explanation for the observation of both configuration retention and inversion at the chiral center of the substrate. For the nonsynchronous concerted mechanism, where the recoil motion of the radical fragment is severely suppressed, only retention is expected at the chiral center. The bound-radical channel with significant recoil/rebound motion would give rise to both inversion and retention, depending on the lifetime of the radical and the time needed to complete a rotation around the C−C axis. The MD simulations revealed that 16.5% of ethane hydroxylation occurs along the concerted pathway, while the rest follows a radical recoil/rebound-type mechanism. The mean lifetime of the ethyl radical is computed to be 320 fs. Since rotation around the C−C axis that would give rise to racemization is expected to be a rapid process, and total racemization of the ethyl radicals in the gas phase is complete in less than 100 fs, the bound-radical pathway is expected to result in a significant amount of racemized product distribution. The degree of racemization is, of course, dependent on the extent of the recoil motion, which in turn dictates the rotational degree of freedom by relaxing the steric hindrance imposed on the ethyl radical at short C···O distances. Figure 15 shows a

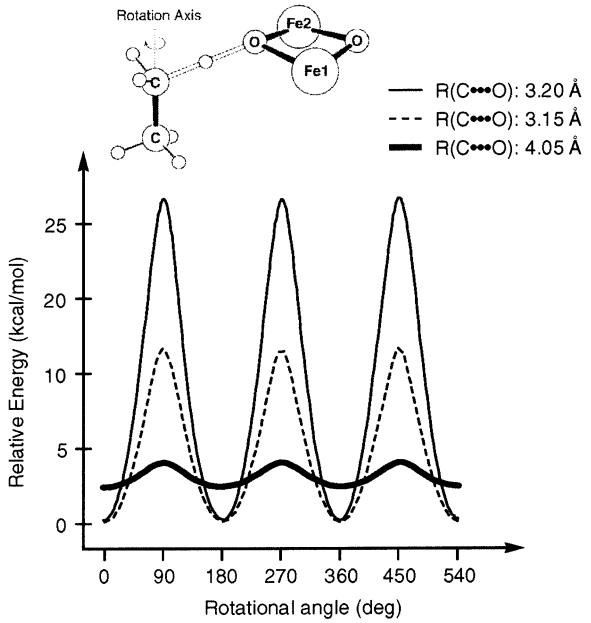

Figure 15. Energy profile for the rotational motion of the ethyl fragment at different C−O distances in the bound-radical intermediate structure. (Reprinted with permission from ref 240. Copyright 2002 American Chemical Society.)

plot of the potential energy surface with respect to rotations around the C−C axis at different distances of the radicaloid ethyl carbon and the oxygen atom from the bridging hydroxide group.

Rotation around the C−C axis is heavily hindered at the computed intermediate structure with a C···O distance of ∼3 Å. Even at a slightly larger distance of 3.2 Å, the rotation barrier is approximately 26 kcal/mol. However, the MD simulation shows that there is a periodic motion along the C···O vector present, resembling a harmonic vibration with a period of ∼200 fs. Half of this period is spent at a C···O distance longer than the 3 Å, computed for the static structure of the bound-radical intermediate. At the outer limit of this motion, where the C···O distance has been increased to 4 Å, the ethyl radical can rotate essentially freely with a barrier of less than 2 kcal/mol (Figure 15). This result provides two significant conclusions. First, the racemization process is suppressed by hindrance of free rotation of the radical fragment, which is another logical characteristic of a bound radical. Second, although the lifetime of the radical has been estimated to be ∼320 fs, only at substantially elongated C···O distances does the radical fragment behave like a distinctive radical with the upper limit of ∼100 fs, which corresponds to half of the "harmonic" period that moves the radical species out of the bound position. Thus, radical clock probes such as *trans*-phenylmethylcyclopropane are not expected to indicate the presence

of radicals. Integrating over the ethyl C−C axis rotational coordinate along the time axis, the configuration retention was predicted to be 69−84%, depending on the initial recoil energy of the radical fragment, which is in good agreement with the experimentally observed retention of 72% using *R*-chiral ethane.

To derive a more qualitative understanding of the molecular features promoting the catalytic reaction, the electronic structure changes of the large-scale model along the reaction pathway were examined recently in a detailed molecular orbital analysis study.[241] A schematic MO diagram of **Q** as computed in the Friesner−Lippard model is shown in Figure 16. There are significant differences between this MO

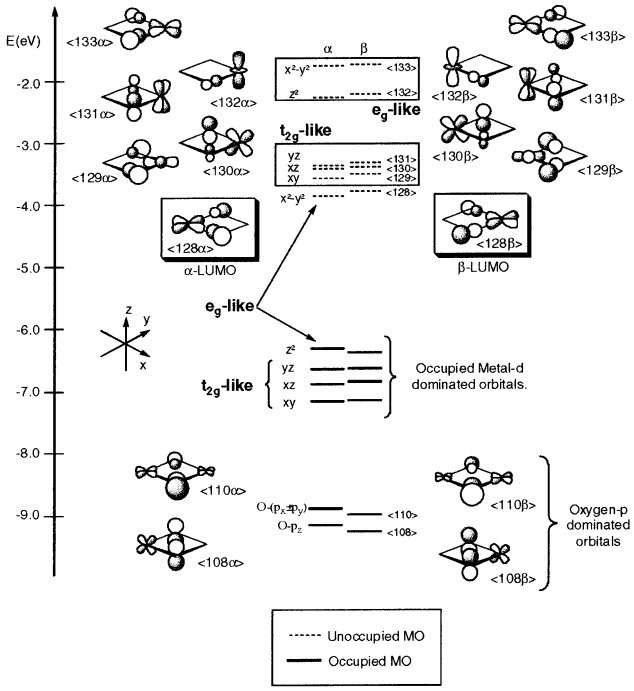

Figure 16. Schematic molecular orbital diagram of **Q** derived using the Friesner−Lippard model and the broken-symmetry orbital approach. (Reprinted with permission from ref 241. Copyright 2002 American Chemical Society.)

diagram and that suggested by Yoshizawa and co-workers. First, the high-spin configuration at both iron centers is reflected in the occupation of eight metal-based MOs with a single electron. It is important to recognize that the unrestricted spin calculation gives rise to two sets of MOs with a maximum occupation number of one electron each. Second, the use of broken-symmetry orbitals gives rise to much more localized MOs compared to the classical MOs analyzed by Yoshizawa and co-workers. To understand the orbital shapes and relative energies of the MOs intuitively, the coordination geometry around each of the iron centers was taken as approximately octahedral. The structure motif of the diiron complex can then be assembled by connecting the two octahedra in an edge-sharing fashion. This simple analysis is generally valid but is particularly appropriate for broken-symmetry orbitals where the usual delocalization by forming in-phase and out-of-phase combinations of the d-atomic orbitals from each of the metal centers is suppressed by default. If the *x*- and *y*-axes are chosen to lie along the bonds between the iron atom and the bridging oxygen atoms, the MO diagram can be understood as a straightforward extension of the familiar t_{2g} and e_g MOs centered around each of the metal centers. Consequently, the HOMOs in both the α- and *β*-orbital spaces are d_{z^2}-dominated MOs, whereas the LUMOs can be recognized as the corresponding $d_{x^2-y^2}$-dominated orbitals that would be expected for a simple d^4-Fe(IV) configuration in an octahedral ligand environment.

Most important for understanding the electronic features of the oxidative activation of the C−H bond are the LUMOs, which serve as acceptors of the electrons originating from the *σ*-bond of the substrate. As shown schematically in Figure 16, the oxygen p-orbitals that are in the Fe_2O_2 plane mix significantly with the metal-based LUMOs and form the electronic basis for reactivity involving a nucleophilic attack at the bridging oxo group. As expected, the LUMO is Fe−O antibonding. The bonding combination MO-⟨110⟩ occurs at substantially lower energy and is dominated by the oxygen p-orbital. This MO is the major constituent of one of the two lone pairs expected for the bridging oxo group. A detailed electronic structure analysis revealed that there is strong coupling between a structural distortion of the Fe_2O_2 core that accompanies the substrate binding at the bridging oxo group and an intramolecular electron transfer. The structural distortion observed at the first transition state **TS1**, which involves an elongation of the Fe2−O4 bond upon substrate binding, is strongly coupled to intramolecular electron transfer from the oxygen-based lone pair MO-⟨110⟩ to the α-LUMO, MO-⟨128α⟩, creating formally a radicaloid oxygen that serves as the direct reaction partner for the hydrocarbon substrate. The intermediate species of both the concerted and bound-radical pathways display unpaired electron density on the methyl fragments. Since this is the result of the first electron transfer from the doubly occupied *σ*-bond between carbon and hydrogen, which involved the α-spin electron, the remaining unpaired electron density is *β*-spin in nature. The antiferromagnetic coupling between the metal centers becomes crucial to connect smoothly the potential energy surfaces of the first and second electron transfers. In the Friesner−Lippard model, the α- and *β*-LUMOs are centered around each of the metal sites, respectively. Thus, whereas the α-electron of the C−H bond was transferred to Fe2 in the first step, the second electron transfer involves the remaining *β*-electron and Fe1, which conveniently is the center of the *β*-LUMO.

The electronic details of the second electron transfer were also studied. The key structural motion in this step is upward rotation of the newly formed O−H group, which was identified to promote intramolecular electron transfer. This motion maximizes overlap of the remaining oxygen lone-pair orbital (MO-⟨108*β*⟩) with the *β*-LUMO and exposes the oxygen to the methyl fragment to give radical recombination, resulting in O−C bond formation to give methanol. The overall spin state of the system is consistently a

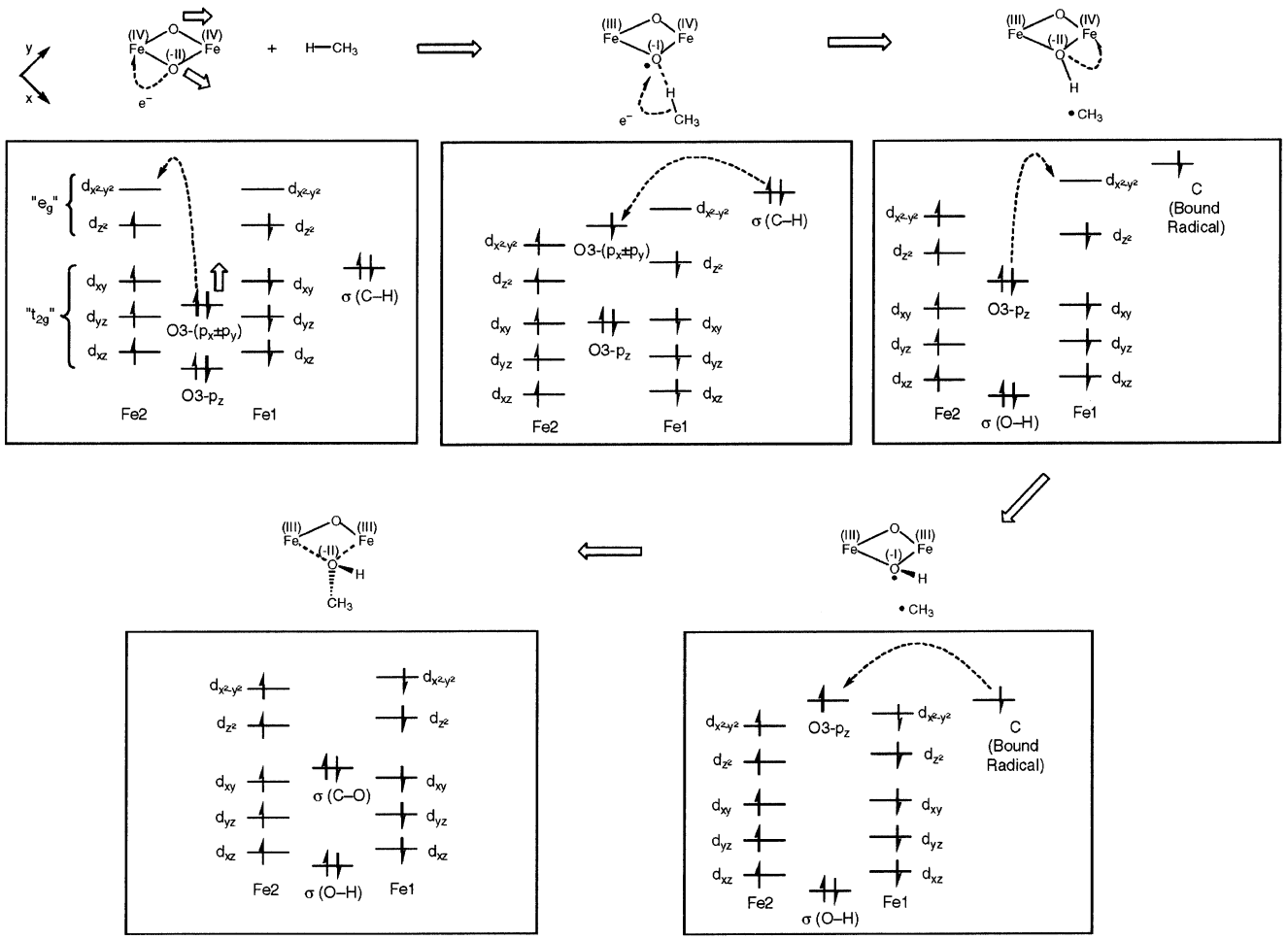

Figure 17. Schematic summary of the electronic changes along the reaction pathway proposed for the Friesner−Lippard model. (Reprinted with permission from ref 241. Copyright 2002 American Chemical Society.)

singlet at all times; consequently, no spontaneous spin flips or spin state crossings are required.

Figure 17 summarizes the electronic features of the whole hydroxylation reaction according to the Friesner−Lippard model. The first step is nucleophilic attack of methane at the bridging oxo group. The electrophilicity of the oxo moiety is greatly enhanced by structural distortion of the diiron core, which can be formally envisioned to promote intramolecular electron transfer. The result is in situ generation of a radicaloid oxygen that carries out the redox reaction. Upon completion of the first electron transfer, the methyl radical moiety can either recoil to follow the bound-radical channel or take the nonsynchronous concerted pathway to complete the reaction. The barriers for this second step are negligibly low in both channels, and the transition states are characterized by rotation of the newly formed O−H group. This motion can be envisioned to promote another intramolecular electron transfer from the second lone-pair orbital of the oxygen atom to the remaining Fe(IV) center, again increasing the electrophilicity of the oxygen moiety, which can react with the methyl radical group to give the final product.

5. Concluding Remarks and Future Directions

In this review we have discussed the experimental evidence for and against the generation of radical intermediates in the reaction of sMMO with methane and related hydrocarbon substrates. The ability to derive unambiguous mechanistic interpretations from substrate probe experiments remains a challenging area of research. A consensus has evolved concerning experimental observations but not the deductions based on these observations. There is agreement that, if transients are formed in sMMO hydroxylations, they are quite short-lived and involve C−H bond homolysis. It is also apparent that some type of cationic species forms in many mechanistic probe studies.

One important question that begs resolution involves results from studies of norcarane oxidations. These probe studies provided seemingly unequivocal evidence for formation of a radical intermediate, but the results contradict studies with chiral substrates and probes that distinguish between cations and radicals as well as the computational results that predict subpicosecond lifetimes for “radicals”. Supporting evidence for the solitary norcarane results should be sought, and the detailed chemistry of the norcarane system might be further explored. Simply stated, if only one piece of unequivocal evidence for radical intermediates can be found in the universe of sMMO studies, then one must conclude that this evidence is unique and that mechanistic generalizations based on it are suspect.

Although there is good experimental agreement that cationic species are involved in some aspect of sMMO hydroxylations, the origins and even the identities of these cationic species are not known. The proposal that cations are formed by oxidation of radical intermediates appears to be flawed. Such an interpretation would require that oxidation reactions occur faster than radical rearrangements, which in some cases have rate constants exceeding 1×10^{11} s^{-1}. Moreover, it is not apparent that an oxidizing species exists after hydrogen abstraction in the computational results. An alternative that has been presented but not yet explored computationally is that a second electrophilic oxidant exists in sMMO, protonated H_{peroxo}, and this species effects oxidation by insertion of OH^+ into a C−H bond to give protonated alcohol products. H_{peroxo} or its protonated product, which cannot be observed spectroscopically, appears to epoxidize propene and other substrates, and further experimental and computational studies of this species might provide important insight. A particular valuable probe would be one that reacted *differentially* with H_{peroxo} and **Q**.

In kinetic isotope effect studies, the large KIEs found for reactions of **Q** with methane conflict with the small KIEs found in k_{cat}. Further work is needed to determine whether the KIE results from **Q** are actually products of an equilibrium binding constant and a rate constant or if the KIE is only in the rate constant of the oxidation reaction. The KIE studies have provided perhaps the most confounding sMMO mechanistic results, and mechanistic conclusions should be withheld until resolution of the KIE contradictions is in hand.

Computational methods have made a significant impact over the past few years in defining a molecular-level understanding of the catalytic cycle. More than in other fields of research, theoretical methods started becoming an equal partner to experimental efforts toward uncovering the mechanistic details of the alkane hydroxylation reaction. Perhaps as a consequence, contradictory conclusions and diverging results have been reported in the recent literature from different groups that follow different philosophies resembling similar trends seen in experimental work. Revisions of model studies, as the computational body of work becomes more sophisticated and more experience is gathered, have taken a promising direction toward sampling different possibilities. So far, some level of agreement has been reached on the following points from computational studies: (1) the reactive site for hydrocarbon oxidation; (2) AF coupling vs F coupling as a determinant in the C−H bond activation pathway; and (3) a bound-radical pathway. These computations are especially valuable, indeed essential, for understanding reactions that are too fast to probe experimentally.

Many challenges remain to be overcome in the future for computational models to become more realistic and provide truly innovative solutions toward a molecular-level understanding of the enzymatic catalysis. The results of the first generation of computational models, reviewed here, will be augmented by larger and more realistic second- and third-generation models. The most recent experimental studies, such as that of the reactions of **Q** with derivatized methane substrates, imply a more complicated interplay of the protein environment and the thermodynamics of the diiron core than had previously been appreciated. Whereas much of the qualitative understanding derived from the purely quantum mechanical studies of small models will most likely prove to be valid to some extent, the sensitive balance of whether substrate uptake and C−H activation becomes rate-limiting cannot be modeled sufficiently with these small models. New technologies for increasing the size of the computational models, such as the combined QM/MM methods, promise more realistic computer models for the future, which will allow for delineating some of the conflicting conclusions that have been highlighted in this review.

6. Glossary of Abbreviations

AF	antiferromagnetic
BS	broken symmetry
CASSCF	complete active space−self-consistent field
CD	circular dichroism
DFT	density functional theory
ENDOR	electron−nuclear double resonance
EPR	electron paramagnetic resonance
ESEEM	electron-spin−echo envelope modulation
EXAFS	extended X-ray absorption fine structure
F	ferromagnetic
FAD	flavin adenine dinucleotide
H_{ox}	MMOH in the Fe(III)−Fe(III) oxidation state
H_{red}	MMOH in the Fe(II)−Fe(II) oxidation state
HOMO	highest occupied molecular orbital
HS	high-spin state
IS	intermediate-spin state
KIE	kinetic isotope effect
LS	low-spin state
LUMO	lowest unoccupied molecular orbital
MD	molecular dynamics
MM	molecular mechanical
MMO	methane monooxygenase
MMOH	hydroxylase component of methane monooxygenase
MMOR	reductase component of methane monooxygenase
MMOB	regulatory component protein of methane monooxygenase
MO	molecular orbital
MP*x*	Møller−Plesset perturbation theory at the *x*th level
NAD^+	nicotinamide adenine dinucleotide, oxidized form
NADH	nicotinamide adenine dinucleotide, reduced form
PCET	proton-coupled electron transfer
pMMO	particulate methane monooxygenase
QM	quantum mechanical
QM/MM	combined quantum mechanical and molecular mechanical method
sMMO	soluble methane monooxygenase

7. Acknowledgment

This work was supported by NIH grants GM48722 to M.N., GM40562 to R.A.F., and GM32134 to S.J.L. This work was partially supported by the National Computational Science Alliance under Grant MCA95C007N and utilized the NCSA SGI/CRAY Origin2000. We thank Professor S. Chan for providing us with the information in ref 144 in advance of

publication and Professors Yoshizawa and Siegbahn for providing the coordinates of the computed structures.

8. References

(1) Hanson, R. S.; Hanson, T. E. *Microbiol. Rev.* **1996**, *60*, 439.
(2) Anthony, C. In *Biology of methylotrophs*; Goldberg, I., Rokem, J. S., Eds.; Butterworth-Heinemann: Stoneham, MA, 1991.
(3) Merkx, M.; Kopp, D. A.; Sazinsky, M. H.; Blazyk, J. L.; Müller, J.; Lippard, S. J. *Angew. Chem., Int. Ed.* **2001**, *40*, 2782.
(4) Feig, A. L.; Lippard, S. J. *Chem. Rev.* **1994**, *94*, 759.
(5) Wallar, B. J.; Lipscomb, J. D. *Chem. Rev.* **1996**, *96*, 2625.
(6) Deeth, R. J.; Dalton, H. *J. Biol. Inorg. Chem.* **1998**, *3*, 302.
(7) Kopp, D. A.; Lippard, S. J. *Curr. Opin. Chem. Biol.* **2002**, *6*, 568.
(8) Liu, K. E.; Lippard, S. J. *Adv. Inorg. Chem.* **1995**, *42*, 263.
(9) Lipscomb, J. D. *Annu. Rev. Microbiol.* **1994**, *48*, 371.
(10) Murrell, J. C.; Gilbert, B.; McDonald, I. R. *Arch. Microbiol.* **2000**, *173*, 325.
(11) Murrell, J. C. *Biodegradation* **1994**, *5*, 145.
(12) Miyaji, A.; Kamachi, T.; Okura, I. *Biotechnol. Lett.* **2002**, *24*, 1883.
(13) Xin, J. Y.; Cui, J. R.; Hu, X. X.; Li, S. B.; Xia, C. G.; Zhu, L. M.; Wang, Y. Q. *Biochem. Biophys. Res. Commun.* **2002**, *295*, 182.
(14) Nguyen, H. H. T.; Elliott, S. J.; Yip, J. H. K.; Chan, S. I. *J. Biol. Chem.* **1998**, *273*, 7957.
(15) Stanley, S. H.; Prior, S. D.; Leak, D. J.; Dalton, H. *Biotechnol. Lett.* **1983**, *5*, 487.
(16) Prior, S. D.; Dalton, H. *J. Gen. Microbiol.* **1985**, *131*, 155.
(17) Gradassi, M. J.; Green, N. W. *Fuel Process. Technol.* **1995**, *42*, 65.
(18) Periana, R. A.; Taube, D. J.; Evitt, E. R.; Löffler, D. G.; Wentrcek, P. R.; Voss, G.; Masuda, T. *Science* **1993**, *259*, 340.
(19) Shilov, A. E.; Shul'pin, G. B. *Chem. Rev.* **1997**, *97*, 2879.
(20) Duetz, W. A.; van Beilen, J. B.; Witholt, B. *Curr. Opin. Biotechnol.* **2001**, *12*, 419.
(21) Tshuva, E. Y.; Lee, D.; Bu, W. M.; Lippard, S. J. *J. Am. Chem. Soc.* **2002**, *124*, 2416.
(22) White, M. C.; Doyle, A. G.; Jacobsen, E. N. *J. Am. Chem. Soc.* **2001**, *123*, 7194.
(23) Fokin, A. A.; Schreiner, P. R. *Chem. Rev.* **2002**, *102*, 1551.
(24) Arakawa, H.; Aresta, M.; Armor, J. N.; Barteau, M. A.; Beckman, E. J.; Bell, A. T.; Bercaw, J. E.; Creutz, C.; Dinjus, E.; Dixon, D. A.; Domen, K.; DuBois, D. L.; Eckert, J.; Fujita, E.; Gibson, D. H.; Goddard, W. A.; Goodman, D. W.; Keller, J.; Kubas, G. J.; Kung, H. H.; Lyons, J. E.; Manzer, L. E.; Marks, T. J.; Morokuma, K.; Nicholas, K. M.; Periana, R.; Que, L.; Rostrup-Nielson, J.; Sachtler, W. M. H.; Schmidt, L. D.; Sen, A.; Somorjai, G. A.; Stair, P. C.; Stults, B. R.; Tumas, W. *Chem. Rev.* **2001**, *101*, 953.
(25) Rappé, A. T.; Skiff, W. M.; Casewit, C. J. *Chem. Rev.* **2000**, *100*, 1435.
(26) Labinger, J. A.; Bercaw, J. E. *Nature* **2002**, *417*, 507.
(27) Crabtree, R. H. *J. Chem. Soc., Dalton Trans.* **2001**, 2437.
(28) Holm, R. H.; Kennepohl, P.; Solomon, E. I. *Chem. Rev.* **1996**, *96*, 2239.
(29) Valentine, A. M.; Lippard, S. J. *J. Chem. Soc., Dalton Trans.* **1997**, 3925.
(30) Rosenzweig, A. C.; Frederick, C. A.; Lippard, S. J.; Nordlund, P. *Nature* **1993**, *366*, 537.
(31) Rosenzweig, A. C.; Nordlund, P.; Takahara, P. M.; Frederick, C. A.; Lippard, S. J. *Chem. Biol.* **1995**, *2*, 409.
(32) Rosenzweig, A. C.; Lippard, S. J. *Acc. Chem. Res.* **1994**, *27*, 229.
(33) Rosenzweig, A. C.; Brandstetter, H.; Whittington, D. A.; Nordlund, P.; Lippard, S. J.; Frederick, C. A. *Proteins—Struct., Funct. Genet.* **1997**, *29*, 141.
(34) Whittington, D. A.; Sazinsky, M. H.; Lippard, S. J. *J. Am. Chem. Soc.* **2001**, *123*, 1794.
(35) Whittington, D. A.; Rosenzweig, A. C.; Frederick, C. A.; Lippard, S. J. *Biochemistry* **2001**, *40*, 3476.
(36) Whittington, D. A.; Lippard, S. J. *J. Am. Chem. Soc.* **2001**, *123*, 827.
(37) Coufal, D. E.; Blazyk, J. L.; Whittington, D. A.; Wu, W. W.; Rosenzweig, A. C.; Lippard, S. J. *Eur. J. Biochem.* **2000**, *267*, 2174.
(38) Elango, N.; Radhakrishnan, R.; Froland, W. A.; Wallar, B. J.; Earhart, C. A.; Lipscomb, J. D.; Ohlendorf, D. H. *Protein Sci.* **1997**, *6*, 556.
(39) Stirling, D. I.; Dalton, H. *Nature* **1981**, *291*, 169.
(40) Stirling, D. I.; Dalton, H. *J. Gen. Microbiol.* **1980**, *116*, 277.
(41) Stirling, D. I.; Dalton, H. *Eur. J. Biochem.* **1979**, *96*, 205.
(42) Stirling, D. I.; Colby, J.; Dalton, H. *Biochem. J.* **1979**, *177*, 361.
(43) Colby, J.; Stirling, D. I.; Dalton, H. *Biochem. J.* **1977**, *165*, 395.
(44) Dalton, H. *Adv. Appl. Microbiol.* **1980**, *26*, 71.
(45) Green, J.; Dalton, H. *J. Biol. Chem.* **1989**, *30*, 17698.
(46) Fox, B. G.; Borneman, J. G.; Wackett, L. P.; Lipscomb, J. D. *Biochemistry* **1990**, *29*, 6419.
(47) Andersson, K. K.; Froland, W. A.; Lee, S. K.; Lipscomb, J. D. *New J. Chem.* **1991**, *15*, 411.
(48) Rataj, M. J.; Kauth, J. E.; Donnelly, M. I. *J. Biol. Chem.* **1991**, *226*, 18684.
(49) Jin, Y.; Lipscomb, J. D. *J. Biol. Inorg. Chem.* **2001**, *6*, 717.
(50) Bosma, T.; Janssen, D. B. *Appl. Microbiol. Biotechnol.* **1998**, *50*, 105.
(51) Fox, B. G.; Froland, W. A.; Dege, J. E.; Lipscomb, J. D. *J. Biol. Chem.* **1989**, *264*, 10023.
(52) Colby, J.; Dalton, H. *Biochem. J.* **1978**, *171*, 461.
(53) Woodland, M. P.; Dalton, H. *J. Biol. Chem.* **1984**, *259*, 53.
(54) Gassner, G. T.; Lippard, S. J. *Biochemistry* **1999**, *38*, 12768.
(55) Kopp, D. A.; Gassner, G. T.; Blazyk, J. L.; Lippard, S. J. *Biochemistry* **2001**, *40*, 14932.
(56) Blazyk, J. L.; Lippard, S. J. *Biochemistry* **2002**, *41*, 15780.
(57) Lund, J.; Dalton, H. *Eur. J. Biochem.* **1985**, *147*, 291.
(58) Lund, J.; Woodland, M. P.; Dalton, H. *Eur. J. Biochem.* **1985**, *147*, 297.
(59) MacArthur, R.; Sazinsky, M. H.; Kühne, H.; Whittington, D. A.; Lippard, S. J.; Brudvig, G. W. *J. Am. Chem. Soc.* **2002**, *124*, 13392.
(60) Walters, K. J.; Gassner, G. T.; Lippard, S. J.; Wagner, G. *Proc. Natl. Acad. Sci. U.S.A.* **1999**, *96*, 7877.
(61) Chang, S. L.; Wallar, B. J.; Lipscomb, J. D.; Mayo, K. H. *Biochemistry* **1999**, *38*, 5799.
(62) Chang, S. L.; Wallar, B. J.; Lipscomb, J. D.; Mayo, K. H. *Biochemistry* **2001**, *40*, 9539.
(63) Müller, J.; Lugovskoy, A. A.; Wagner, G.; Lippard, S. J. *Biochemistry* **2002**, *41*, 42.
(64) Wallar, B. J.; Lipscomb, J. D. *Biochemistry* **2001**, *40*, 2220.
(65) Balendra, S.; Lesieur, C.; Smith, T. J.; Dalton, H. *Biochemistry* **2002**, *41*, 2571.
(66) Callaghan, A. J.; Smith, T. J.; Slade, S. E.; Dalton, H. *Eur. J. Biochem.* **2002**, *269*, 1835.
(67) Merkx, M.; Lippard, S. J. *J. Biol. Chem.* **2002**, *277*, 5858.
(68) Brandstetter, H.; Whittington, D. A.; Lippard, S. J.; Frederick, C. A. *Chem. Biol.* **1999**, *6*, 441.
(69) Kochkina, V. M.; Morozov, I. A.; Harutyunyan, E. G. *Mol. Biol.* **2001**, *35*, 730.
(70) DeWitt, J. G.; Bentsen, J. G.; Rosenzweig, A. C.; Hedman, B.; Green, J.; Pilkington, S.; Papaefthymiou, G. C.; Dalton, H.; Hodgson, K. O.; Lippard, S. J. *J. Am. Chem. Soc.* **1991**, *113*, 9219.
(71) Woodland, M. P.; Patil, D. S.; Cammack, R.; Dalton, H. *Biochim. Biophys. Acta* **1986**, *873*, 237.
(72) Fox, B. G.; Liu, Y.; Dege, J. E.; Lipscomb, J. D. *J. Biol. Chem.* **1991**, *266*, 540.
(73) Fox, B. G.; Surerus, K. K.; Münck, E.; Lipscomb, J. D. *J. Biol. Chem.* **1988**, *263*, 10553.
(74) Fox, B. G.; Hendrich, M. P.; Surerus, K. K.; Andersson, K. K.; Froland, W. A.; Lipscomb, J. D.; Münck, E. *J. Am. Chem. Soc.* **1993**, *115*, 3688.
(75) Froland, W. A.; Andersson, K. K.; Lee, S. K.; Liu, Y.; Lipscomb, J. D. *J. Biol. Chem.* **1992**, *267*, 17588.
(76) Hendrich, M. P.; Münck, E.; Fox, B. G.; Lipscomb, J. D. *J. Am. Chem. Soc.* **1990**, *112*, 5861.
(77) Davydov, A.; Davydov, R.; Gräslund, A.; Lipscomb, J. D.; Andersson, K. K. *J. Biol. Chem.* **1997**, *272*, 7022.
(78) Davydov, R.; Valentine, A. M.; Komar-Panicucci, S.; Hoffman, B. M.; Lippard, S. J. *Biochemistry* **1999**, *38*, 4188.
(79) Green, J.; Dalton, H. *J. Biol. Chem.* **1988**, *263*, 17561.
(80) Smoukov, S. K.; Kopp, D. A.; Valentine, A. M.; Davydov, R.; Lippard, S. J.; Hoffman, B. M. *J. Am. Chem. Soc.* **2002**, *124*, 2657.
(81) Willems, J. P.; Valentine, A. M.; Gurbiel, R.; Lippard, S. J.; Hoffman, B. M. *J. Am. Chem. Soc.* **1998**, *120*, 9410.
(82) Hendrich, M. P.; Fox, B. G.; Andersson, K. K.; Debrunner, P. G.; Lipscomb, J. D. *J. Biol. Chem.* **1992**, *267*, 261.
(83) Thomann, H.; Bernardo, M.; McCormick, J. M.; Pulver, S.; Andersson, K. K.; Lipscomb, J. D.; Solomon, E. I. *J. Am. Chem. Soc.* **1993**, *115*, 8881.
(84) DeRose, V. J.; Liu, K. E.; Kurtz, D. M.; Hoffman, B. M.; Lippard, S. J. *J. Am. Chem. Soc.* **1993**, *115*, 6440.
(85) Hoffman, B. M.; Sturgeon, B. E.; Doan, P. E.; DeRose, V. J.; Liu, K. E.; Lippard, S. J. *J. Am. Chem. Soc.* **1994**, *116*, 6023.
(86) Hoffman, B. M. *J. Phys. Chem.* **1994**, *98*, 11657.
(87) Bender, C. J.; Rosenzweig, A. C.; Lippard, S. J.; Peisach, J. *J. Biol. Chem.* **1994**, *269*, 15993.
(88) DeRose, V. J.; Liu, K. E.; Lippard, S. J.; Hoffman, B. M. *J. Am. Chem. Soc.* **1996**, *118*, 121.
(89) Sturgeon, B. E.; Doan, P. E.; Liu, K. E.; Burdi, D.; Tong, W. H.; Nocek, J. M.; Gupta, N.; Stubbe, J.; Kurtz, D. M.; Lippard, S. J.; Hoffman, B. M. *J. Am. Chem. Soc.* **1997**, *119*, 375.
(90) Ericson, A.; Hedman, B.; Hodgson, K. O.; Green, J.; Dalton, H.; Bentsen, J. G.; Beer, R. H.; Lippard, S. J. *J. Am. Chem. Soc.* **1988**, *110*, 2330.
(91) DeWitt, J.; Hedman, B.; Ericson, A.; Hodgson, K. O.; Bentsen, J.; Beer, R.; Lippard, S. J.; Green, J.; Dalton, H. *Physica B* **1989**, *158*, 97.

(92) DeWitt, J. G.; Rosenzweig, A. C.; Salifoglou, A.; Hedman, B.; Lippard, S. J.; Hodgson, K. O. *Inorg. Chem.* **1995**, *34*, 2505.
(93) Shu, L. J.; Liu, Y.; Lipscomb, J. D.; Que, L. *J. Biol. Inorg. Chem.* **1996**, *1*, 297.
(94) Que, L. *Pure Appl. Chem.* **1998**, *70*, 947.
(95) Pulver, S. C.; Froland, W. A.; Lipscomb, J. D.; Solomon, E. I. *J. Am. Chem. Soc.* **1997**, *119*, 387.
(96) Pulver, S.; Froland, W. A.; Fox, B. G.; Lipscomb, J. D.; Solomon, E. I. *J. Am. Chem. Soc.* **1993**, *115*, 12409.
(97) Solomon, E. I. *Inorg. Chem.* **2001**, *40*, 3656.
(98) Drummond, D.; Smith, S.; Dalton, H. *Eur. J. Biochem.* **1992**, *210*, 629.
(99) Liu, K. E.; Valentine, A. M.; Wang, D. L.; Huynh, B. H.; Edmondson, D. E.; Salifoglou, A.; Lippard, S. J. *J. Am. Chem. Soc.* **1995**, *117*, 10174.
(100) Valentine, A. M.; Tavares, P.; Pereira, A. S.; Davydov, R.; Krebs, C.; Hoffman, B. M.; Edmondson, D. E.; Huynh, B. H.; Lippard, S. J. *J. Am. Chem. Soc.* **1998**, *120*, 2190.
(101) Parr, R. G.; Yang, W. *Density Functional Theory of Atoms and Molecules*; Oxford University Press: New York, 1989.
(102) Ziegler, T. *Chem. Rev.* **1991**, *91*, 651.
(103) Sears, T. J.; Johnson, P. M.; Jin, P.; Oatis, S. *J. Chem. Phys.* **1996**, *104*, 781.
(104) Newcomb, M.; Choi, S. Y.; Horner, J. H. *J. Org. Chem.* **1999**, *64*, 1225.
(105) Bowry, V. W.; Lusztyk, J.; Ingold, K. U. *J. Am. Chem. Soc.* **1991**, *113*, 5687.
(106) Choi, S. Y.; Newcomb, M. *Tetrahedron* **1995**, *51*, 657.
(107) Newcomb, M.; Johnson, C. C.; Manek, M. B.; Varick, T. R. *J. Am. Chem. Soc.* **1992**, *114*, 10915.
(108) Newcomb, M.; Chestney, D. L. *J. Am. Chem. Soc.* **1994**, *116*, 9753.
(109) Le Tadic-Biadatti, M. H.; Newcomb, M. *J. Chem. Soc., Perkin Trans. 2* **1996**, 1467.
(110) Eaton, P. E.; Yip, Y. C. *J. Am. Chem. Soc.* **1991**, *113*, 7692.
(111) Choi, S.-Y.; Eaton, P. E.; Newcomb, M.; Yip, Y.-C. *J. Am. Chem. Soc.* **1992**, *114*, 6326.
(112) Della, E. W.; Janowski, W. K. *J. Org. Chem.* **1995**, *60*, 7756.
(113) Friedrich, E. C.; Holmstead, R. L. *J. Org. Chem.* **1972**, *37*, 2550.
(114) Friedrich, E. C.; Jassawalla, J. D. C. *J. Org. Chem.* **1979**, *44*, 4224.
(115) Ruzicka, F.; Huang, D.-S.; Donnelly, M. I.; Frey, P. A. *Biochemistry* **1990**, *29*, 1696.
(116) Choi, S. Y.; Eaton, P. E.; Hollenberg, P. F.; Liu, K. E.; Lippard, S. J.; Newcomb, M.; Putt, D. A.; Upadhyaya, S. P.; Xiong, Y. *J. Am. Chem. Soc.* **1996**, *118*, 6547.
(117) Jin, Y.; Lipscomb, J. D. *Biochemistry* **1999**, *38*, 6178.
(118) Choi, S. Y.; Eaton, P. E.; Kopp, D. A.; Lippard, S. J.; Newcomb, M.; Shen, R. N. *J. Am. Chem. Soc.* **1999**, *121*, 12198.
(119) Brazeau, B. J.; Austin, R. N.; Tarr, C.; Groves, J. T.; Lipscomb, J. D. *J. Am. Chem. Soc.* **2001**, *123*, 11831.
(120) Groves, J. T.; Subramanian, D. V. *J. Am. Chem. Soc.* **1984**, *106*, 2177.
(121) Groves, J. T.; McClusky, G. A.; White, R. E.; Coon, M. J. *Biochem. Biophys. Res. Commun.* **1978**, *81*, 154.
(122) Sustmann, R.; Trill, H. *J. Am. Chem. Soc.* **1974**, *96*, 4343.
(123) Stearns, R. A.; Ortiz de Montellano, P. R. *J. Am. Chem. Soc.* **1985**, *107*, 4081.
(124) Green, J.; Dalton, H. *Biochem. J.* **1986**, *236*, 155.
(125) Dalton, H.; Golding, B. T.; Waters, B. W.; Higgins, R.; Taylor, J. A. *J. Chem. Soc., Chem. Commun.* **1981**, 482.
(126) Liu, K. E.; Johnson, C. C.; Newcomb, M.; Lippard, S. J. *J. Am. Chem. Soc.* **1993**, *115*, 939.
(127) Valentine, A. M.; Le Tadic-Biadatti, M. H.; Toy, P. H.; Newcomb, M.; Lippard, S. J. *J. Biol. Chem.* **1999**, *274*, 10771.
(128) Jin, Y.; Lipscomb, J. D. *Biochim. Biophys. Acta—Protein Struct. Mol. Enzymol.* **2000**, *1543*, 47.
(129) White, R. E.; Groves, J. T.; McClusky, G. A. *Acta Biol. Med. Ger.* **1979**, *38*, 475.
(130) Austin, R. N.; Chang, H. K.; Zylstra, G. J.; Groves, J. T. *J. Am. Chem. Soc.* **2000**, *122*, 11747.
(131) Fu, H.; Look, G. C.; Zhang, W.; Jacobsen, E. N.; Wong, C.-H. *J. Org. Chem.* **1991**, *56*, 6497.
(132) Newcomb, M.; Shen, R. N.; Lu, Y.; Coon, M. J.; Hollenberg, P. F.; Kopp, D. A.; Lippard, S. J. *J. Am. Chem. Soc.* **2002**, *124*, 6879.
(133) Auclair, K.; Hu, Z.; Little, D. M.; Ortiz de Montellano, P. R.; Groves, J. T. *J. Am. Chem. Soc.* **2002**, *124*, 6020.
(134) Valentine, A. M.; Wilkinson, B.; Liu, K. E.; Komar-Panicucci, S.; Priestley, N. D.; Williams, P. G.; Morimoto, H.; Floss, H. G.; Lippard, S. J. *J. Am. Chem. Soc.* **1997**, *119*, 1818.
(135) Priestley, N. D.; Floss, H. G.; Froland, W. A.; Lipscomb, J. D.; Williams, P. G.; Morimoto, H. *J. Am. Chem. Soc.* **1992**, *114*, 7561.
(136) Wilkinson, B.; Zhu, M.; Priestley, N. D.; Nguyen, H. H. T.; Morimoto, H.; Williams, P. G.; Chan, S. I.; Floss, H. G. *J. Am. Chem. Soc.* **1996**, *118*, 921.
(137) Kwart, H. *Acc. Chem. Res.* **1982**, *15*, 401.
(138) Yoshizawa, K. *Coord. Chem. Rev.* **2002**, *226*, 251.
(139) Iyer, K. R.; Jones, J. P.; Darbyshire, J. F.; Trager, W. F. *Biochemistry* **1997**, *36*, 7136.
(140) Belova, V. S.; Gvozdev, R. I.; Malashenko, Y. R.; Sadkov, A. P.; Yurchenko, V. V. *Biokhimiya* **1976**, *41*, 1903.
(141) Nesheim, J. C.; Lipscomb, J. D. *Biochemistry* **1996**, *35*, 10240.
(142) Wilkins, P. C.; Dalton, H.; Samuel, C. J.; Green, J. *Eur. J. Biochem.* **1994**, *226*, 555.
(143) Hanzlik, R. P.; Ling, K.-H. *J. Org. Chem.* **1990**, *55*, 3992.
(144) Huang, D.-S.; Wu, S.-H.; Wang, Y.-S.; Yu, S. S.-F.; Chan, S. I. *Chem. Biochem.* **2002**, *3*, 760.
(145) Stahl, S. S.; Francisco, W. A.; Merkx, M.; Klinman, J. P.; Lippard, S. J. *J. Biol. Chem.* **2001**, *276*, 4549.
(146) Lee, S. Y.; Lipscomb, J. D. *Biochemistry* **1999**, *38*, 4423.
(147) Brazeau, B. J.; Lipscomb, J. D. *Biochemistry* **2000**, *39*, 13503.
(148) Brazeau, B. J.; Wallar, B. J.; Lipscomb, J. D. *J. Am. Chem. Soc.* **2001**, *123*, 10421.
(149) Valentine, A. M.; Stahl, S. S.; Lippard, S. J. *J. Am. Chem. Soc.* **1999**, *121*, 3876.
(150) Ambundo, E. A.; Friesner, R. A.; Lippard, S. J. *J. Am. Chem. Soc.* **2002**, *124*, 8770.
(151) Maseras, F.; Morokuma, K. *J. Comput. Chem.* **1995**, *16*, 1170.
(152) Kairys, V.; Jensen, J. H. *J. Phys. Chem. A* **2000**, *104*, 6656.
(153) Bash, P. A.; Field, M. J.; Karplus, M. *J. Am. Chem. Soc.* **1987**, *109*, 8092.
(154) Singh, U. C.; Kollman, P. A. *J. Comput. Chem.* **1986**, *7*, 718.
(155) Woo, T. K.; Cavallo, L.; Ziegler, T. *Theor. Chem. Acc.* **1998**, *100*, 307.
(156) Gao, J. L.; Amara, P.; Alhambra, C.; Field, M. J. *J. Phys. Chem. A* **1998**, *102*, 4714.
(157) Zhang, Y. K.; Lee, T. S.; Yang, W. T. *J. Chem. Phys.* **1999**, *110*, 46.
(158) Murphy, R. B.; Philipp, D. M.; Friesner, R. A. *J. Comput. Chem.* **2000**, *21*, 1442.
(159) Murphy, R. B.; Philipp, D. M.; Friesner, R. A. *Chem. Phys. Lett.* **2000**, *321*, 113.
(160) Philipp, D. M.; Friesner, R. A. *J. Comput. Chem.* **1999**, *20*, 1468.
(161) Torrent, M.; Vreven, T.; Musaev, D. G.; Morokuma, K.; Farkas, Ö.; Schlegel, H. B. *J. Am. Chem. Soc.* **2002**, *124*, 192.
(162) Friesner, R. A.; Baik, M.-H.; Gherman, B. F.; Guallar, V.; Wirstam, M.; Murphy, R. B.; Lippard, S. J. *Coord. Chem. Rev.* **2003**, *238—239*, 267.
(163) Becke, A. D. *J. Chem. Phys.* **1993**, *98*, 5648.
(164) Lee, C. T.; Yang, W. T.; Parr, R. G. *Phys. Rev. B* **1988**, *37*, 785.
(165) Curtiss, L. A.; Raghavachari, K.; Redfern, P. C.; Pople, J. A. *J. Chem. Phys.* **1997**, *106*, 1063.
(166) Curtiss, L. A.; Redfern, P. C.; Raghavachari, K.; Pople, J. A. *J. Chem. Phys.* **1998**, *109*, 42.
(167) Becke, A. D. *Phys. Rev. A* **1988**, *38*, 3098.
(168) Vosko, S. H.; Wilk, L.; Nusair, M. *Can. J. Phys.* **1980**, *58*, 1200.
(169) Perdew, J. P.; Wang, Y. *Phys. Rev. B* **1992**, *45*, 13244.
(170) Nakao, Y.; Hirao, K.; Taketsugu, T. *J. Chem. Phys.* **2001**, *114*, 7935.
(171) Nakao, Y.; Hirao, K.; Taketsugu, T. *J. Chem. Phys.* **2001**, *114*, 5216.
(172) Gill, P. M. W.; Johnson, B. G.; Pople, J. A.; Frisch, M. J. *Chem. Phys. Lett.* **1992**, *197*, 499.
(173) Hay, P. J.; Wadt, W. R. *J. Chem. Phys.* **1985**, *82*, 270.
(174) Hay, P. J.; Wadt, W. R. *J. Chem. Phys.* **1985**, *82*, 299.
(175) Wadt, W. R.; Hay, P. J. *J. Chem. Phys.* **1985**, *82*, 284.
(176) Stevens, W. J.; Basch, H.; Krauss, M. *J. Chem. Phys.* **1984**, *81*, 6026.
(177) Stevens, W. J.; Krauss, M.; Basch, H.; Jasien, P. G. *Can. J. Chem.* **1992**, *70*, 612.
(178) Baik, M.-H.; Lee, D.; Friesner, R. A.; Lippard, S. J. *Isr. J. Chem.* **2001**, *41*, 173.
(179) Liu, K. E.; Wang, D. L.; Huynh, B. H.; Edmondson, D. E.; Salifoglou, A.; Lippard, S. J. *J. Am. Chem. Soc.* **1994**, *116*, 7465.
(180) Lee, S. K.; Fox, B. G.; Froland, W. A.; Lipscomb, J. D.; Münck, E. *J. Am. Chem. Soc.* **1993**, *115*, 6450.
(181) Andersson, K.; Malmqvist, P. A.; Roos, B. O. *J. Chem. Phys.* **1992**, *96*, 1218.
(182) Andersson, K.; Malmqvist, P. A.; Roos, B. O.; Sadlej, A. J.; Wolinski, K. *J. Phys. Chem.* **1990**, *94*, 5483.
(183) Noodleman, L. *J. Chem. Phys.* **1981**, *74*, 5737.
(184) Yamaguchi, K.; Jensen, F.; Dorigo, A.; Houk, K. N. *Chem. Phys. Lett.* **1988**, *149*, 537.
(185) Yoshizawa, K.; Suzuki, A.; Shiota, Y.; Yamabe, T. *Bull. Chem. Soc. Jpn.* **2000**, *73*, 815.
(186) Torrent, M.; Musaev, D. G.; Basch, H.; Morokuma, K. *J. Comput. Chem.* **2002**, *23*, 59.
(187) McGrady, J. E.; Stranger, R.; Lovell, T. *J. Phys. Chem. A* **1997**, *101*, 6265.
(188) Zhao, X. G.; Richardson, W. H.; Chen, J. L.; Li, J.; Noodleman, L.; Tsai, H. L.; Hendrickson, D. N. *Inorg. Chem.* **1997**, *36*, 1198.
(189) Dunietz, B. D.; Beachy, M. D.; Cao, Y. X.; Whittington, D. A.; Lippard, S. J.; Friesner, R. A. *J. Am. Chem. Soc.* **2000**, *122*, 2828.
(190) Lovell, T.; Han, W.-G.; Liu, T.; Noodleman, L. *J. Am. Chem. Soc.* **2002**, *124*, 5890.
(191) Stowasser, R.; Hoffmann, R. *J. Am. Chem. Soc.* **1999**, *121*, 3414.
(192) Baerends, E. J.; Gritsenko, O. V. *J. Phys. Chem. A* **1997**, *101*, 5383.

(193) Kohn, W.; Becke, A. D.; Parr, R. G. *J. Phys. Chem.* **1996**, *100*, 12974.
(194) Zhao, Q. S.; Morrison, R. C.; Parr, R. G. *Phys. Rev. A* **1994**, *50*, 2138.
(195) Perdew, J. P.; Levy, M. *Phys. Rev. Lett.* **1983**, *51*, 1884.
(196) Ziegler, T.; Rauk, A. *Inorg. Chem.* **1979**, *18*, 1558.
(197) Ziegler, T.; Rauk, A. *Inorg. Chem.* **1979**, *18*, 1755.
(198) Mulliken, R. S. *J. Chem. Phys.* **1955**, *23*, 1833.
(199) Szabo, A.; Ostlund, N. S. *Modern Quantum Chemistry*; McGraw-Hill: New York, 1989.
(200) Yoshizawa, K.; Ohta, T.; Yamabe, T.; Hoffmann, R. *J. Am. Chem. Soc.* **1997**, *119*, 12311.
(201) Shu, L. J.; Nesheim, J. C.; Kauffmann, K.; Münck, E.; Lipscomb, J. D.; Que, L. *Science* **1997**, *275*, 515.
(202) Schröder, D.; Schwarz, H. *Angew. Chem., Int. Ed. Engl.* **1995**, *34*, 1973.
(203) Fiedler, A.; Schröder, D.; Shaik, S.; Schwarz, H. *J. Am. Chem. Soc.* **1994**, *116*, 10734.
(204) Schröder, D.; Schwarz, H. *Angew. Chem., Int. Ed. Engl.* **1990**, *29*, 1433.
(205) Shiota, Y.; Yoshizawa, K. *J. Am. Chem. Soc.* **2000**, *122*, 12317.
(206) Yoshizawa, K.; Shiota, Y.; Yamabe, T. *Chem. Eur. J.* **1997**, *3*, 1160.
(207) Yoshizawa, K.; Yamabe, T.; Hoffmann, R. *New J. Chem.* **1997**, *21*, 151.
(208) Yoshizawa, K.; Hoffmann, R. *Inorg. Chem.* **1996**, *35*, 2409.
(209) Yoshizawa, K.; Yokomichi, Y.; Shiota, Y.; Ohta, T.; Yamabe, T. *Chem. Lett.* **1997**, 587.
(210) Yoshizawa, K. *J. Biol. Inorg. Chem.* **1998**, *3*, 318.
(211) Yoshizawa, K.; Shiota, Y.; Yamabe, T. *J. Am. Chem. Soc.* **1998**, *120*, 564.
(212) Yoshizawa, K.; Ohta, T.; Yamabe, T. *Bull. Chem. Soc. Jpn.* **1998**, *71*, 1899.
(213) Yoshizawa, K. *J. Inorg. Biochem.* **2000**, *78*, 23.
(214) Yoshizawa, K. *J. Organomet. Chem.* **2001**, *635*, 100.
(215) Whittington, D. A.; Valentine, A. M.; Lippard, S. J. *J. Biol. Inorg. Chem.* **1998**, *3*, 307.
(216) m, molecular mass; I, moment of inertia; q_v, vibrational partition function; E, activation energy. Supercripts R and # denote the reactant and transition states, respectively.
(217) Shaik, S.; Danovich, D.; Fiedler, A.; Schröder, D.; Schwarz, H. *Helv. Chim. Acta* **1995**, *78*, 1393.
(218) Shaik, S.; Filatov, M.; Schröder, D.; Schwarz, H. *Chem. Eur. J.* **1998**, *4*, 193.
(219) Shaik, S.; de Visser, S. P.; Ogliaro, F.; Schwarz, H.; Schröder, D. *Curr. Opin. Chem. Biol.* **2002**, *6*, 556.
(220) Basch, H.; Mogi, K.; Musaev, D. G.; Morokuma, K. *J. Am. Chem. Soc.* **1999**, *121*, 7249.
(221) Basch, H.; Musaev, D. G.; Morokuma, K. *J. Phys. Chem. B* **2001**, *105*, 8452.
(222) Torrent, M.; Mogi, K.; Basch, H.; Musaev, D. G.; Morokuma, K. *J. Phys. Chem. B* **2001**, *105*, 8616.
(223) Torrent, M.; Musaev, D. G.; Morokuma, K.; Basch, H. *J. Phys. Chem. B* **2001**, *105*, 4453.
(224) Basch, H.; Musaev, D. G.; Mogi, K.; Morokuma, K. *J. Phys. Chem. A* **2001**, *105*, 3615.
(225) Torrent, M.; Musaev, D. G.; Morokuma, K. *J. Phys. Chem. B* **2001**, *105*, 322.
(226) Musaev, D. G.; Basch, H.; Morokuma, K. *J. Am. Chem. Soc.* **2002**, *124*, 4135.
(227) Hrovat, D. A.; Borden, W. T. *J. Am. Chem. Soc.* **1994**, *116*, 6459.
(228) Lide, D. R. *Handbook of Chemistry and Physics*, 74th ed.; CRC Press: Boca Raton, FL, 1994.
(229) Siegbahn, P. E. M.; Crabtree, R. H. *J. Am. Chem. Soc.* **1997**, *119*, 3103.
(230) Siegbahn, P. E. M. *Inorg. Chem.* **1999**, *38*, 2880.
(231) Siegbahn, P. E. M. *Chem. Phys. Lett.* **2002**, *351*, 311.
(232) Siegbahn, P. E. M.; Blomberg, M. R. A. *Chem. Rev.* **2000**, *100*, 421.
(233) Siegbahn, P. E. M.; Crabtree, R. H. *Struct. Bonding* **2000**, *97*, 125.
(234) Siegbahn, P. E. M.; Crabtree, R. H.; Nordlund, P. *J. Biol. Inorg. Chem.* **1998**, *3*, 314.
(235) Blomberg, M. R. A.; Siegbahn, P. E. M. *J. Phys. Chem. B* **2001**, *105*, 9375.
(236) Siegbahn, P. E. M. *J. Biol. Inorg. Chem.* **2001**, *6*, 27.
(237) Gherman, B. F.; Dunietz, B. D.; Whittington, D. A.; Lippard, S. J.; Friesner, R. A. *J. Am. Chem. Soc.* **2001**, *123*, 3836.
(238) Friesner, R. A.; Dunietz, B. D. *Acc. Chem. Res.* **2001**, *34*, 351.
(239) Guallar, V.; Gherman, B. F.; Lippard, S. J.; Friesner, R. A. *Curr. Opin. Chem. Biol.* **2002**, *6*, 236.
(240) Guallar, V.; Gherman, B. F.; Miller, W. H.; Lippard, S. J.; Friesner, R. A. *J. Am. Chem. Soc.* **2002**, *124*, 3377.
(241) Baik, M.-H.; Gherman, B. F.; Friesner, R. F.; Lippard, S. J. *J. Am. Chem. Soc.* **2002**, *124*, 14608.
(242) Lovell, T.; Li, J.; Noodleman, L. *Inorg. Chem.* **2001**, *40*, 5251.
(243) Lovell, T.; Li, J.; Noodleman, L. *Inorg. Chem.* **2001**, *40*, 5267.
(244) Lovell, T.; Li, J.; Noodleman, L. *J. Biol. Inorg. Chem.* **2002**, *7*, 799.
(245) Berkowitz, J.; Ellison, G. B.; Gutman, D. *J. Phys. Chem.* **1994**, *98*, 2744.
(246) Halgren, T. A.; Roberts, J. D.; Horner, J. H.; Martinez, F. N.; Tronche, C.; Newcomb, M. *J. Am. Chem. Soc.* **2000**, *122*, 2988.

CR950244F